NOV-3341-NT-3284
Issue 1 – Rev 1

Report on the validation of MERIS IBAER land products

Aerosol Optical Thickness and surface reflectance

Attention to: Peter REGNER, ESA/ESRIN
Luc GOVAERTS, ESA/ESRIN

	Function	Name	Signature	Date
Prepared by	Project Engineer	Véronique BRUNIQUEL Béatrice BERTHELOT W. Von HoyningenHuene		
Verified by	Project Manager	Béatrice BERTHELOT		
Authorised by	General Manager	Richard BRU		

Noveltis
Parc Technologique du Canal – 2, Avenue de l'Europe – 31520 Ramonville-Saint-Agne – France
Tél. : +33 (0)562 88 11 11 – Fax : +33 (0)562 88 11 12 – E-mail : Noveltis@Noveltis.fr

Indexing form

Customer	**ESA/ESRIN**	**Contract N°**	**-**

Confidentiality codes				**Document management**	
Company / Programme		Defence			
Non-protected	☐	Non-protected	☒	None	☐
Reserved	☒	Limited diffusion	☐	Internal	☒
Confidential	☐	Defence confidentiality	☐	Customer	☐

Contractual document	**Project N°**	**Work Package**
Yes ☒ No ☐	3341	WP100

Report on the validation of MERIS IBAER land products

Aerosol Optical Thickness and surface reflectance

Summary

This document contains the elements of the validation of the BAER processor.

Document			
File name	NOV-3341-NT-3284_v1.5.doc	Nbr of pages	141
Project	MERIS extension	Nbr of tables	7
Software	Microsoft Office Word	Nbr of figures	38
Language	English	Nbr of appendices	5

Document reference					
Internal	NOV-3341-NT-3284	Issue	1	Date	31/03/06
External	-	Revision	1	Date	07/04/06

Author(s)	**Verified by**	**Authorised by**
Véronique BRUNIQUEL Béatrice BERTHELOT W. Von HoyningenHuene	Béatrice BERTHELOT	Richard BRU

Distribution list

INTERNAL	EXTERNAL	
Name	Name	Company / Organisation
Documentation Noveltis Richard BRU Béatrice BERTHELOT Véronique BRUNIQUEL	Peter REGNER Wolfgang von HOYNINGEN-HUENE	ESA/ESRIN Bremen University

Document status

Report on the validation of MERIS IBAER land products Aerosol Optical Thickness and surface reflectance			
Issue	**Revision**	**Date**	**Reason for the revision**
1	1	07/04/06	Modification of the document

Modification status				
Issue	Rev	Status *	Modified pages	Reason for the modification
1	1	M	all	Additional information has been added

* *I = Inserted* *D = deleted* *M = Modified*

Acronyms

AAI	Aerosol Absorbed Index
AATSR	Advanced Along Track Scanning radiometer
ACE	Aerosol Characterisation experiment
AERONET	Aerosol Robotic Network
AOT	Aerosol Optical Thickness
ASCAR	Algorithm Survey and Critical Analysis Report
ATBD	Algorithm Theoretical Basis Document
ATSR-2	Along Track Scanning radiometer
AVHRR	Advances Very High Resolution Radiometer
BAER	Bremen AERosol algorithm for MERIS
BEAM	Basic Envisat AATSR MERIS toolbox
DDV	Dark Dense Vegetation
DWD	Deutscher Wetterdienst
ENVISAT	ESA satellite
GOMETRAN	GOME radiative TRANsfer model
HDF	Hierarchical Data Format
IBAER	Integrated BAER processor
IGOS	Integrated Global Observing Strategy
IPCC	Intergovernemental Panel Climate Change
KNMI	Koninklijk Nederlands Meteorologisch Instituut
L1	Level 1
L2	Level 2
LACE	Lindenberg Aerosol Characterisation experiment
LUT	Look Up Table
MERCI	Catalogue and Inventory for MERIS RR Data Products
MERIS	Moderate Imaging Spectrometer
MISR	Multiangle Imaging Spectrometer
MODIS	Moderate Resolution Imaging SpectroRadiometer
NIR	Near Infra Red
NDVI	Normalised Difference Vegetation Index
POLDER	Polarisation and Directionaly of the Earth's Reflectances
RMSD	Root Mean Square Deviation
RTM	Radiative Transfer Model
SCIAMACHY	SCanning Imaging Absorption Spectrometer for Atmospheric CHartograpHY
SCIATRAN	SCIAMACHY radiative TRANsfer model
SDS	Scientific Data Set
SeaWiFS	Sea Viewing Wide Field of View Sensor
SURF	Surface
SW	ShortWave
SW-VIS	Short Wave -Visible
TOMS	Total Ozone Mapping Spectrometer
VIS	Visible

Reference documents

[RD1] BAER processor – Input Output Data Document, NOVETIS technical note, NOV-3341-NT-3711 v.1.0

[RD2] Algorithm for Remote Sensing of Tropospheric Aerosol From MODIS, Product ID: MOD04, Y. J. Kaufman and D. Tanré, version October 26, 1998

[RD3] An ATBD for the ENVISAT radiometer MERIS;, Determination of aerosol optical thickness over land surfaces, using Bremen Aerosol Retrieval (BAER) and its application to atmospheric correction over lands, W. Von Hoyningen-Huene, B. Berthelot, A. Kokhanovsky, J.P. Burrows, NOV-3341-NT-3352.pdf, April, 2006.

[RD4] Santer et al., 2000,

[RD5] Berthelot and Quesney, 2005. Assessment of the cloud mask in the frame of the GLOBCOVER project., NOV-3325-NT-3440.pdf

[RD6] Annexe to the validation report, NOV-3341-NT-3229, B. Berthelot.

List of figures

List of tables

Table of contents

1. Introduction

1.1. Scope of the document

ESA's Medium Resolution Imaging Spectrometer (MERIS) on board Envisat has been continuously observing the Earth for the last four years. This instrument acquires multispectral imagery in 15 spectral bands from 0.4 to 0.9 µm of the ocean, land and atmosphere. This spectral range and high spatial resolution with global coverage make MERIS a potentially valuable sensor for the measurement and the monitoring of the Earth.
This study focused on the "***Development of algorithms for the exploitation of MERIS data over land***" It aims at developing algorithms to characterise the aerosol content in the atmosphere, in order to complete the atmospheric correction scheme over land of the Level 2 MERIS data, and developing algorithm to retrieve the biophysical vegetation products, useful for environmental studies at global or regional scale.
This document is the validation report, reporting for the aerosol correction scheme developed in the frame of the MERIS data exploitation activities. The results are based on the exploitation of the BAER method (described in the ATBD [RD3]), which allow to estimate the aerosol optical thickness and perform the aerosol correction to provide land surface reflectances.
The algorithm has been developed to monitor the aerosol optical thickness (proportional to the aerosol total loading), over most of part of the continents. The aerosol information is used in a second step to perform atmospheric corrections, using either the SMAC processor or the UBAC processor, to derive the remotely sensed surface reflectance over the land. The processing is made on a pixel-by pixel basis

The report is presented in four main sections, the presentation of the data used for the validation (section 2), the cloud detection (section 3), the aerosol optical thickness retrieval (section 4), the surface reflectance estimation (section 5). Papers written during the project are referred in the ATBD.

1.2. Algorithm overview

It has been shown that the retrieval of the aerosol content over land is a difficult task on a global scale since the surface albedo is generally unknown and variable with wavelength. Over the dark dense vegetation, some algorithms have been developed (Kaufman and Tanré, 1988; Holben et al. 1992) taking advantage of the low level of the reflectance in the blue and red regions to extend the derivation of aerosol optical thickness to additional brighter surfaces.
The BAER method (Bremen AErosol Retrieval) is an algorithm for remote sensing of aerosols from MERIS data over land. It is based on the same physical principles, i.e. the use of the MERIS blue bands (channel 1 and 2, 412nm, and 440 nm) to estimate the aerosol scattering and relate it to the aerosol content.

The actual MERIS Level 2 product provides reflectance data with an incomplete atmospheric correction over land. The atmospheric correction is made for Rayleigh scattering only and the variable aerosol influence is not considered. Thus, an additional step of atmospheric correction for L2 data over land is required, considering the effect of the atmospheric aerosol.

The original approach has been developed to retrieve AOT over land from SeaWiFS L1 data. It determines the spectral aerosol optical thickness (AOT) from nadir looking multi-wavelength radiometers. The method is based on the determination of the aerosol reflectance over 'dark surfaces', using the UV and short-wave-VIS range below the red-edge of the vegetation spectrum. This requires a proper separation of the variable surface effects, other atmospheric effects and aerosol effect.

For L2 data over land, the variability of the vegetation cover and the kind of the vegetation will be considered dynamically by means of a surface reflectance model tuned from the satellite scene self by the NDVI. The aerosol reflectance is obtained by removing the estimation of the surface effect. Look-up-tables of the relationship between AOT - aerosol reflectance and the use of constraints enable the determination of the AOT for 7 MERIS channels in a spectral range of 0.412 - 0.670 µm. AOT is extrapolated, using Angström power law with parameters estimated from the retrieved AOT. Others terms of radiative transfer (aerosol reflectance, total transmittance and hemispheric reflectance) are computed once the AOT known to correct the Top Of Aerosol reflectance from aerosol effect.

Once the aerosol optical thickness estimated, it is used as input of the atmospheric correction method (either SMAC or UBAC) to perform the aerosol correction and to provide the surface reflectance in the 13 MERIS channels.

1.3. Objectives of the validation

The objective of this study is to provide some validation elements of the aerosol optical thickness, angstrom exponent and surface reflectances products derived from the Integrated BAER algorithm (Von Hoynyngen-Huene et al;, 2005). The algorithm is fully described in the ATBD, referred by "Aerosol Optical Thickness and surface reflectance "in the document NOV-3341-NT-3352v1.0 [RD3].

The algorithm has been developed to be applied on MERIS L2 data to determine the aerosol optical thickness over land and complete the atmospheric correction by removing the aerosol signal from the Level 2 MERIS land products.

The full processing procedure is subdivided into 3 steps:

1. Cloud screening
2. Retrieval of aerosol optical thickness by the BAER approach
3. Atmospheric correction of aerosol effects in L2 reflectance data over land, using SMAC (Simplified Model of Atmospheric Correction, c.f. Dedieu *et al.*, 1994) or UBAC (University Bremen Atmospheric Correction, ATBD)

The validation of the products provides user the accuracy of the products derived from the Integrated BAER processor. A large number of MERIS L2 data has been processed in this exercise to cover a wide range of situations, i.e. the retrieval is performed over different surface types, various locations and dates. The accuracy is achieved by comparison to ground measured values (**direct validation** with AERONET measurements) and other equivalent products obtained from MERIS and MODIS sensors (**indirect validation** with MODIS Atmosphere products and MERIS standard outputs over DDV pixels).

This document presents the validation of each of the three modules.

1.4. MERIS products used for the validation

The selected Level 2 MERIS data correspond to 11 areas well distributed around the world chosen for representing various cover types at different seasons. They have been taken from the MERCI database[1]. The geographic coordinates are noted in Table 1 and the sites are located in Figure 1. It is important to note that these sites have been also chosen because an AERONET station is present on each of these areas. Each MERIS product has been also displayed and selected manually to keep the products the clearest from the cloud point of view. The number of selected products is mentioned in Table 1. The full list of all selected MERIS products is available in Annex 1.

Due to the constraint of the MERIS data available in the MERCI database, the MERIS data selected for the validation correspond to the 2003 period.

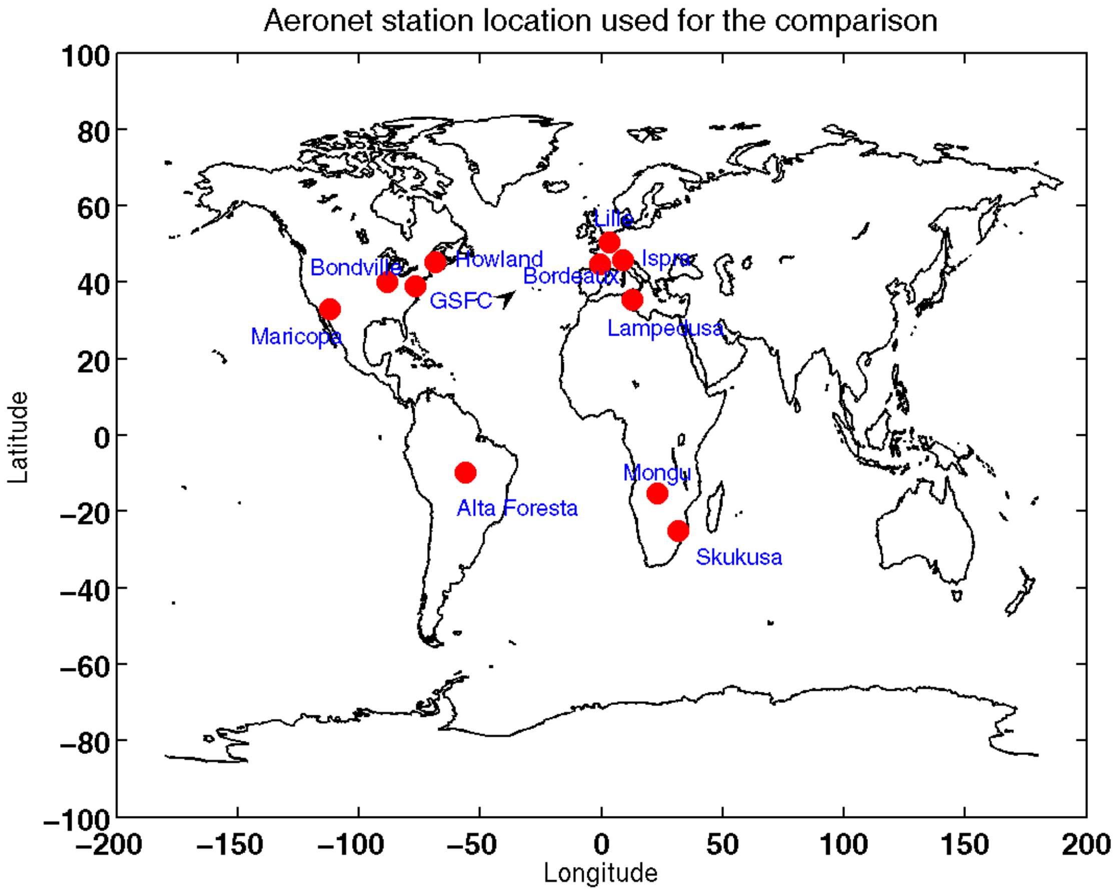

Figure 1: Validation site locations

The MERIS sites also correspond to different site characteristics: for instance, conifer area near Bordeaux, tropical forest for Alta Foresta. A true colour image and the land classification map corresponding are provided in Table 1 for each site.

[1] They have been selected among the available MERIS products of the MERCI database (http://141.4.215.11/merci/welcome.do).

Table 1: Definition of the validation sites and number of selected MERIS images

Site name	Latitude (°)/ Longitude (°)	Number of selected MERIS images	View of the site
France	[55-35, -10,10]	1	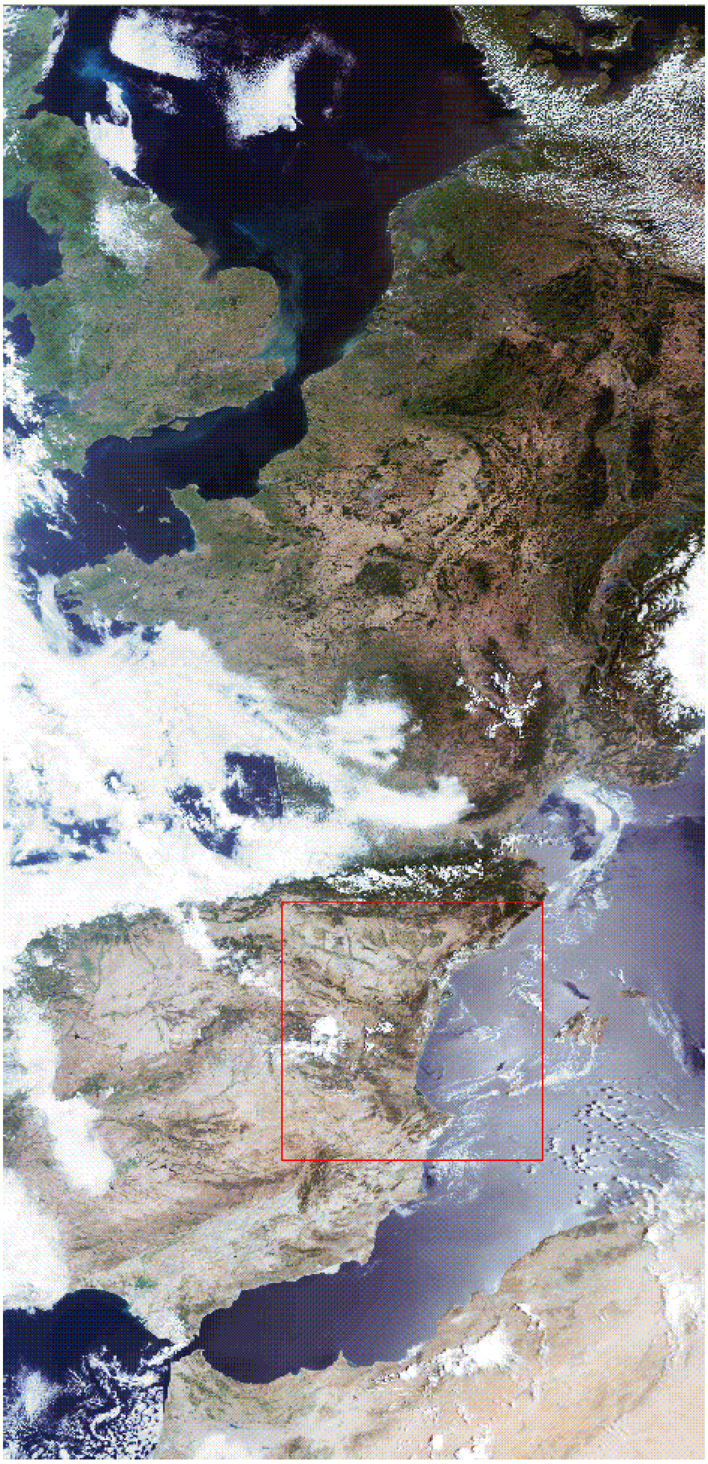

Site name	Latitude (°)/ Longitude (°)	Number of selected MERIS images	View of the site
Alta_Foresta	-9.916 -56.017	4	 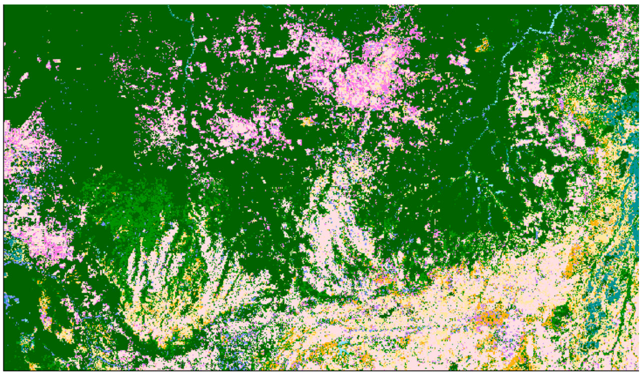
Bondville	40.053 -88.372	9	 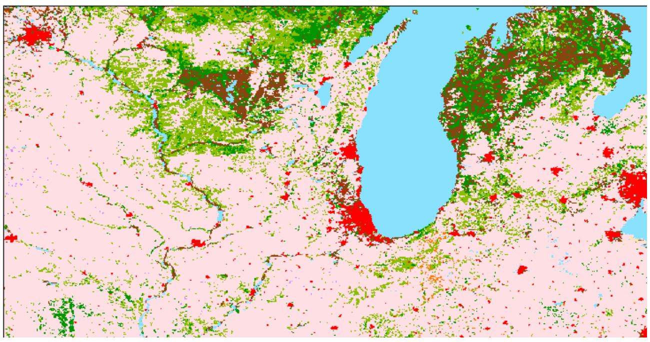

Site name	Latitude (°)/ Longitude (°)	Number of selected MERIS images	View of the site
Bordeaux	44.788 -0.579	5	 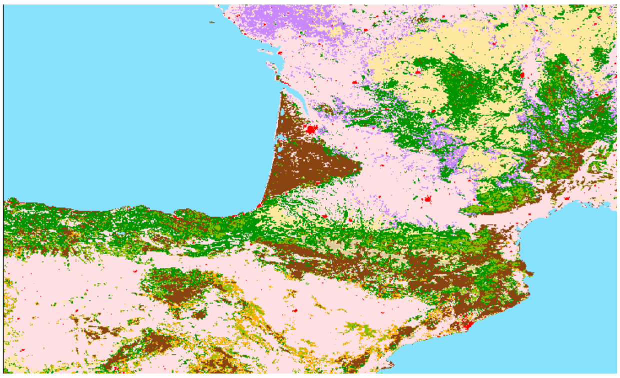
GSFC	39.03 -76.88	4	 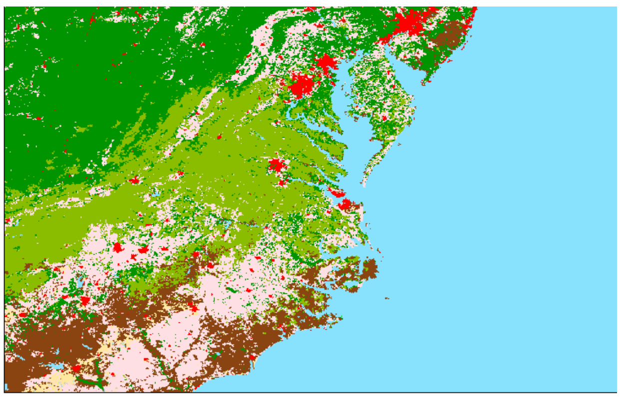

Site name	**Latitude (°)/ Longitude (°)**	**Number of selected MERIS images**	**View of the site**
Howland	45.2 -68.733	1	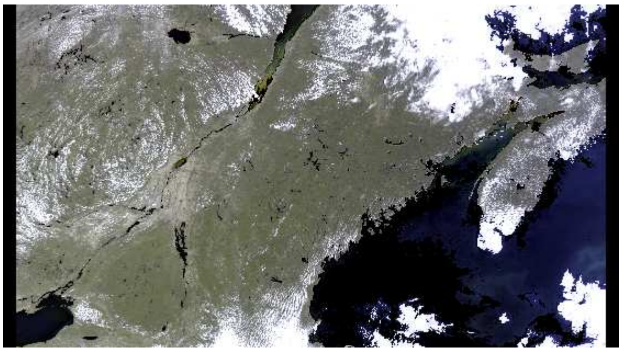 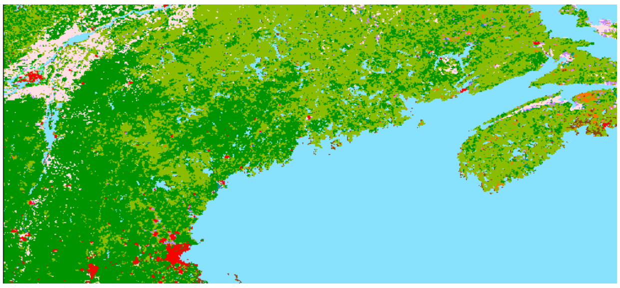
Ispra	45.803 8.626	9	 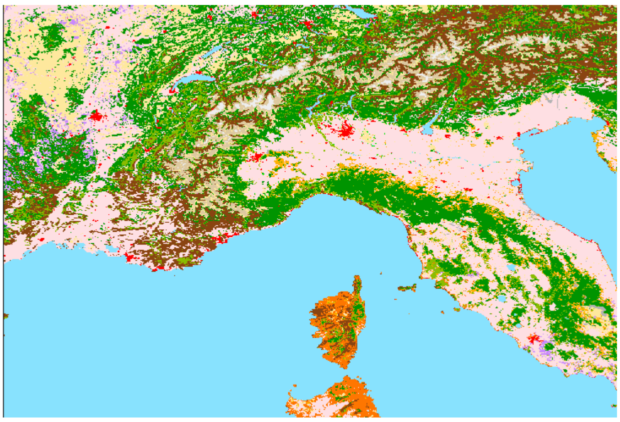

Site name	Latitude (°)/ Longitude (°)	Number of selected MERIS images	View of the site
Lampedusa	35.517 12.632	3	 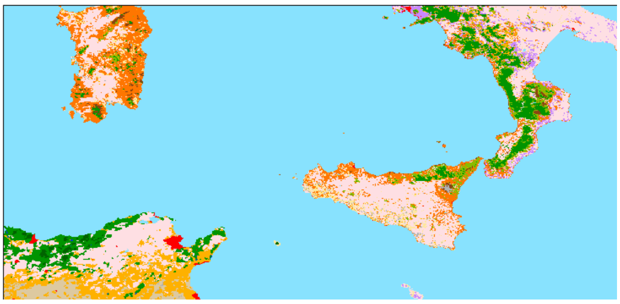
Lille	50.612 3.142	4	 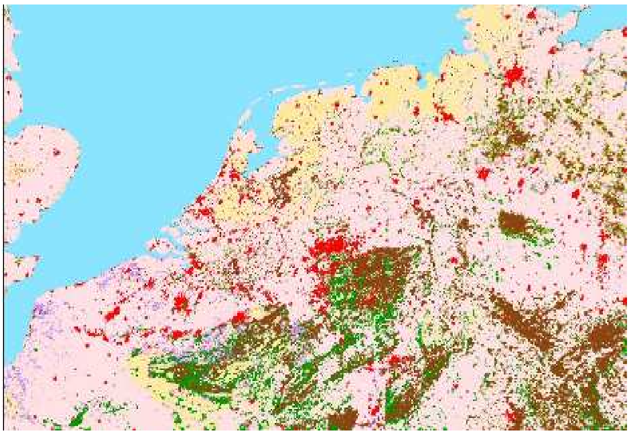

Site name	Latitude (°)/ Longitude (°)	Number of selected MERIS images	View of the site
Maricopa	33.069 -111.972	29	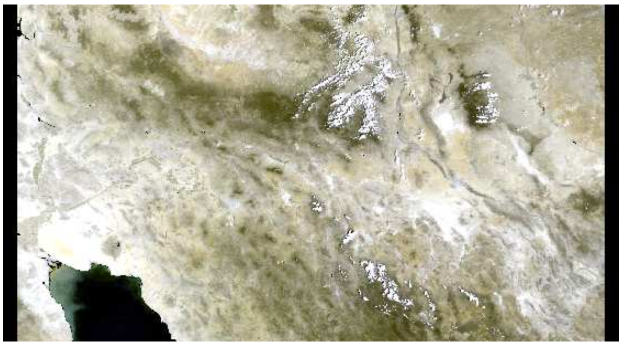 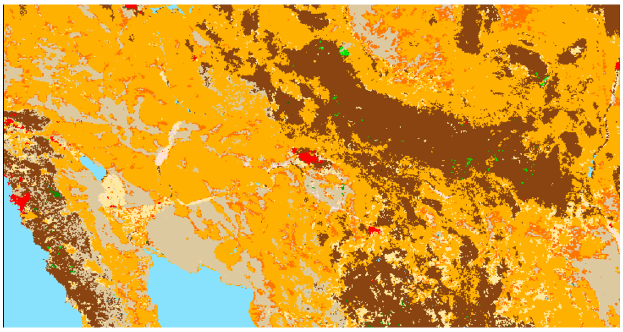
Mongu	-15.257 23.151	6	 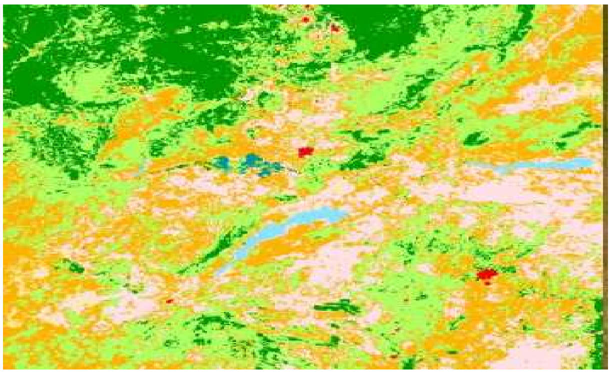

Site name	Latitude (°)/ Longitude (°)	Number of selected MERIS images	View of the site
Skukusa	-24.99 31.587	4	 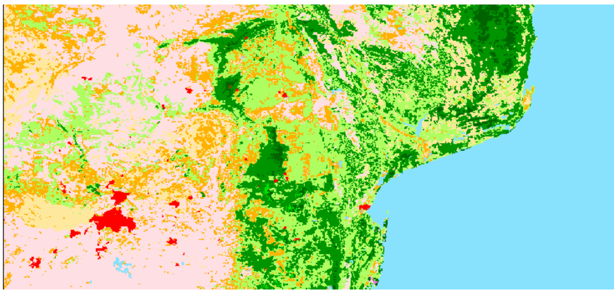

Figure 2: Legend of the ecoclimap 2000 classification

2. Data used for the validation

2.1. Aerosol optical thickness data used for the validation

2.1.1. MERIS AOT over ddv

The Aerosol optical thickness over land is a Level 2 product. In this study, It is called in this study “official aerosol product”. The AOT is computed using the Santer et al. 2000 algorithm, described in [RD4]. The ddv pixels are identified using a threshold applied to a spectral index, the Atmospheric Resistant Vegetation Index (ARVI), threshold above which pixels are considered as ddv with known reflectance. Once the ddv surfaces have been identified, the aerosol properties are retrieved. An illustration of both aerosol optical thickness and angstrom coefficient is shown on the next figure.

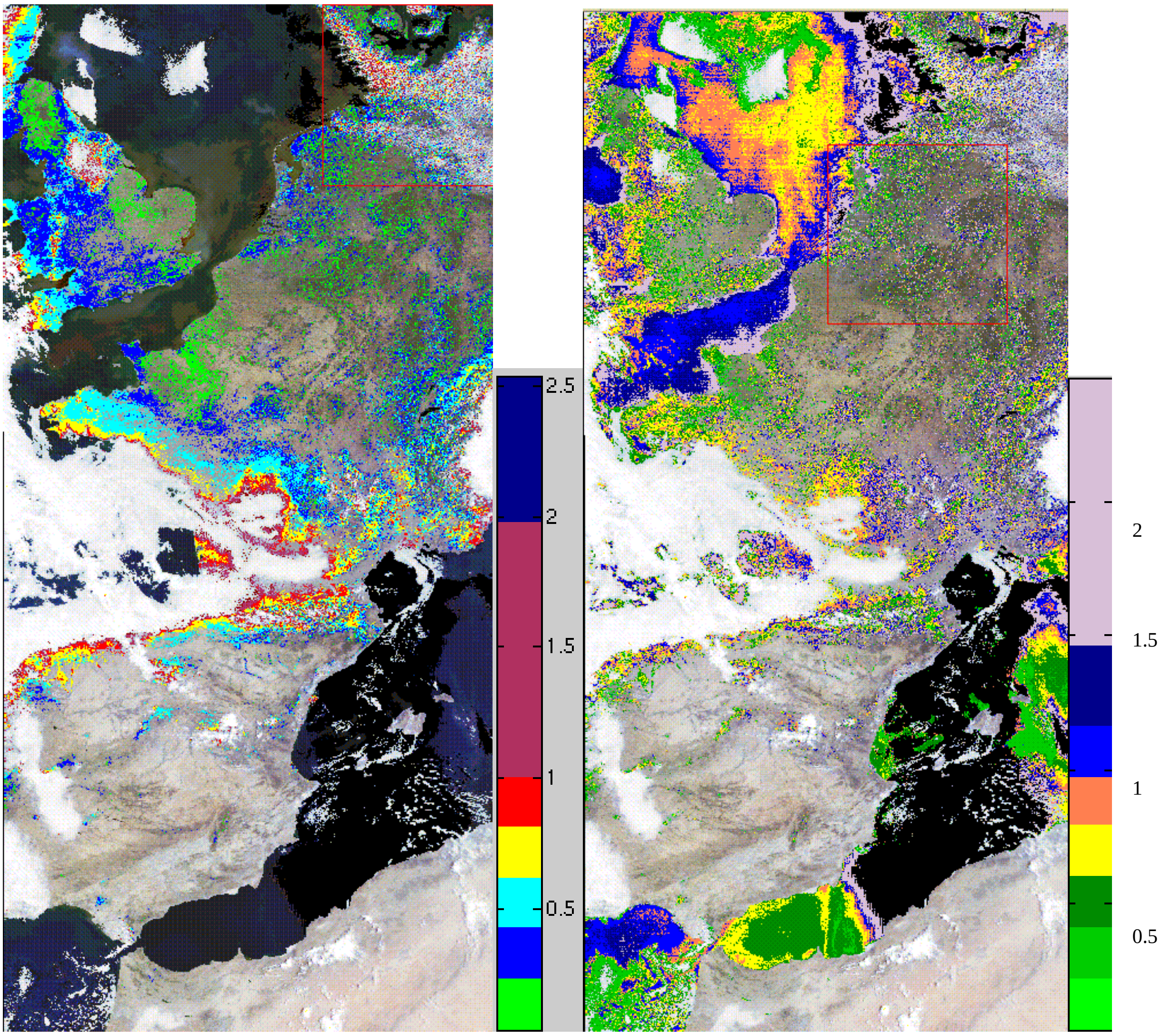

Figure 3: AOT at 443 nm (left plot) and angstrom coefficient (right plot). France 14/07/2003.

2.1.2. MODIS data

2.1.2.1. MODIS product type

The **MOD04 and MYD04 daily level 2 products** correspond to MODIS Aerosol Products processed from data collected by the instruments respectively on the TERRA (10:30 UTC local overpass time) and the AQUA (13:30 UTC local overpass time) platforms. The characteristics of these two products are similar. These products provide AOT estimations at a daily frequency and at a spatial resolution of a 10x10 1-km (at nadir). The related ATBD corresponding to these products is [RD2].

2.1.2.2. MOD04 coverage

Each MOD04 product (or granule) covers a five-minute time interval that implies a typical size of each product of 135 columns and 203 lines (except for every tenth granule that has 204 lines). An example of the AOT product is given in Figure 4.

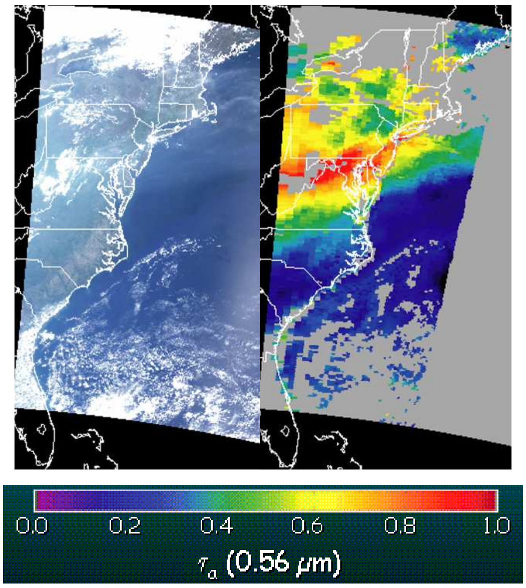

Figure 4: Example of MOD04 Granule Coverage; RGB image on the left; AOT at 560 nm on the right

2.1.2.3. MOD04 product format

The format of the MOD04 products is HDF. A code to read and extract the MOD04 parameters has been developed from HDF library subroutines and functions available on the official MODIS web site (http://modis.gsfc.nasa.gov/).

2.1.2.4. MOD04 parameters

The MOD04 products contain 53 parameters stored as a SDS within the HDF file. Among all these parameters, the following ones summarised in Table 2, have been extracted in view of comparison with BAER-MERIS outputs:

Table 2: Extracted MOD04 and MYD04 parameters

Parameter name	Description	Valid Range
Longitude	Geodetic Longitude	-180 to +180 degrees east
Latitude	Geodetic Latitude	- 90 to +90 degrees north
Optical_Depth_Land_And Ocean	AOT at 0.55 µm for both Ocean (best) and Land (corrected)	0 to 3
Aerosol_Type_Land	Aerosol Type	0 to 3 with 0 = mixed, 1 = dust, 2 = sulfate, 3 = smoke
Continental_Optical_Depth_Land	Continental Optical Thickness at 0.47 and 0.66 µm	0 to 3
Corrected_Optical_Depth_Land	Corrected Optical Thickness at 0.47, 0.55 and 0.66 µm	0 to 3
Angstrom_Exponent_Land	Angstrom Exponent at 0.47 and 0.67 µm	-0.5 to 3
Cloud_Fraction_Land	Cloud Fraction (%)	0 to 100

2.1.3. Selected MOD04 products

2.1.3.1. Ordering of the MODIS products

All the required MOD04 and MYD04 data products have been ordered via the MODIS data ordering system available at http://disc.gsfc.nasa.gov/daac-bin/MODIS/Data_order.pl?PRINT=1. The MOD04 products are available at no charge.

2.1.3.2. Selected MOD04 products for the validation activities

All the MOD04 and MYD04 granules available for each site and for the day of acquisition of the selected MERIS images have been ordered. Table 3 presents the number of MOD04 and MYD04 products selected depending on the site of interest.

Table 3 : Number of MODIS granules selected in view of the validation activities

Site name	Number of selected MERIS images	Number of MOD04 granules	Number of MYD04 granules
France	1	2	0
Alta_Foresta	4	7	4
Bondville	9	13	15

Bordeaux	5	10	9
GSFC	4	9	8
Howland	1	1	1
Ispra	9	18	14
Lampedusa	3	4	5
Lille	4	5	8
Maricopa	29	38	39
Mongu	6	11	11
Skukusa	4	6	5

2.1.4. AERONET measurements

2.1.4.1. Definition of the AERONET products

The AERONET program allows to assess aerosol optical properties and validate satellite retrievals via a ground-based remote sensing aerosol network of 355 sites (Figure 5) distributed all over the world.

The network hardware consists of automatic sun-sky scanning spectral radiometers (CIMEL Electronique 318A). Data provides globally distributed near real time observations of aerosol spectral optical thickness (AOT), aerosol size distributions, and precipitable water in diverse aerosol regimes.

Several AERONET products can be downloaded (raw data, AOT, Almucantar retrievals, daily or monthly averages…) at no charge on the dedicated web site http://aeronet.gsfc.nasa.gov/.

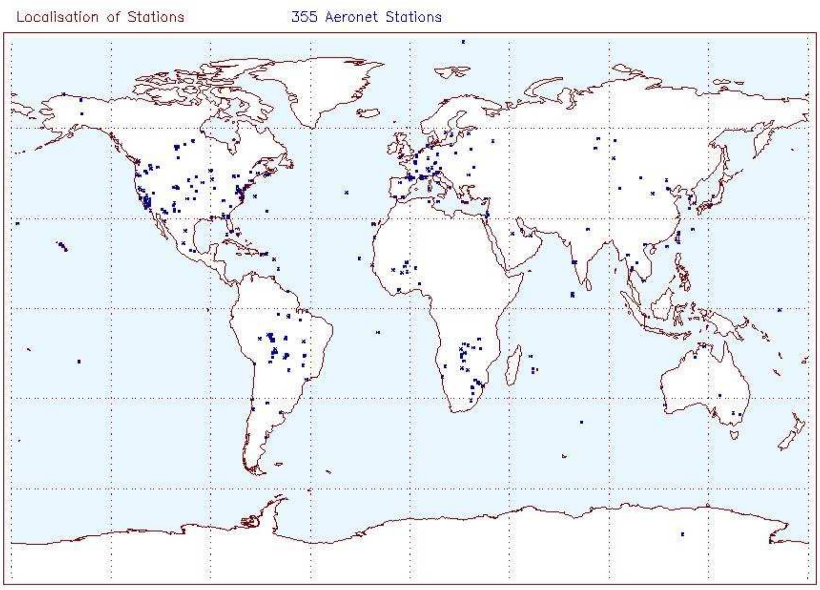

Figure 5: Location of the AERONET stations

2.1.4.2. AERONET product type

Three levels of data are available: level 1.0 (raw data), level 1.5 (cloud screened data) and level 2.0 (cloud screened data and quality-assured).

Here, only AERONET level 2.0 data have been used to lead the validation activities excepted for the Alta_Foresta site for which only level 1.5 data was available.

2.1.4.3. AERONET data file format and content

The AERONET measurements are organised in one file per station for the required temporal period of observation. The provided data file is in ASCII format.

The file structure consists in four header lines that contain for example the product level, the station location, the column field names, …. The following data lines correspond to one line per measurement.

An example of level 2.0 file is displayed hereafter:

Level 2.0. Quality Assured Data.<p>The following data are pre and post field calibrated automatically cloud cleared and manually inspected.

Location=Ispra long=8.627 lat=45.803 elev=235 Nmeas=4 PI=Giuseppe_Zibordi Email=giuseppe.zibordi@jrc.it

AOT Level 2.0 All Points UNITS can be found at http://aeronet.gsfc.nasa.gov/data_menu.html

Date(dd-mm-yy) Time(hh:mm:ss) Julian_Day AOT_1020 AOT_870 AOT_670 AOT_500 AOT_440 AOT_380 AOT_340 AOT_532 AOT_535 AOT_1640 Water(cm) %TripletVar_1020 %TripletVar_870 %TripletVar_670 %TripletVar_500 %TripletVar_440 %TripletVar_380 %TripletVar_340 %TripletVar_532 %TripletVar_535 %TripletVar_1640 %WaterError 440-870Angstrom 380-500Angstrom 440-675Angstrom 500-870Angstrom 340-440Angstrom 440-675Angstrom(Polar) Last_Processing_Date Solar_Zenith_Angle

01/01/2003 11:14:33 1.468438 0.038325 0.044806 0.073269 0.119589 0.141780 0.166634 0.189546 N/A N/A N/A 0.845367 0.456265 0.504388 0.642881 0.617031 0.599185 0.921647 0.620208 N/A N/A N/A N/A 1.697046 1.193891 1.561534 1.774134 1.121407 N/A 07/03/2003 68.852826

01/01/2003 11:29:34 1.478866 0.038223 0.043845 0.071269 0.115022 0.137066 0.160989 0.182626 N/A N/A N/A 0.845144 0.568005 0.506470 0.529941 0.274644 0.256582 0.451597 0.441289 N/A N/A N/A N/A 1.675067 1.209493 1.543050 1.742699 1.108846 N/A 07/03/2003 68.775057

01/01/2003 11:44:32 1.489259 0.052641 0.054112 0.075488 0.112628 0.130354 0.152941 0.173960 N/A N/A N/A 0.873528 1.410212 1.112757 0.706326 0.754266 0.860590 1.093634 1.156840 N/A N/A N/A N/A 1.302694 1.103076 1.289067 1.328175 1.114234 N/A 07/03/2003 68.865395

…

2.1.4.4. AERONET parameters

The line 4 of the header of level 2.0 file lists all the AERONET measured parameters:

- Date of acquisition: Date, Time and Julian day
- Aerosol Optical Thickness at 1640, 1020, 870, 670, 535, 532, 500, 440, 380, 340 nm
- Angstrom coefficients
- Auxiliary data: Precipitation, Solar zenith angle

An example of the products is shown in the next figure.

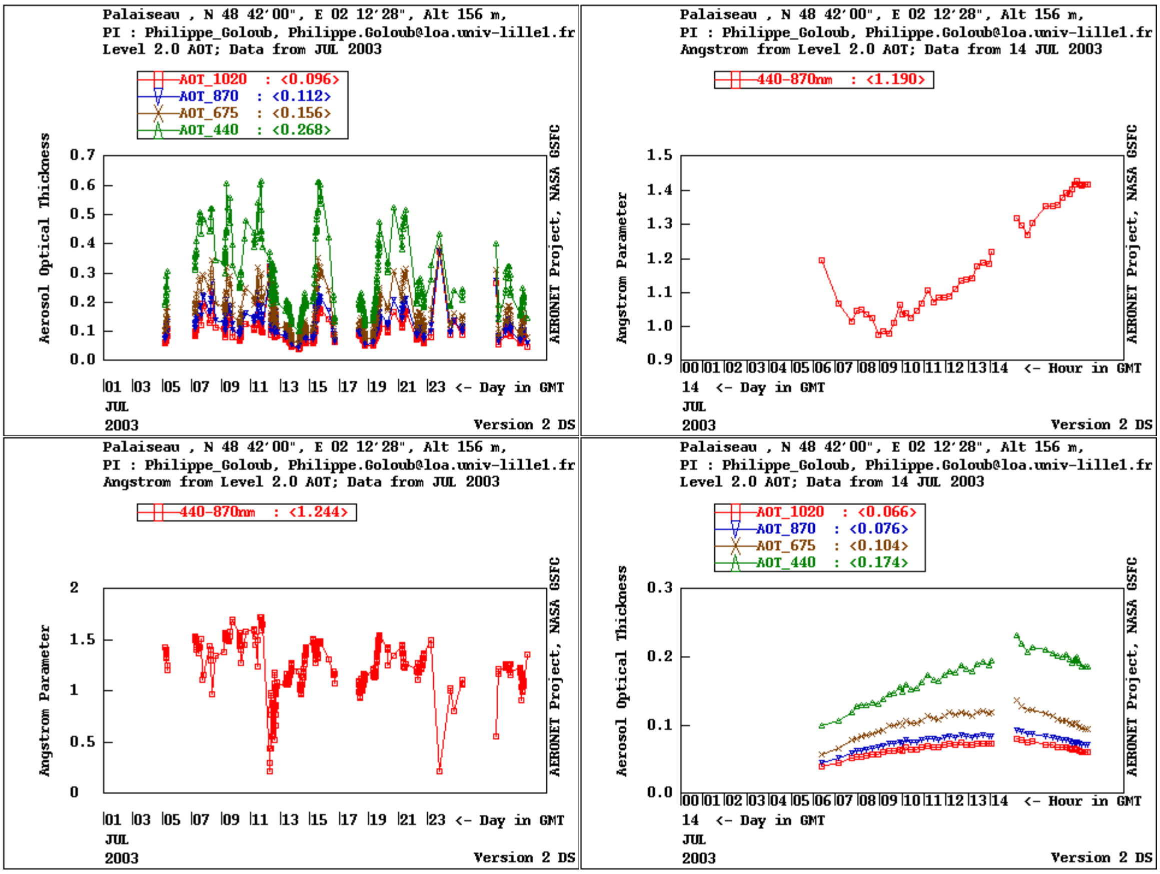

Figure 6: AOTs and angstrom coefficient temporal variation during one month (left plots) and over one day (right plot).

2.1.4.5. Ordering of the AERONET measurements

The AERONET measurements can be downloaded using an easy web interface available at http://aeronet.gsfc.nasa.gov/ and allowing the users to select data depending on several options: station, date, level of processing, type of data, average data, etc.

2.1.4.6. Selected AERONET data

The downloaded AERONET data have been selected for each validation site and for the nearest date/hour of MERIS acquisition.

AERONET measurements are averaged if several acquisitions are available in an interval of –10 .. + 10 mn around the MERIS acquisition.

No AERONET data is selected if no acquisition has been done in this same interval.

The number of available AERONET measurements corresponding to the MERIS images is presented in Table 4. We can note that no AERONET data has been done in Bordeaux and Howland in 2003.

Table 4: Number of available AERONET measurements selected in view of validation activities

Site name	Number of selected MERIS images	Number of AERONET measurements
France	1	5
Alta_Foresta	4	3
Bondville	9	6
Bordeaux	5	0
GSFC	4	4
Howland	1	0
Ispra	9	9
Lampedusa	3	2
Lille	4	3
Maricopa	29	29
Mongu	6	6
Skukusa	4	4

3. Cloud screening assessment

3.1. Introduction

The BAER algorithm proposed in this study applies to clear-sky observations, which are those that went through cloud screening procedures. In the framework of aerosol content estimation, the cloud screening is one of the most critical steps required to get reliable aerosol optical thickness estimation, and in a second step surface level products from satellite observations in the solar reflective spectral domain.

The preprocessing of the MERIS Level 2 data provides a cloud mask, integrated in the Level 2 flag. Since the quality of the Level 2 flag is poorly achieved, a new cloud mask based on single and constant threshold applied to the L2 reflectance in the visible channels, has been developed in the framework of the study, and integrated into the processor. The quality of the available cloud masks are assessed by comparing the cloud masks produced by three available methods:

- The official MERIS Level 2 cloud mask,
- The IBAER method (which integrates the L2 cloud mask)
- The official MERIS Level 1 bright cloud mask when both L1b and L2 are available.

The performance analysis of the mask is assessed directly by visual comparison and reported in the next subsections.

3.2. MERIS Cloud mask intercomparison

3.2.1. Level 2 cloud mask and mask computed by Integrated BAER processor

The IBAER mask is compared to the L2 cloud mask in the following images. A true colour image is displayed to locate the clouds and the same image is plotted with the IBAER cloud mask super-imposed. Two colours are used. The blue colour corresponds to the Level 2 cloud mask. The red colour corresponds to the IBAER cloud mask improvement against the cloud mask level 2. The Image acquired by MERIS on July, 14, 2003 is used for the comparison. The assessment has been made for all the MERIS dataset, and is reported by the same representation in the annexe of the document.

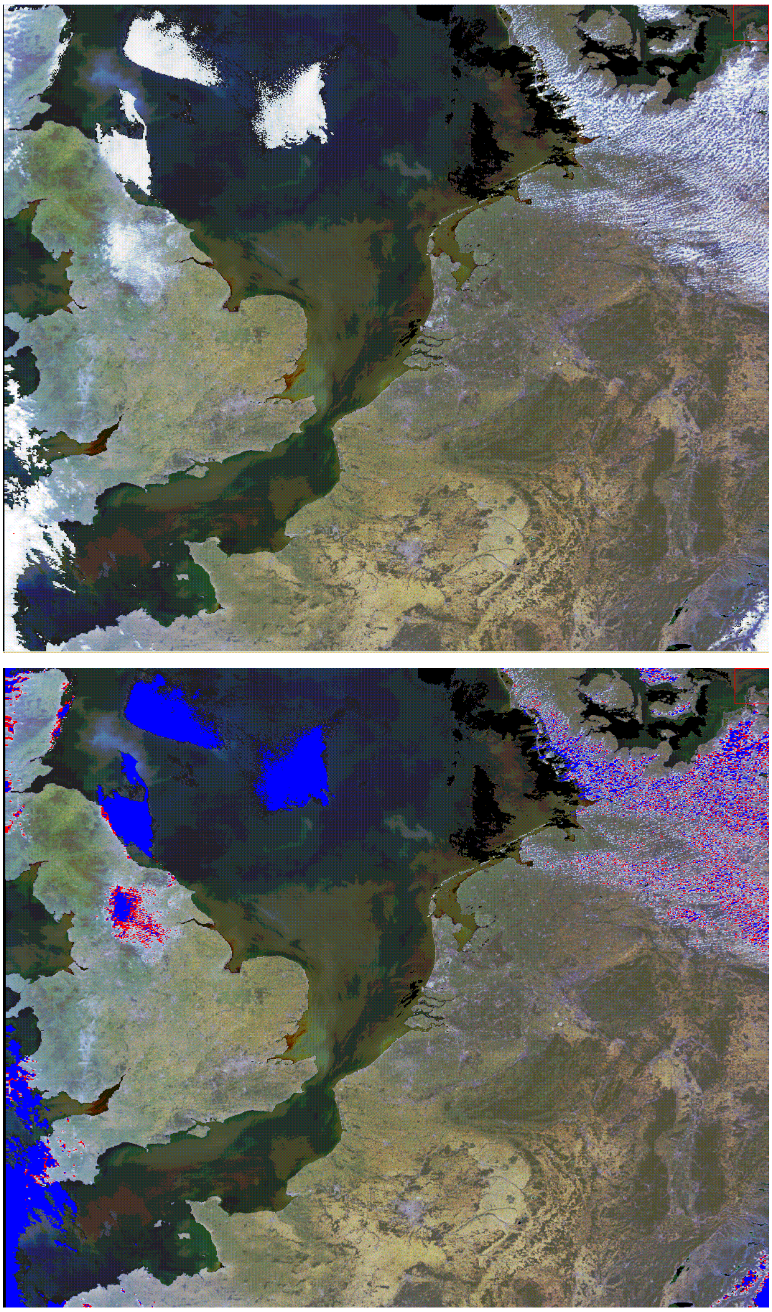

Figure 7: Coloured composition of MERIS LEVEL 2 data. RGB colour (Top image) and corresponding cloud mask. The blue colour flags the Level 2 cloud mask. The red colour flags the cloud detected by IBAER

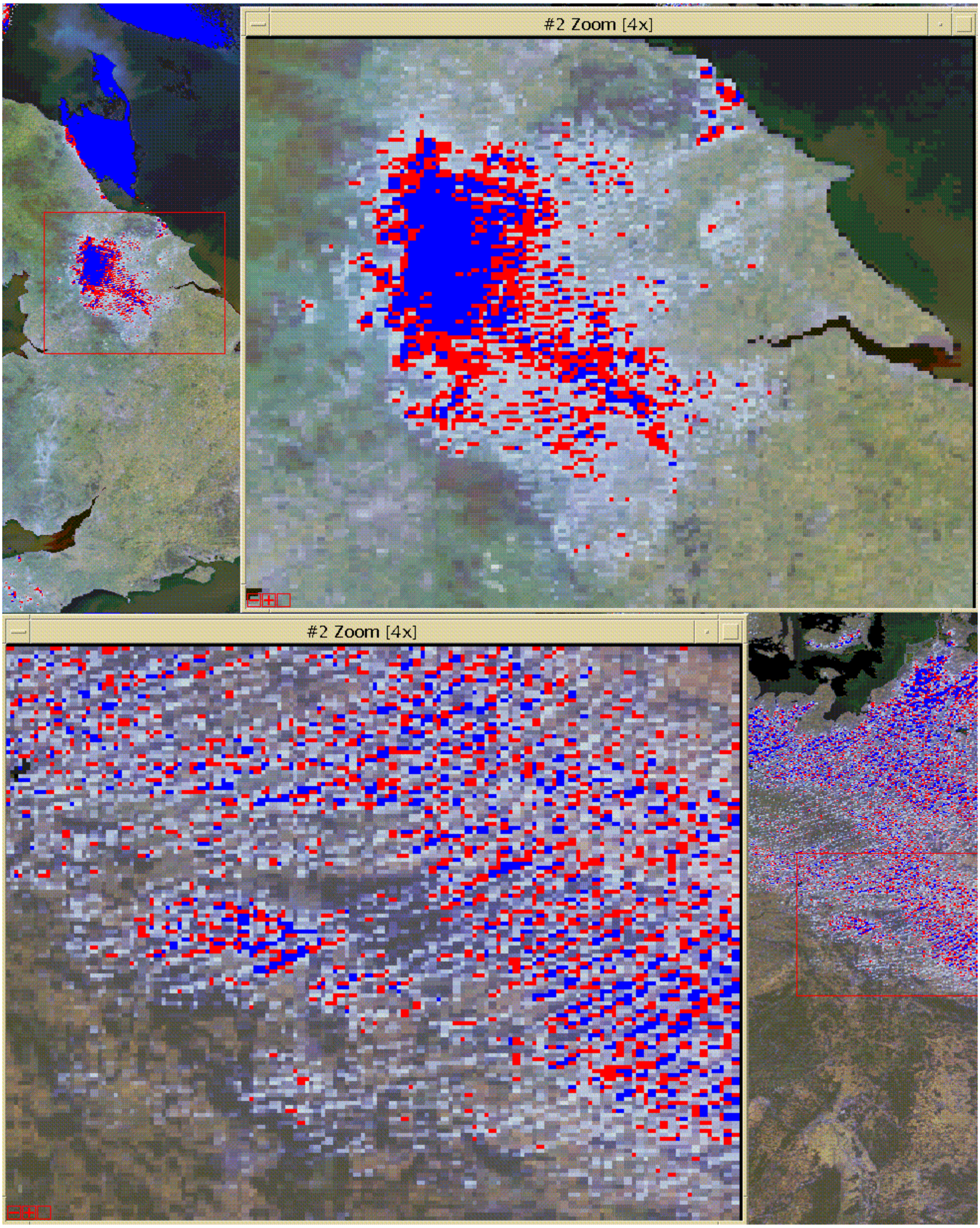

Figure 8: Zoom of the cloud mask. The blue colour flags the Level 2 cloud mask. The red colour flags the cloud detected by IBAER

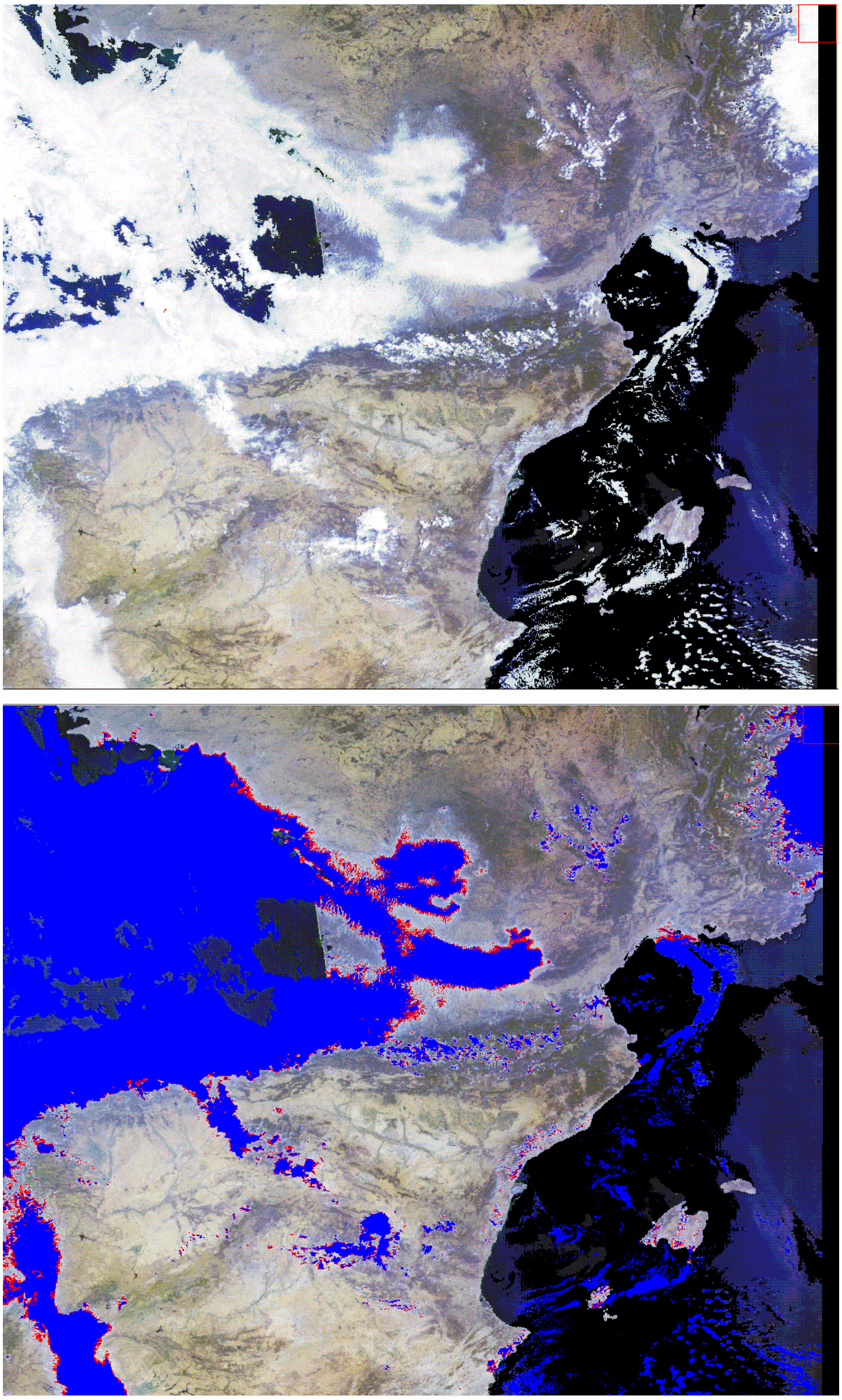

Figure 9: Coloured composition of MERIS LEVEL 2 data. RGB colour (Top image) and corresponding cloud mask. The blue colour flags the Level 2 cloud mask. The red colour flags the cloud detected by IBAER

3.2.2. Level 1b bright cloud mask and IBAER cloud mask

The L1b bright cloud flag and the Level 2 cloud flag at Reduced resolution are compared over the same area for July, 14, 2003 (Figure 10). The coloured composition at L1b is shown in the following image with the bright flag coloured in red. The coloured composition at L2 is shown in the following image with the cloud coloured in blue (Cloud flag at L2) and red (IBAER cloud flag). Three areas are zoomed from these images to allow the comparisons (Figure 11).

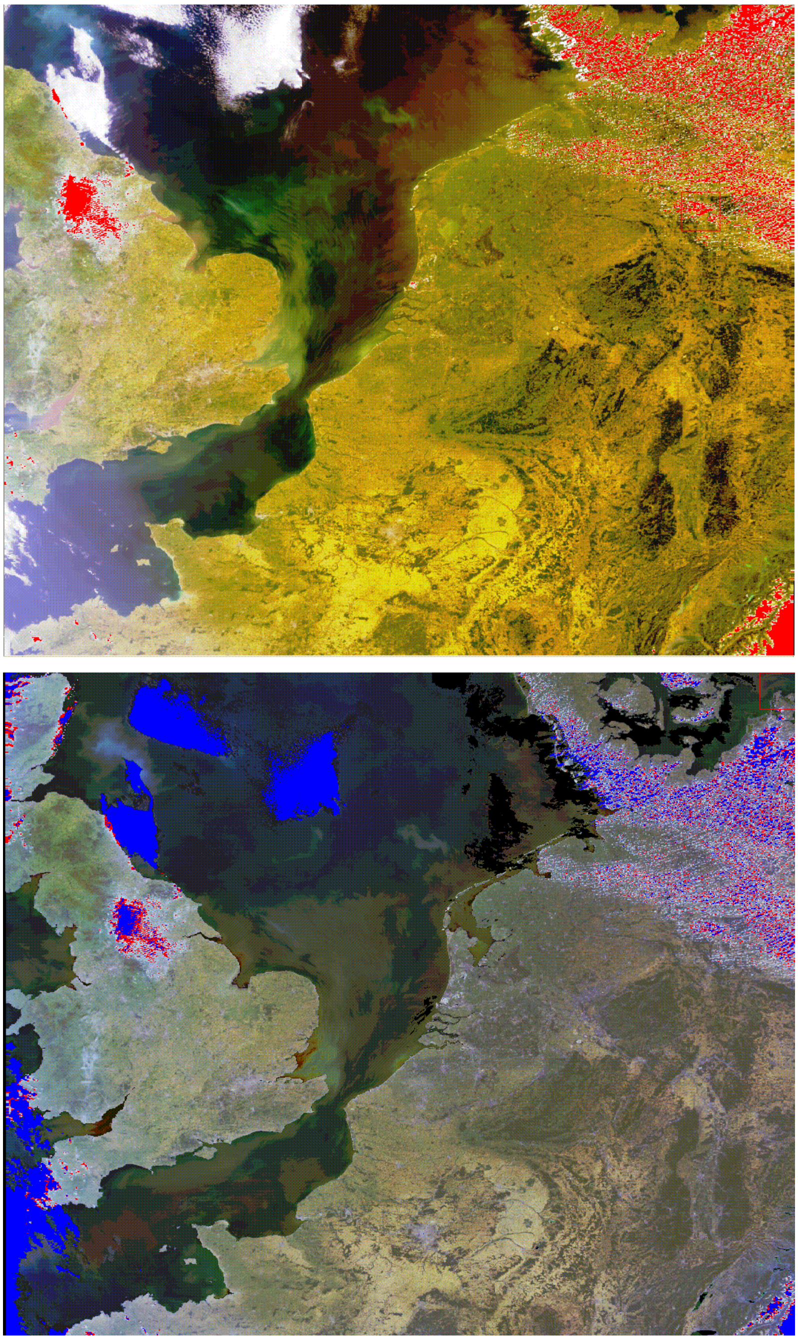

Figure 10: Cloud masks at Level 1 (top) and level 2 (bottom) comparison on MERIS image acquired in July, 2003.

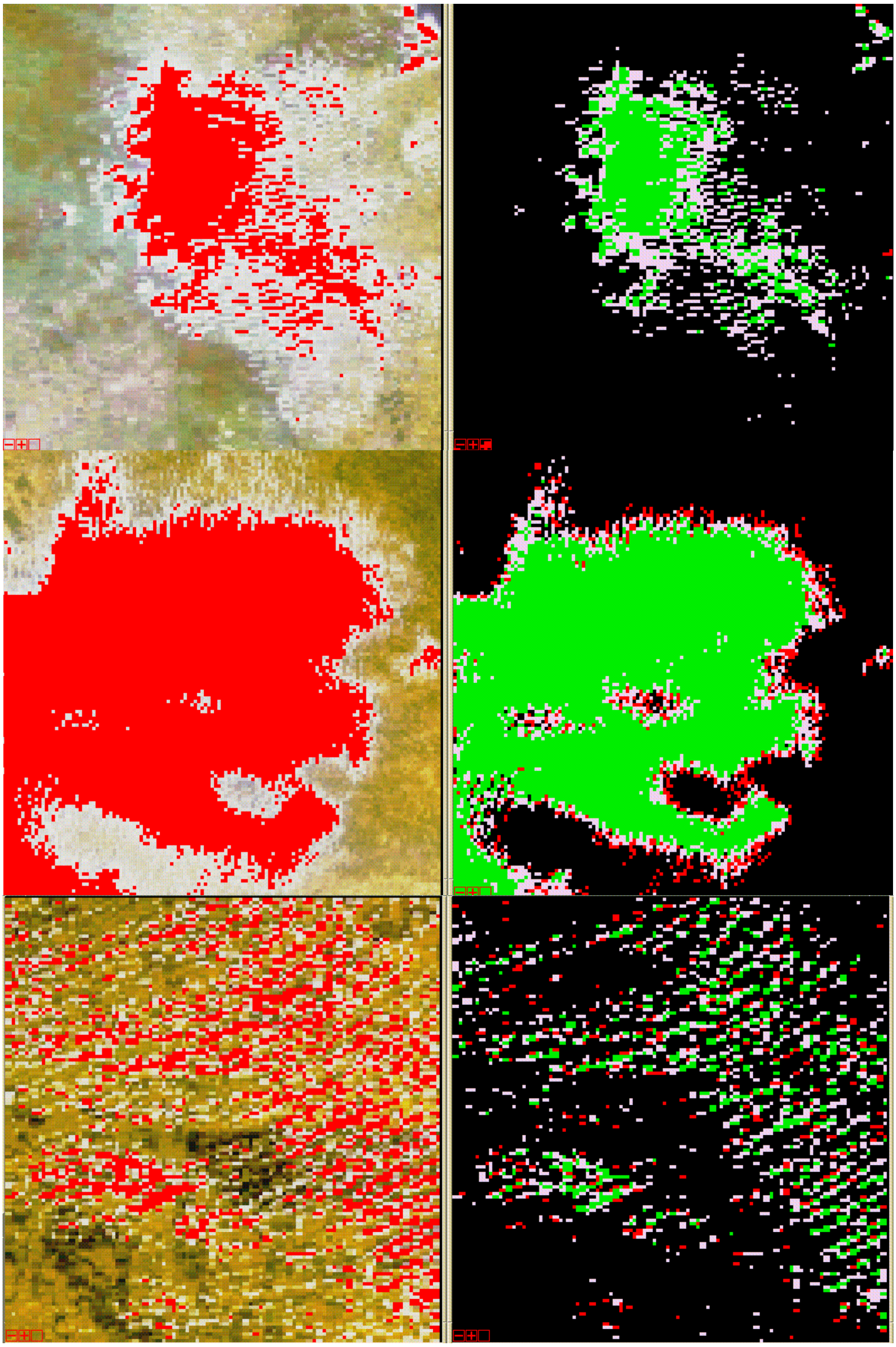

Figure 11: Cloud detected at Level 1 (on the left) and 2 (on the right). The red colour indicates the clouds detected on the L1b data. The green colour indicates the clouds detected on the L2 data. The clear pink colour indicates the clouds detected by IBAER.

3.2.3. Impact of the spatial resolution on cloud detection

In order to assess the quality of the cloud detection with the spatial resolution, the IBAER cloud detection has been applied to an image acquired in the full and reduced spatial resolutions.

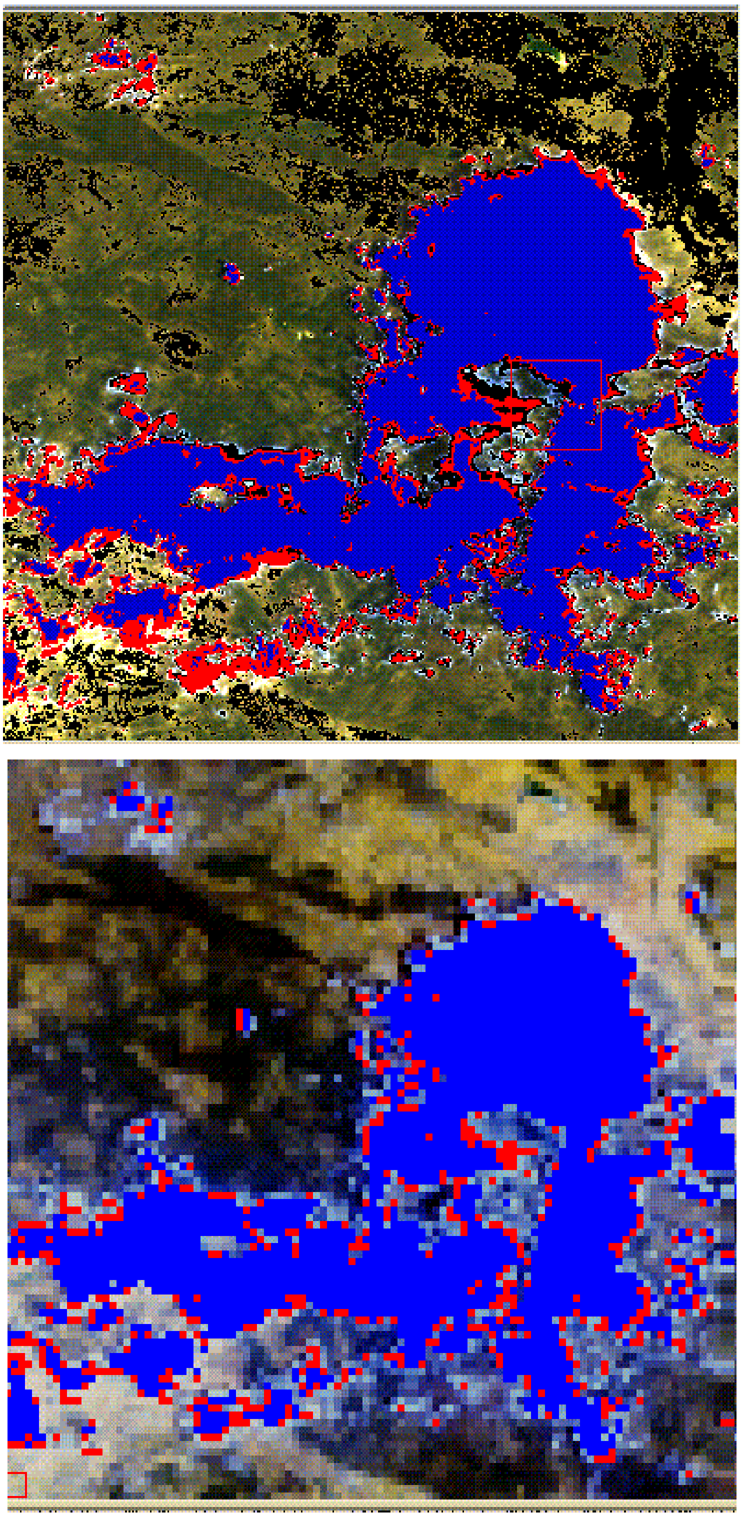

Figure 12: Level 2 Cloud mask 2 in full resolution (top) and reduced resolution (bottom) on MERIS image acquired in July, 2003.

3.3. Conclusion

3.3.1. Cloud mask comparison

- Assessment of the cloud Level 2 mask: This mask detects the dense and bright flags, but does not detect the small clouds, or the semi transparent clouds. There are still a lot of pixels contaminated by cloud. It can be seen on presented figures (Figure 7 to Figure 9), and annexe 2) that the pixels coloured in blue underestimate the area covered by the clouds. Moreover, cirrus clouds are not detected.
- Assessment of the cloud Level 2 mask plus IBAER: The addition of the IBAER cloud mask improves the cloud detection, but is not probably severe enough. This is well illustrated on the previous figure (Figure 7 to Figure 9), where the IBAER contributes to extend the cloud detection.
- Assessment of the IBAER mask against the Level 1b bright flag: Figure 10 and Figure 11 allow the comparison between IBAER cloud and the level 1 b cloud mask. We can see that the level 1b cloud mask is better than the IBAER cloud mask, even the cloud boarders are not detected. The comparison of the zoom shows that the green an pink colours which correspond to the IBAER cloud mask are inside the area covered by the level 1 b cloud mask bright.
- Assessment of the contribution of the full spatial resolution against the reduced resolution in the cloud detection. Figure 12 presents the same area acquired in both resolutions, 300 m and 1.1 km. The improvement of IBAER method against Level 2 cloud mask is important, since the cloud boarders are better detected. At higher resolution, thin clouds and partially cloudy pixels are more sensitive to the underlying spectral properties of the surface. These pixels are detected as clouds by IBAER, whereas they are not seen by the Level 2 cloud mask.

3.3.2. Performances of the algorithm

The IBAER cloud mask is an additional step that is required due to the limitations in the official cloud detection algorithm. It improves the identification of the cloud mask provided in the Level 2 MERIS data, and make more confident the processing of remaining pixels in case of cloud free conditions. However, this method has not been fully validated over bright surfaces, such as desert or snow or ice.

3.3.3. Possible improvements

The IBAER cloud detection method is based on a simple threshold method, using three channels in the visible part of the solar spectrum. However, advanced methods, based also on threshold methods and developed for MERIS level 1b data have demonstrated their capacities to improve the cloud detection, allowing the detection of dense and bright clouds, but also cirrus and snow (Berthelot and Quesney, 2005, [RD5]). The methods have been assessed over a large dataset. Their advantages result in the high speed of execution, and the facility to set up the method, that is important for an integration into the BEAM toolbox.

Based on these results, the same approach could be done to improve the cloud detection on level 2 MERIS data, and integrate it into the BEAM toolbox.

Some additional information could be provided with the cloud channel.

- The cloud shadows could be removed from the processing.
- The cloud mask could be extended to at least 2 pixels in order to remove the environment effects due to the clouds.

4. Validation of the Atmosphere products

4.1. Introduction

The aerosol retrieval over land using MERIS data is a difficult task, which need to be done by checking its consistency and compare it to available aerosol optical thickness, retrieved using satellite data or ground measurements.

This section presents the methodology used to lead the validation activities and the results obtained in the frame of three inter-comparisons:

- between BAER outputs and the standard MERIS products, particularly over DDV pixels
- between BAER outputs and the MOD04 parameters
- between BAER outputs and the AERONET measurements

The retrieval of the AOT has been performed on the full dataset of MERIS images (see annexe 1). The results are provided in the next sub sections, summarised on tables site by site and for all dates.

4.2. Assessment of the BAER output

This first assessment is made in order to check the consistency of the BAER product, in terms of spatial coherence, range of both AOT and angstrom coefficient values. Figure 13 and Figure 14 present spectral AOT and Alpha exponent maps calculated by the IBAER processor over the Ispra site. Ispra site is covered by cultivated and managed area, and tree cover and natural vegetation.

The official outputs of the BAER processor defined in the IODD [RD 1] are the AOTs at 412, 440 and 550 nm and the Alpha exponent. The other spectral AOT maps hereafter shown have been derived using the classical Angstrom power law and the Alpha exponent.

We can note that:

- The spatial variations of the AOT are coherent without abrupt variations from one pixel to its neighbour.
- Large Alpha values (> 2.0) are obtained for flagged pixels. The Alpha values obtained over the North if Italy are high whereas they seem to be low (~ 0.5) in the south.

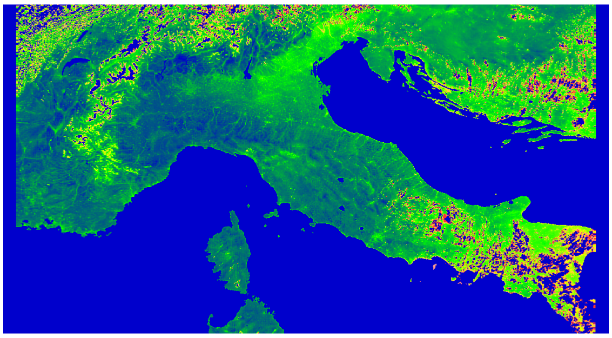

AOT@412

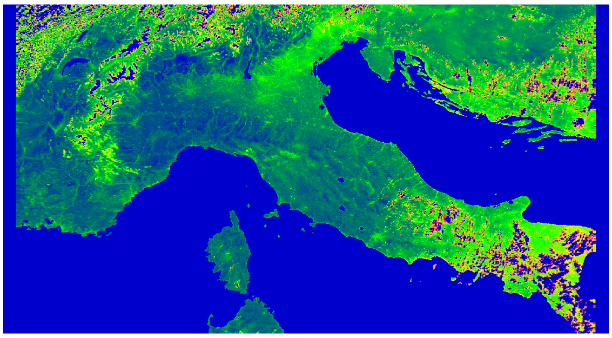

AOT@440

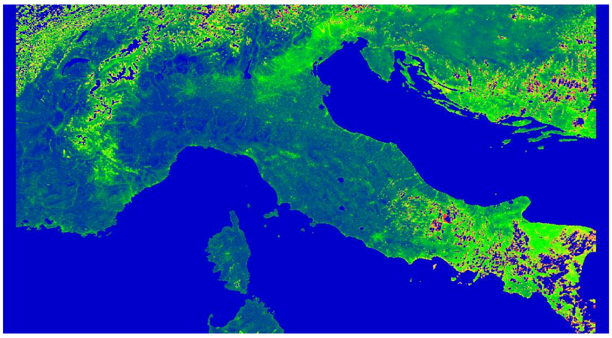

AOT@550

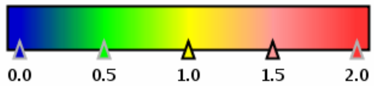

Figure 13: Spectral AOT maps processed with BAER. The MERIS source image corresponds to an acquisition done on 2003/06/20 at 09:46:22

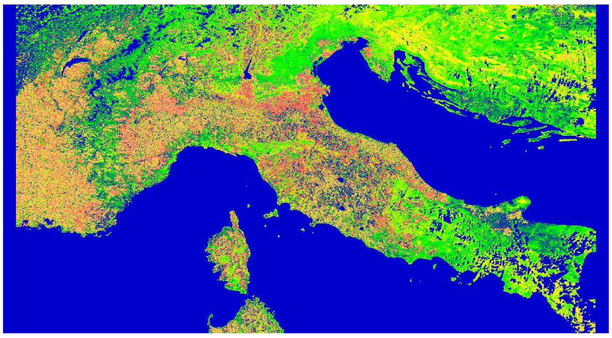

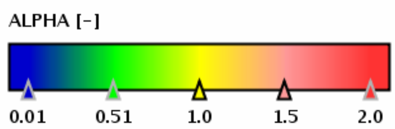

Figure 14: Alpha exponent processed with BAER The MERIS source image corresponds to an acquisition done on 2003/06/20 at 09:46:22.

4.3. Indirect validation

4.3.1. Comparison between BAER outputs and standard MERIS products

4.3.1.1. Introduction

The BAER algorithm has been applied on the MERIS L2 dataset presented previously. The outputs (required for the validation) are the AOT at 412, 565, 865 nm, the angstrom coefficient, and a flag indicating the quality of the retrieval.

The selection of the pixels is made using the DDV flags present in the L2 products. For each pixel identified as a dark target, the values between BAER and DDV are compared. Comparison is made for different channels over land for spectral AOT at 412, 560, 865, and the angstrom coefficient.

The totality of the results is given in another report (NOV-3341-NT-3292.doc, [RD6]). The statistics are provided within the figures, like the spatial area covered by the validation. An example is given hereafter for the Lille image.

Figure 15 displays the area where both the AOT have been computed using the BAER method and DDV. The pixels for which the retrieval has been achieved are coloured in red. The pixels for which the AOT over DDV has been estimated are plot in blue colour in the same figure.

The figure allows to see the large surface area cover by the BAER retrieval against the area covered by the retrieval over DDV.

The scatterplots between BAER variables and DDV variables are also plot in this document. An example is seen in Figure 16.

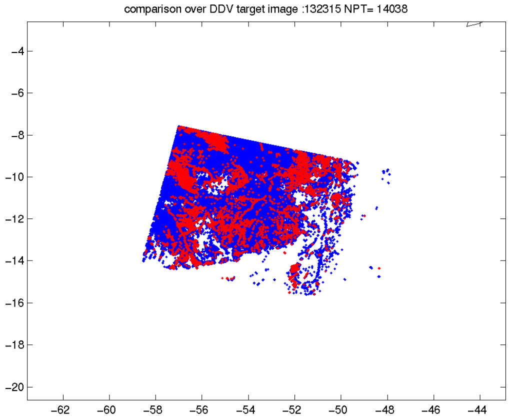

Figure 15: Area covered by the validation. Pixels in red are the pixels where the BAER retrieval is made. These pixels are overplotted by a blue colour which indicates the location of ddv pixels. The number of pixels allowed for the comparison is indicated in the title.

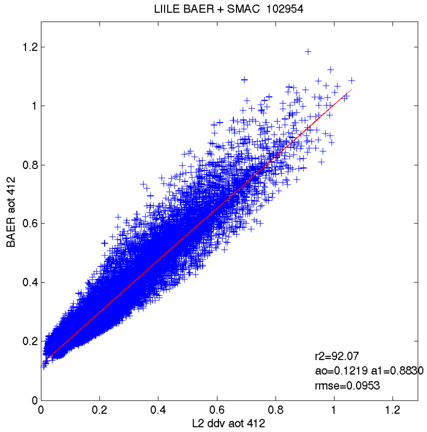

Figure 16: Example of the result comparison (here aot at 412nm). The rmse, determination coefficient and regression coefficient are indicated in the image.

4.3.1.2. Result synthesis

The statistical analysis has been made for the whole dataset (50 images) at the specified wavelengths. A table is drawn below indicating site by site, and image by image, the values of the linear regression (offset and slope), the mean, rmse, r^2, and standard deviation. The tables are provided with the annexe 4, and summarised hereafter.

4.3.1.2.1 Comparison over the France-Spain area

The AOT estimated in the blue channel (443 nm) for BAER and DDV target is displayed in Figure 17 to illustrate the coverage of the AOT retrieval with BAER approach against the DDV.

The AOT is estimated over largest areas than with the DDV method. The spatial continuity is good and consistent with the AOT estimated over DDV. The range of values is the same in both images, except on the cloud boarders but the problem will be solved by extending the cloud mask, or by applying another cloud mask. The AOT varies between 0 and 0.6. The AOT over cities is high around 0.4 and 0.5.

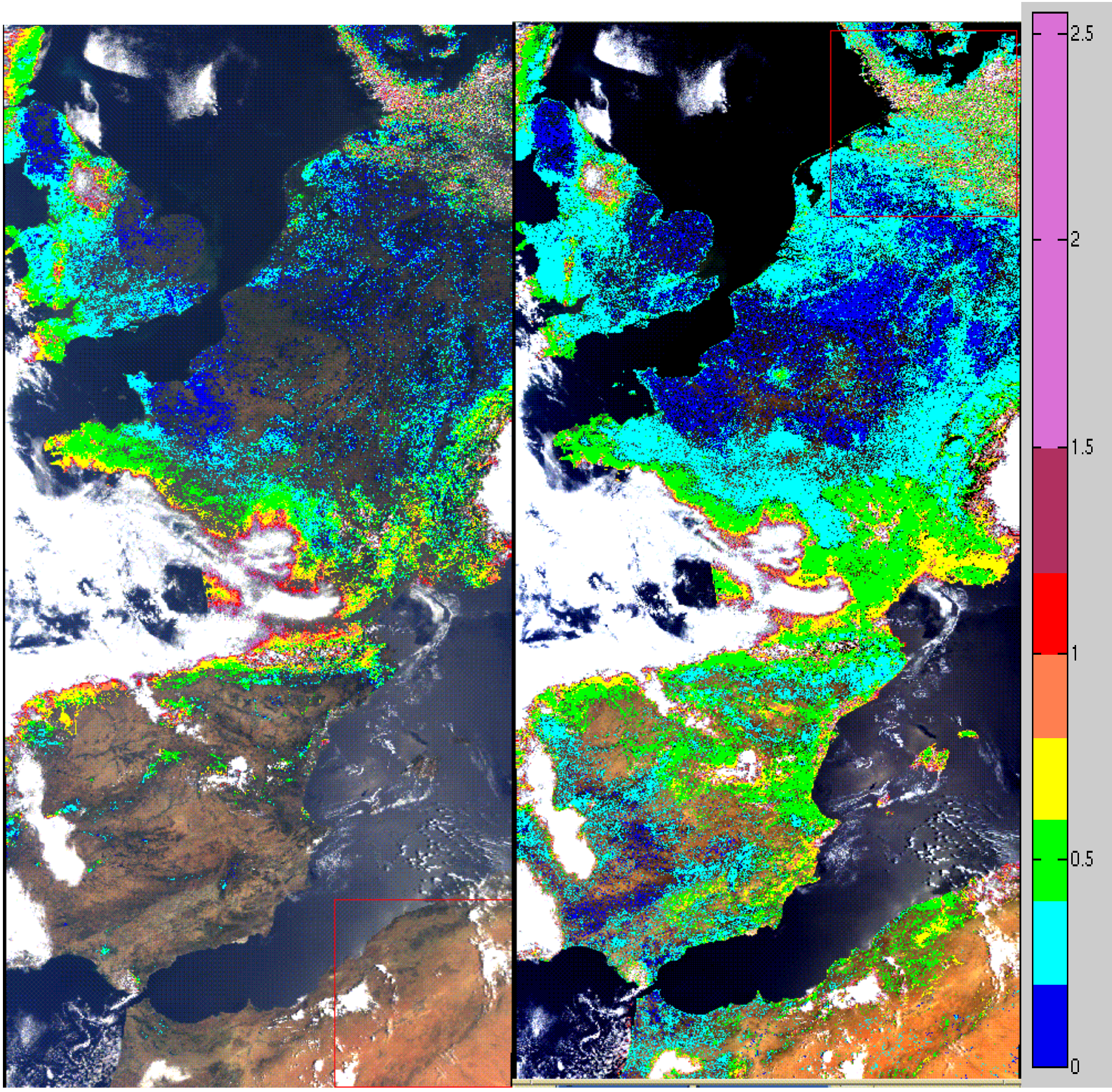

Figure 17: AOT in channel 2 over DDV (left image) and using BAER method (right image)

The angstrom coefficient is represented for both retrievals in the next figure. The results are different, heterogeneous in each image. The angstrom coefficient is however higher in the DDV scene than in the BAER scene.

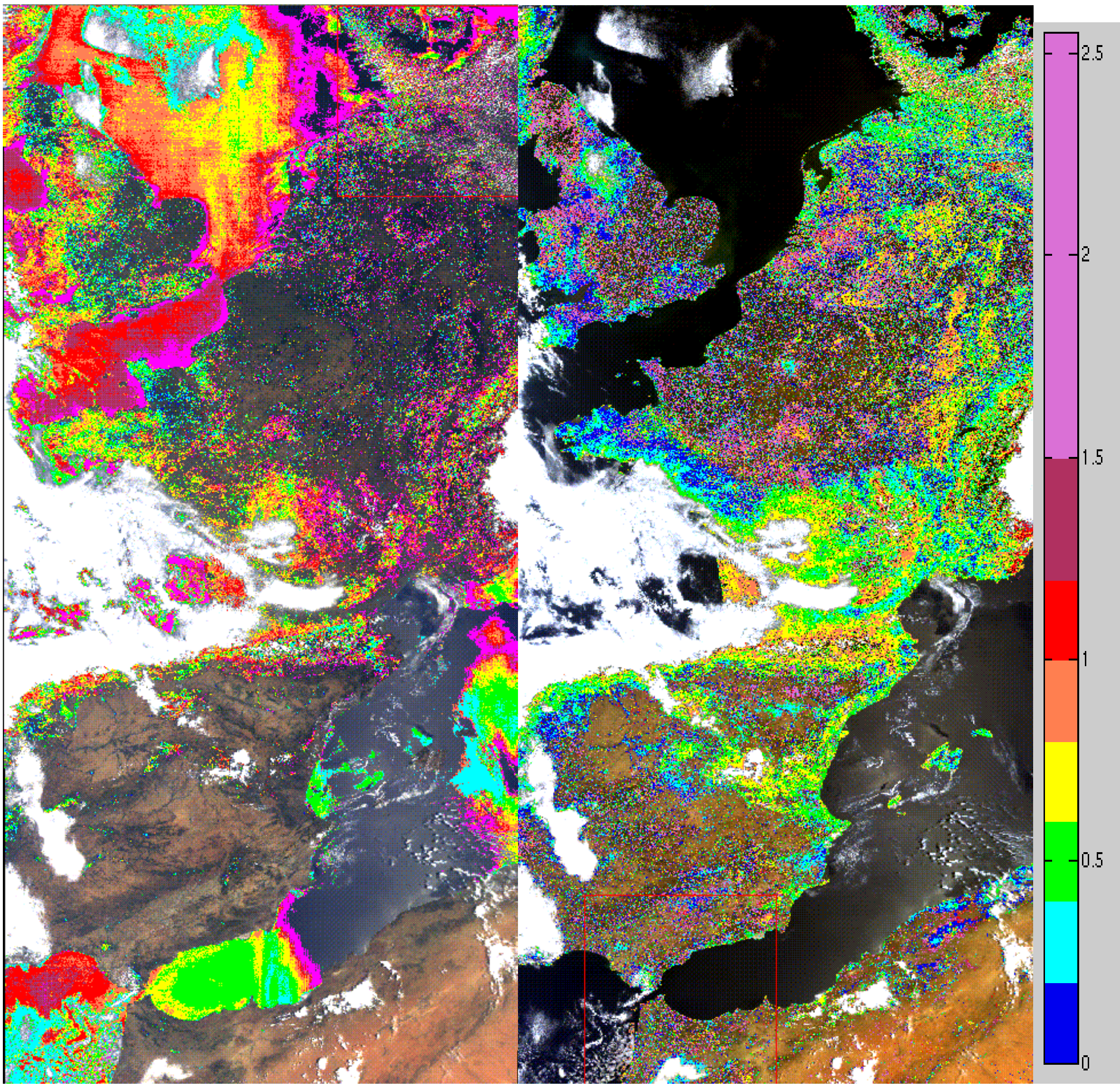

Figure 18: angstrom coefficient over DDV (left image) and using BAER method (right image)

4.3.1.2.2 Validation over the 11 sites

4.3.1.2.2.1 Angstrom coefficient estimation

The analysis of the spatial consistency between the two products shows that the angstrom coefficient is very variable, from one pixel to its neighbour, so that the spatial consistency is difficult to assess. The angstrom coefficient estimated by BAER are generally lower than those of the DDV, The mean is less than 1 for almost all the images, for both products except for the MONGU site where the angstrom coefficient varies between 1.3 and 1.5 for the DDV pixels. The standard deviation for both estimations is high, varying 0.2 and 0.5. In addition, no correlation is found between both angstrom coefficients.

4.3.1.2.2.2 Aerosol optical thickness estimation

The comparison of AOT estimation at 412 nm provided very good results. The coefficient of determination (r^2) is high, greater than 90 % for most of sites except for the sites where the number of DDV pixel is low (this is the case for instance of the GFSC site and the Maricopa site). The mean of the BAER AOT are slightly superior as those obtained for the ddv target. The range of the mean values varies between 0.1 and 0.5 which is a high value, with a standard deviation varying between 0.1 and 0.2. The rmse is good for Alta_foresta, Bondville, Lille (less than 0.07), is acceptable for most of site (around 0.1) and not good for Mongu and Maricopa sites where it is greater than 0.2. These sites are located over bright surfaces, and we know the AOT retrieval over these types of surfaces is difficult. The number of pixels used for the regression is less than 1000[2], whereas it is varies between 20000 and 100000 for the other sites.

The accuracy of the estimation at 560 nm is good for most of sites (except the two bright sites). The rmse is less than 0.05. The correlation is around 80%.

This result is important because the AOT at 550 nm is the variable that is used in input of the most of atmospheric correction method or radiative transfer model. This is the case of the SMAC method which has been integrated into the IBAER processor.

4.3.1.3. Conclusion

To sum up the results, the comparison of both products (BAER and DDV) provides good results over most studied images. Although BAER tends to overestimate the results obtained over DDV, the results at 412 nm are good. The determination coefficient is greater than 80 %, whatever the location of the site. At 560 nm, the correlation varies from 60% to 80%, except for images where the clouds are not well filtered, and over bright surfaces. The correlation decreases with the increase of the wavelength. The results at 865 nm are not less good than at 412 nm. But the knowledge of the AOT at this wavelength is less important because this variable is not used into the correction of atmospheric effects.

An offset appears for low aerosol optical thickness (whatever the spectral band is). This offset varies between 0.05 and 0.1, depending on the number of pixels processed in the regression.

No correlation is found when comparing the angstrom coefficient.

[2] The size of the image is 600x1121

4.3.2. Comparison between BAER outputs and MOD04 parameters

Mainly, this validation consists in comparing the estimated BAER AOTs with the AOTs derived from the MODIS data.

4.3.2.1. Validation methodology

The BAER outputs and the MOD04 parameters are not directly comparable, because of different instrument channels of MERIS and MODIS over land:

1. the official BAER outputs defined in RD1 are the AOT at 412 and 560 nm and the MOD04 AOT are defined at 470, 550 and 660 nm. Consequently, the BAER AOT needs to be interpolated in the MODIS bands in order to be comparable;
2. The BAER products and the MOD04 products have not the same spatial resolution and their product grid also differs. Consequently, the 1 x 1 km BAER outputs needs to be averaged in order to be comparable to the MOD04 spatial resolution and they need also to be mapped in the MOD04 product grid.

In answer to item 1, new temporary BAER AOTs are estimated at 470, 550 and 660 in order to lead the validation. These estimations are done following the classical Angstrom power law with 412 nm as reference band:

$$\tau_{470} = \tau_{412} * \left(\frac{470}{412}\right)^{\alpha_{412}}$$

The AOT at 550 and 660 nm are similarly obtained replacing 470 by 550 and then by 660. The α_{412} coefficient is the Angstrom exponent estimated by the BAER processor at 412 nm.

Concerning item 2, a simple processing is applied on the BAER AOT maps in order to be comparable to the MOD04 AOT maps. If possible, "average BAER pixels" are calculated for each MOD04 pixel. The average consists in estimating the AOT mean of a BAER 5x5 window centred on the BAER pixel the nearest of the MOD04 pixel. The BAER pixels taken into account in the computation of the AOT mean have to be:

- LAND pixels
- With an AOT in a valid range from 0 to 2.
- With an Alpha Angstrom coefficient at 412 nm in a valid range from 0.0 to 1.5

4.3.2.2. Results for MERIS image over France

The AOT for the MODIS aerosol optical thickness and BAER optical thickness is represented in the next figure. The spatial resolution is not the same, 10 km for MODIS, 1 km for BAER, but these images allow to compare the spatial consistency of the products.

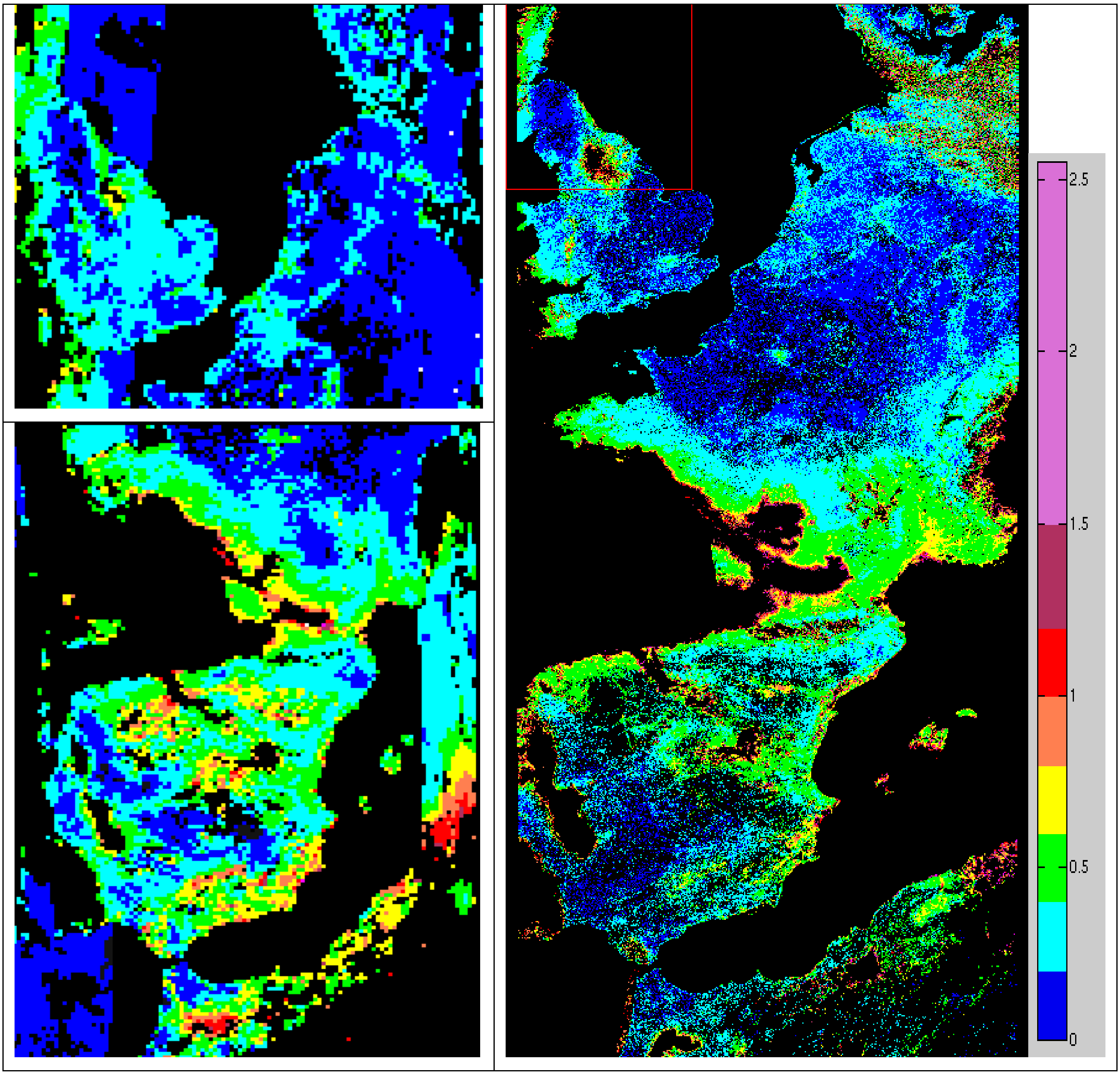

Figure 19: MODIS and BAER AOT at 550 nm

The spatial comparison of the AOT at 550 nm allow to see the good agreement between the two product. In MODIS data which cover sea and land, we can see that there is also large regions where the retrieval fails.

4.3.2.3. Comparisons between BAER AOT and MOD04

Figure 20 to Figure 29 show the relationships between the MERIS AOT and the MODIS AOT at 470, 550 and 660 nm over the Bordeaux site.

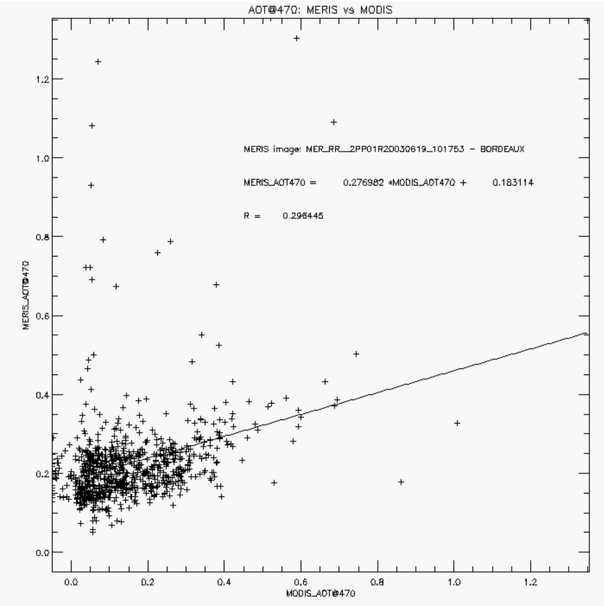

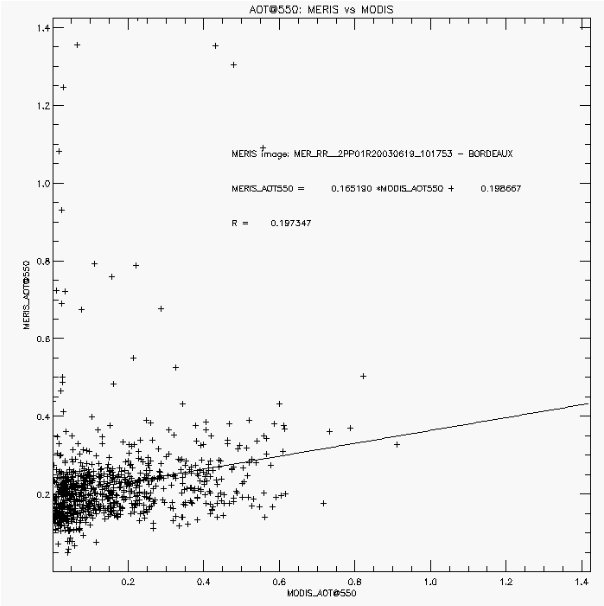

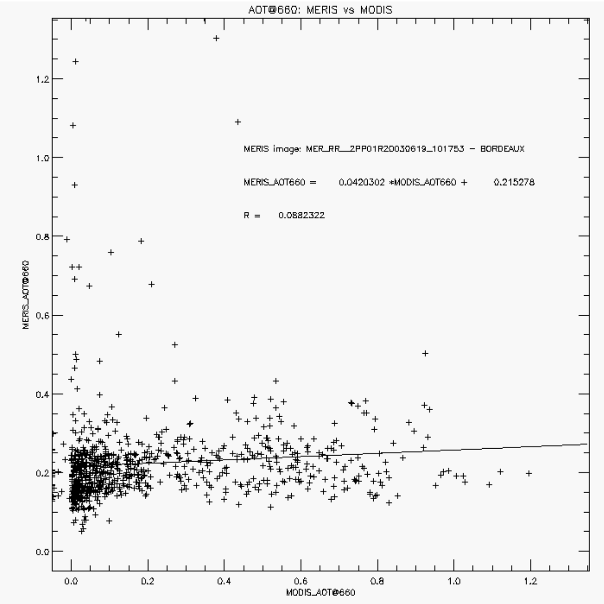

Figure 20: AOT comparisons at 470, 550 and 660
Site Bordeaux
MERIS image – Date: 2003/06/19 10:17
MYD04 product – Date: 2003/06/19 12:55

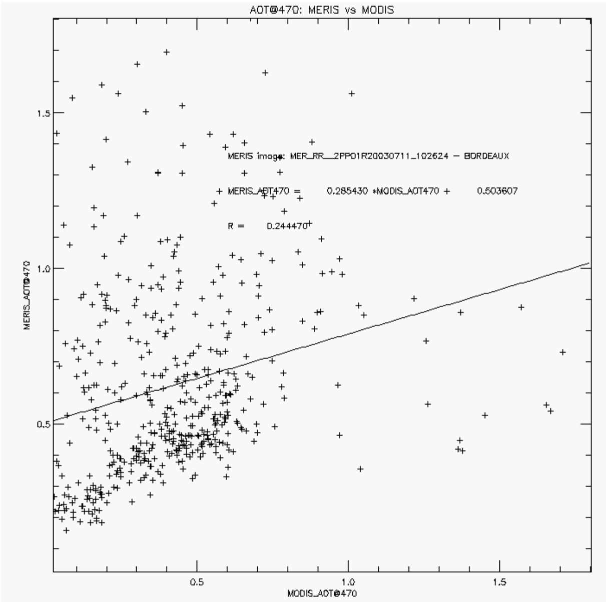

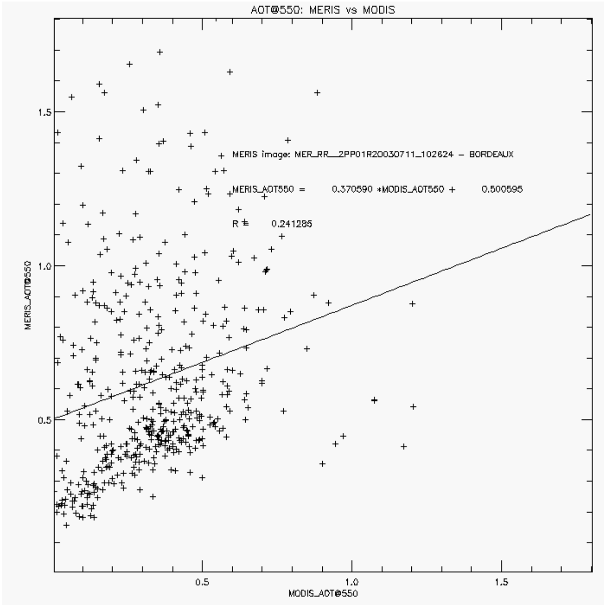

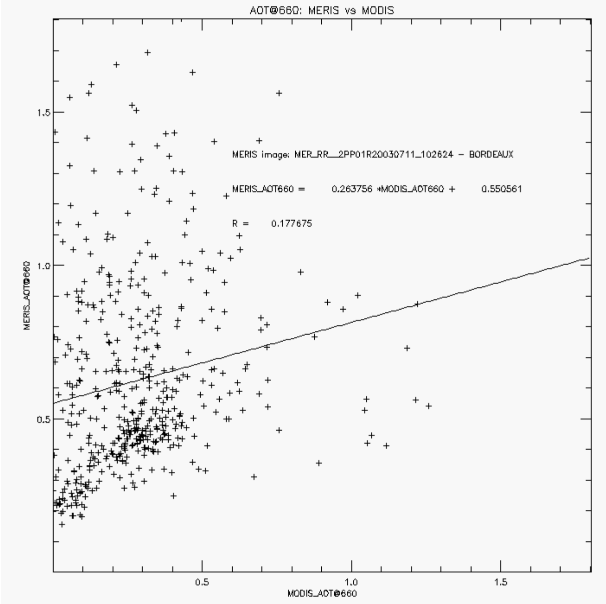

Figure 21: AOT comparisons at 470, 550 and 660
Site Bordeaux
MERIS image – Date: 2003/07/11 10:26
MYD04 product – Date: 2003/07/11 12:15

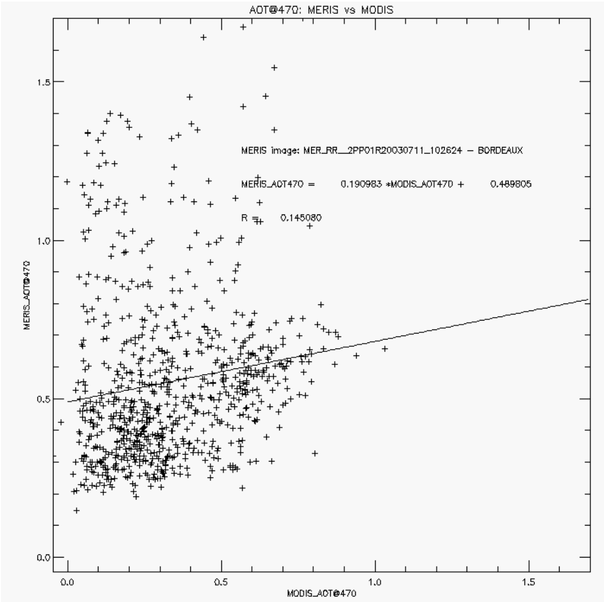

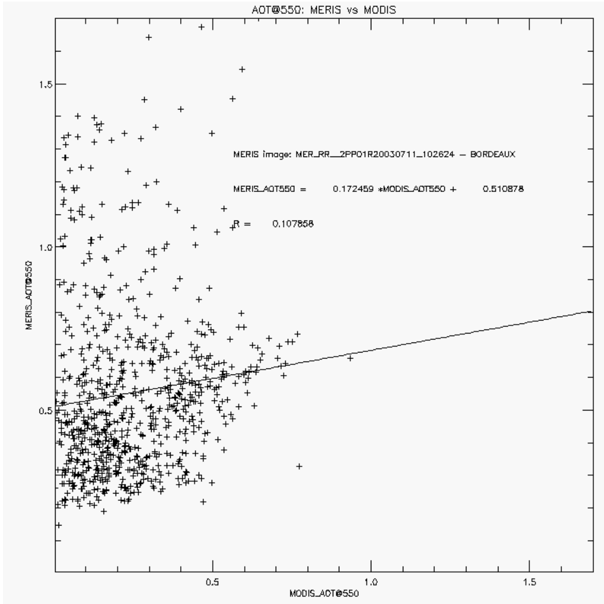

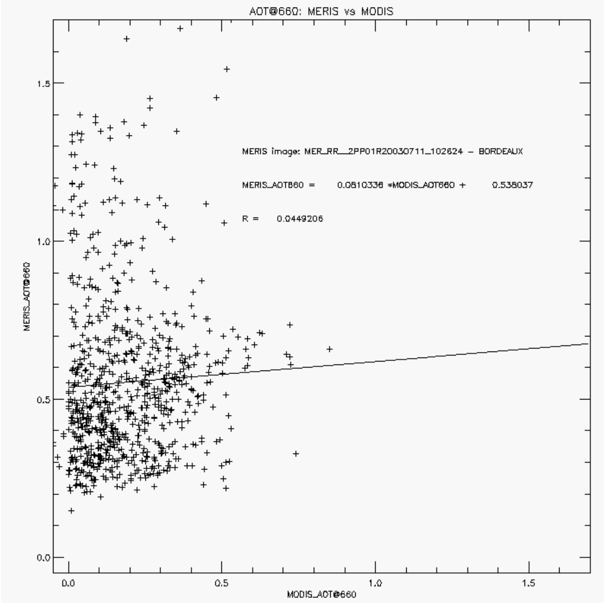

Figure 22: AOT comparisons at 470, 550 and 660
Site Bordeaux
MERIS image – Date: 2003/07/11 10:26
MYD04 product – Date: 2003/07/11 12:20

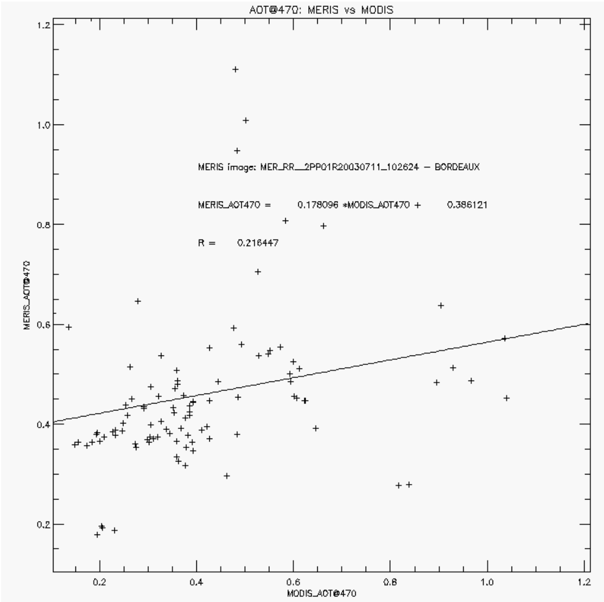

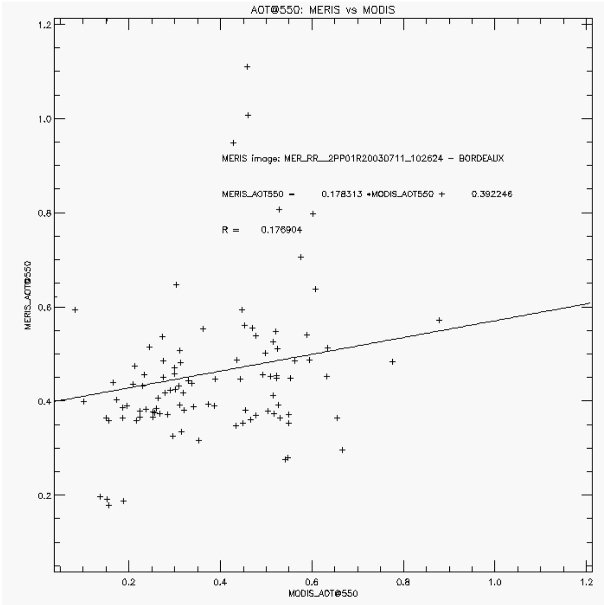

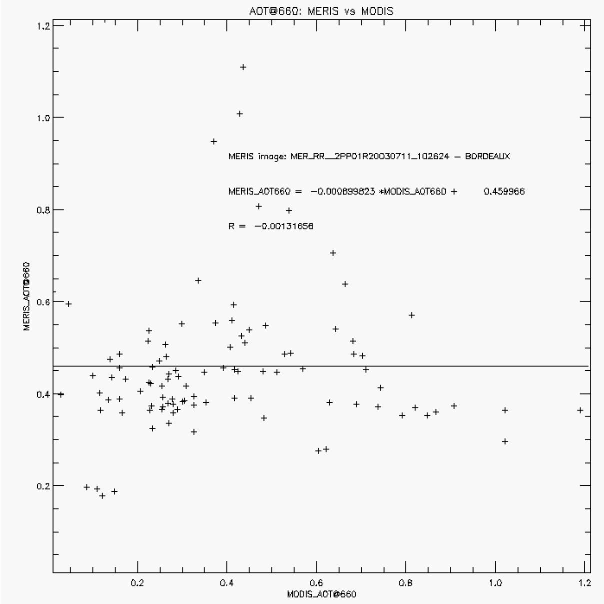

Figure 23: AOT comparisons at 470, 550 and 660
Site Bordeaux
MERIS image – Date: 2003/07/11 10:26
MYD04 product – Date: 2003/07/11 13:55

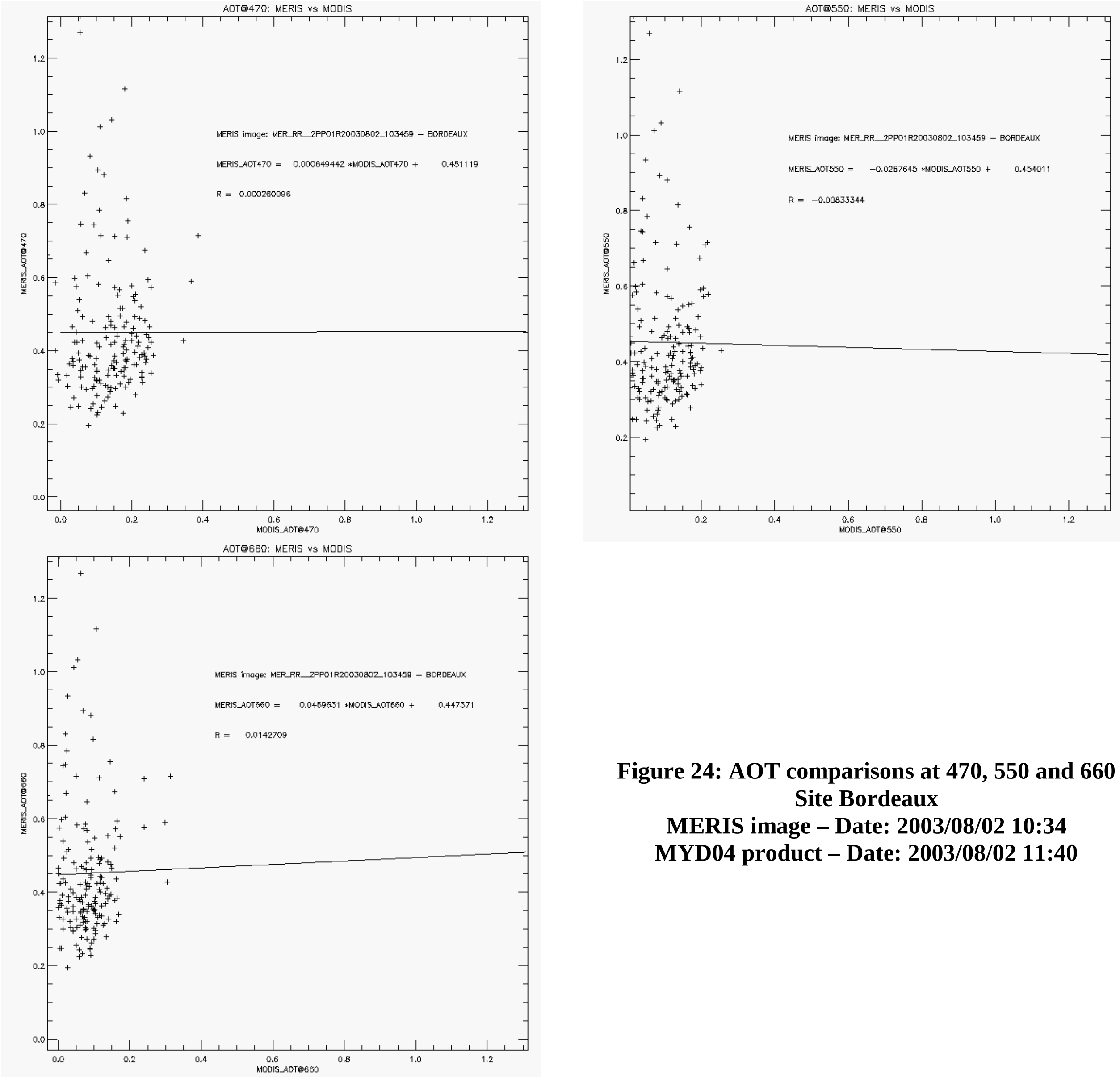

Figure 24: AOT comparisons at 470, 550 and 660
Site Bordeaux
MERIS image – Date: 2003/08/02 10:34
MYD04 product – Date: 2003/08/02 11:40

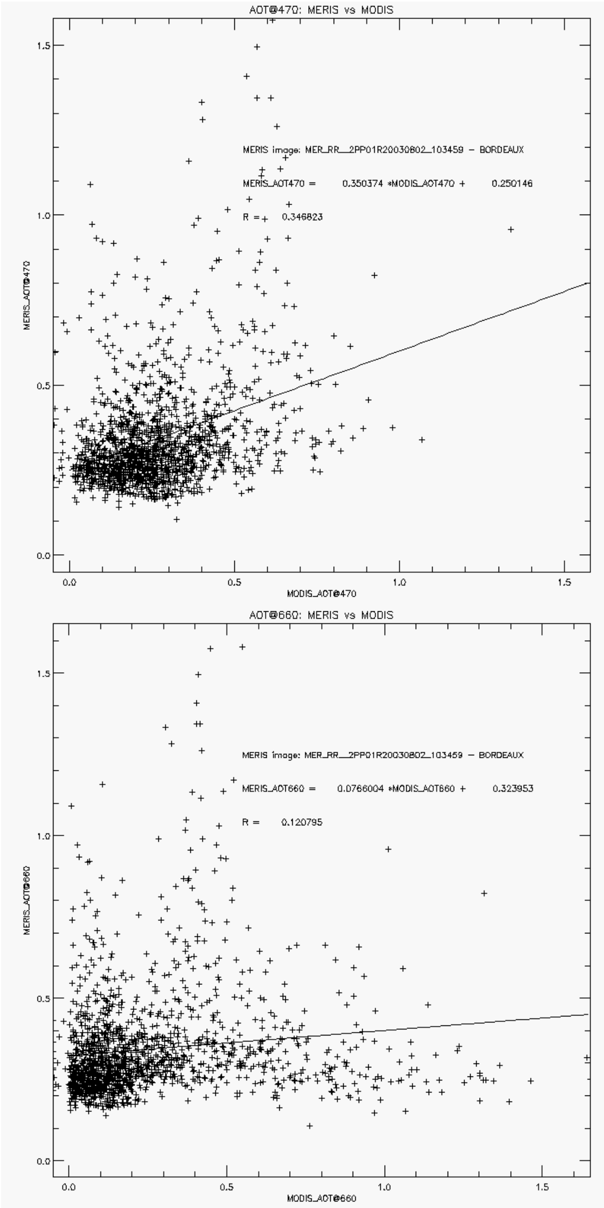

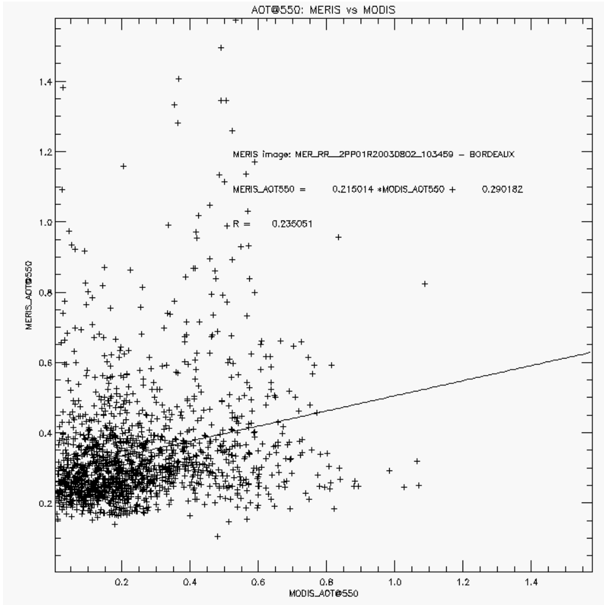

Figure 25: AOT comparisons at 470, 550 and 660
Site Bordeaux
MERIS image – Date: 2003/08/02 10:34
MYD04 product – Date: 2003/08/02 13:20

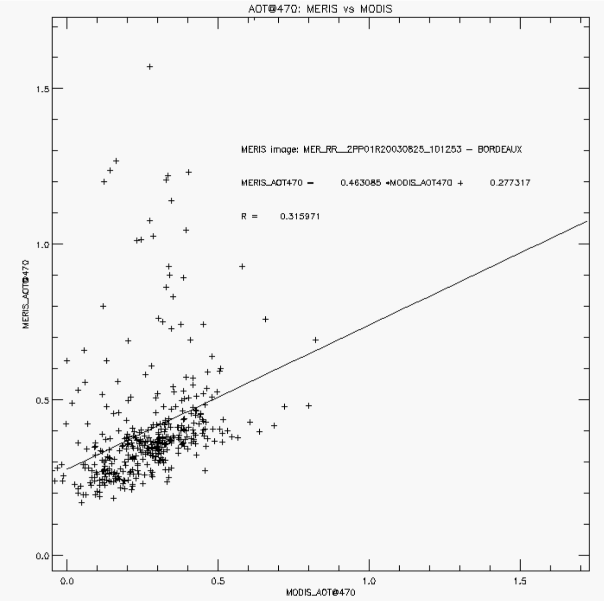

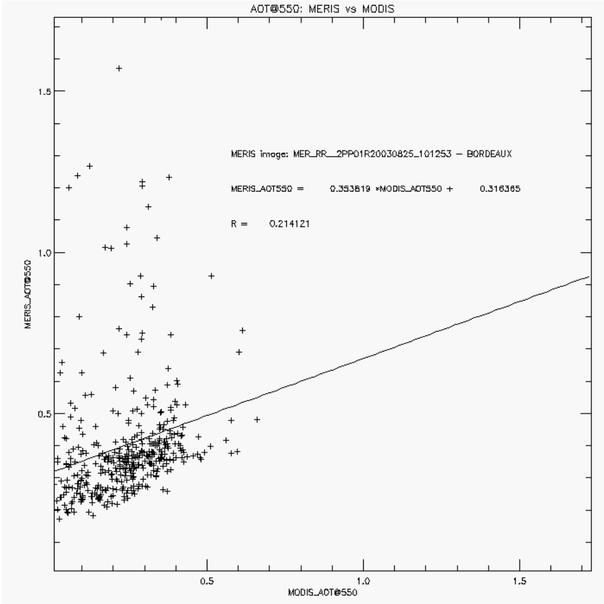

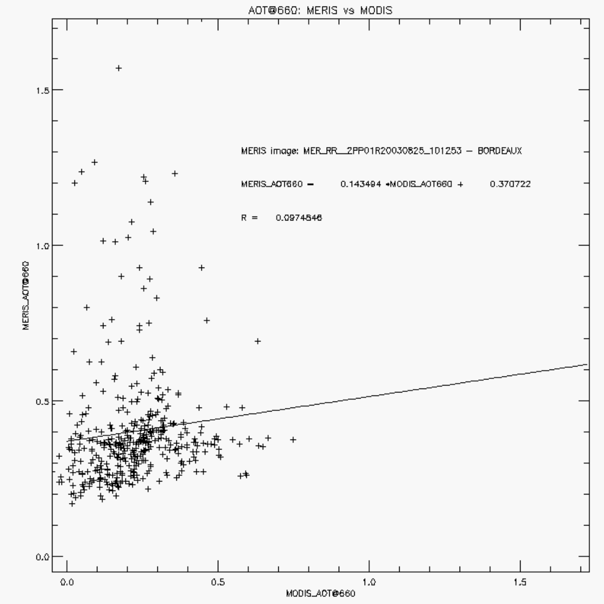

Figure 26: AOT comparisons at 470, 550 and 660
Site Bordeaux
MERIS image – Date: 2003/08/25 10:12
MYD04 product – Date: 2003/08/25 13:25

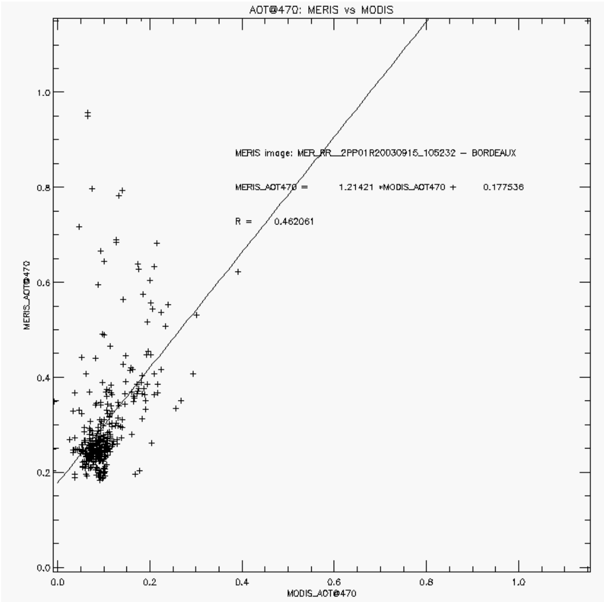

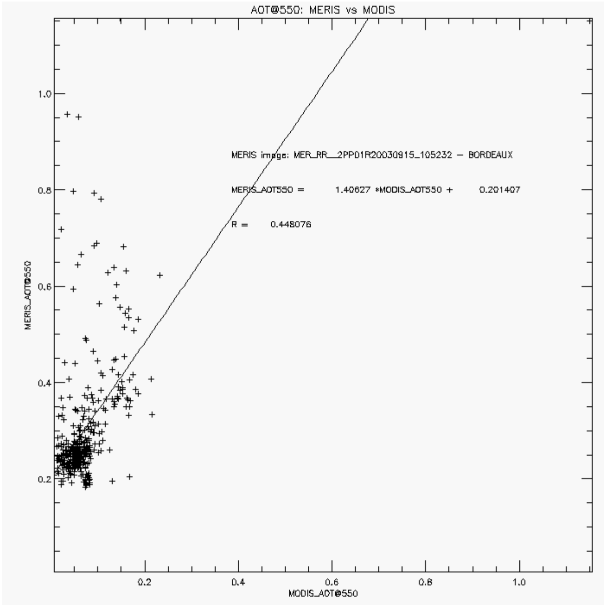

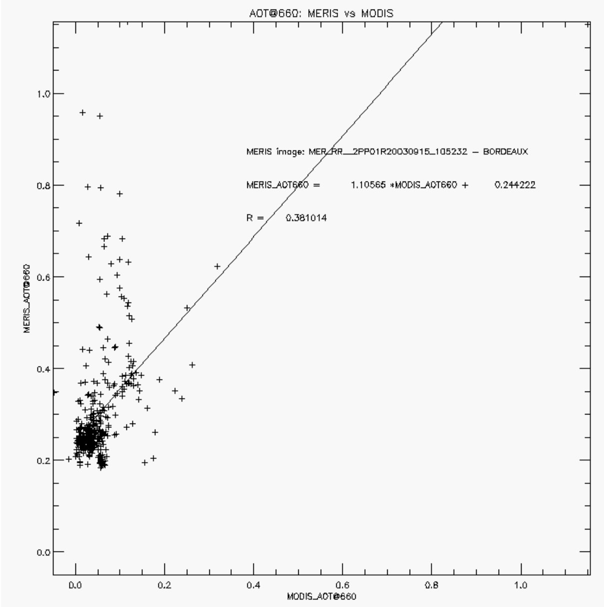

Figure 27: AOT comparisons at 470, 550 and 660
Site Bordeaux
MERIS image – Date: 2003/09/15 10:52
MYD04 product – Date: 2003/09/15 12:05

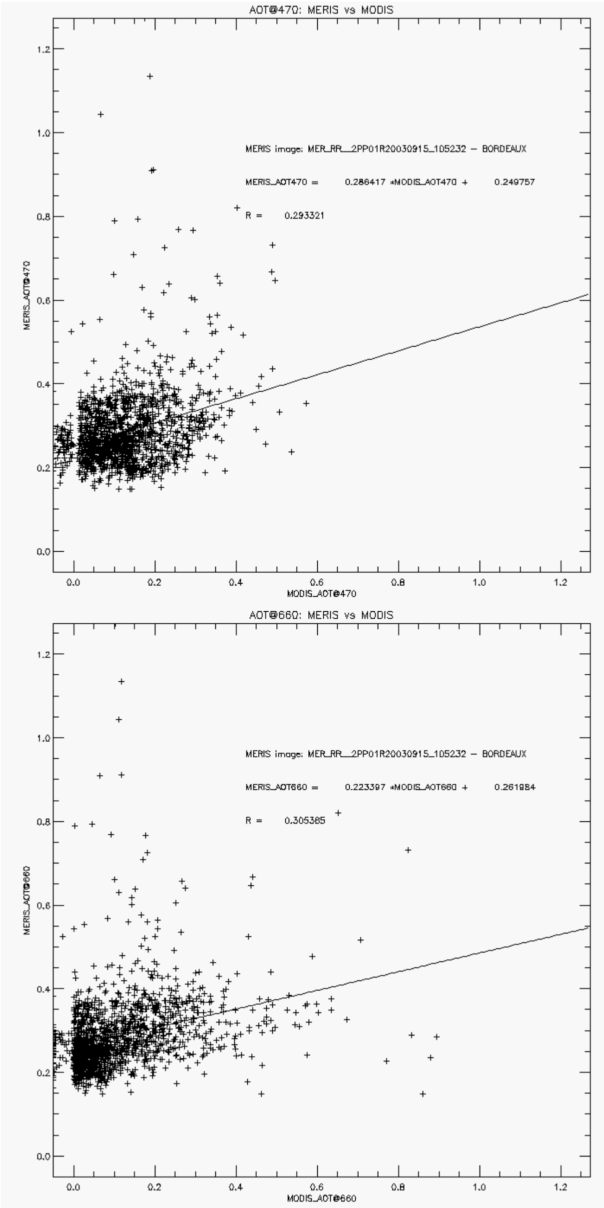

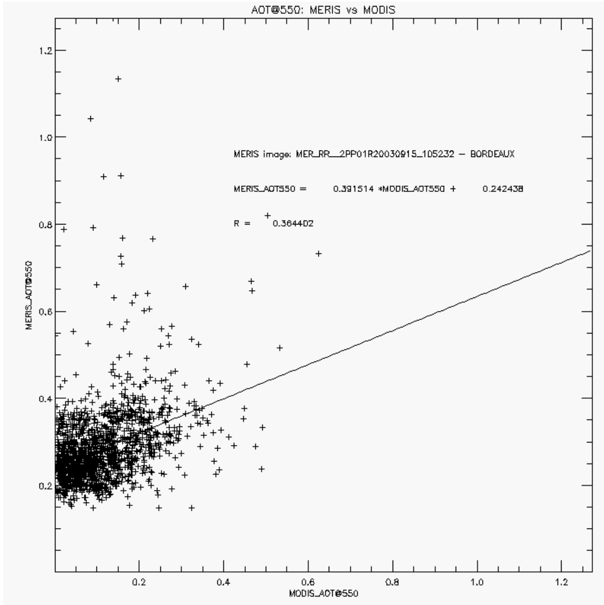

Figure 28: AOT comparisons at 470, 550 and 660
Site Bordeaux
MERIS image – Date: 2003/09/15 10:52
MYD04 product – Date: 2003/09/15 13:45

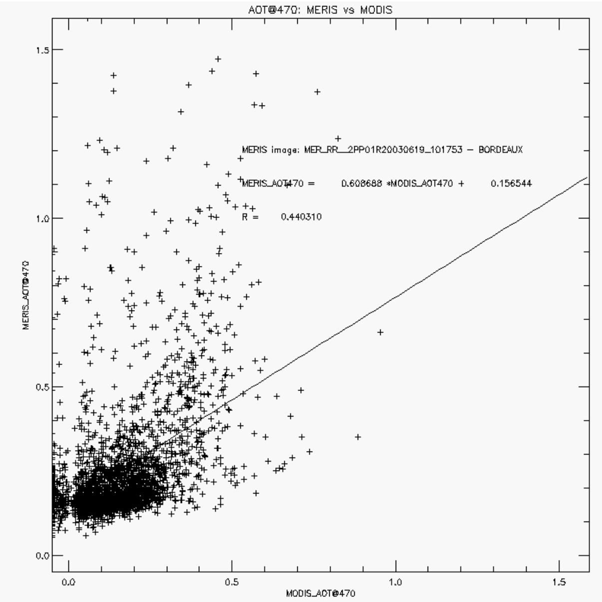

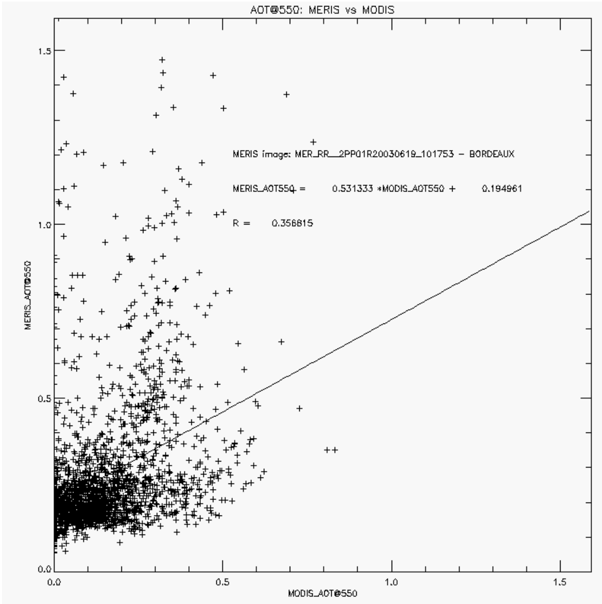

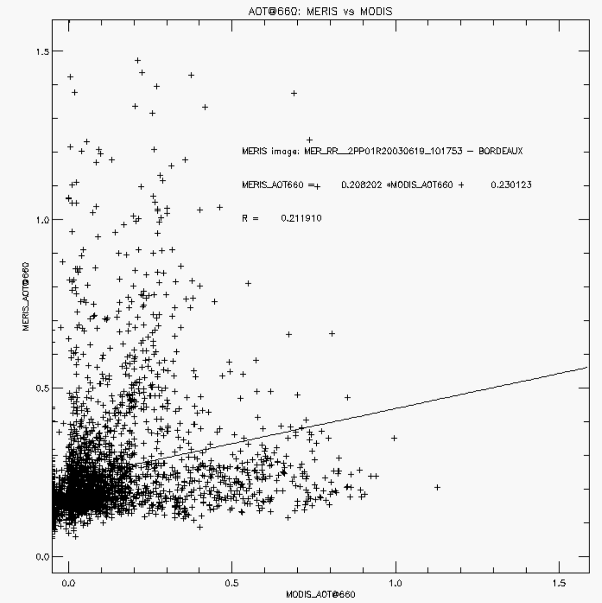

Figure 29: AOT comparisons at 470, 550 and 660
Site Bordeaux
MERIS image – Date: 2003/06/19 10:17
MOD04 product – Date: 2003/06/19 11:15

We can note that:

- a bias of about 0.2 is systematically observed for all the bands.
- the correlation coefficient (r) decreases with the wavelength; the band that is the best correlated is 470 nm.
- the plot scattering is usually very large.
- outstanding values of BAER are caused by different cloud screening methods and the averaged character of MODIS results.
- The AOT of the MODIS products start at 0 or has even negative values, which are unrealistic. Even under very clear conditions there is some aerosol, giving a minimum AOT of about 0.05 at 0.440 nm. This also caused an apparent bias in the comparisons.

4.4. Direct validation

The direct validation aims at comparing BAER output with the data of the sunphotometers of the AERONET network (Holben 1992).

4.4.1. Results for MERIS image over France

For this image, data of 9 AERONET stations are available. The daily variations of AOT and angstrom coefficient observed are represented for each site.

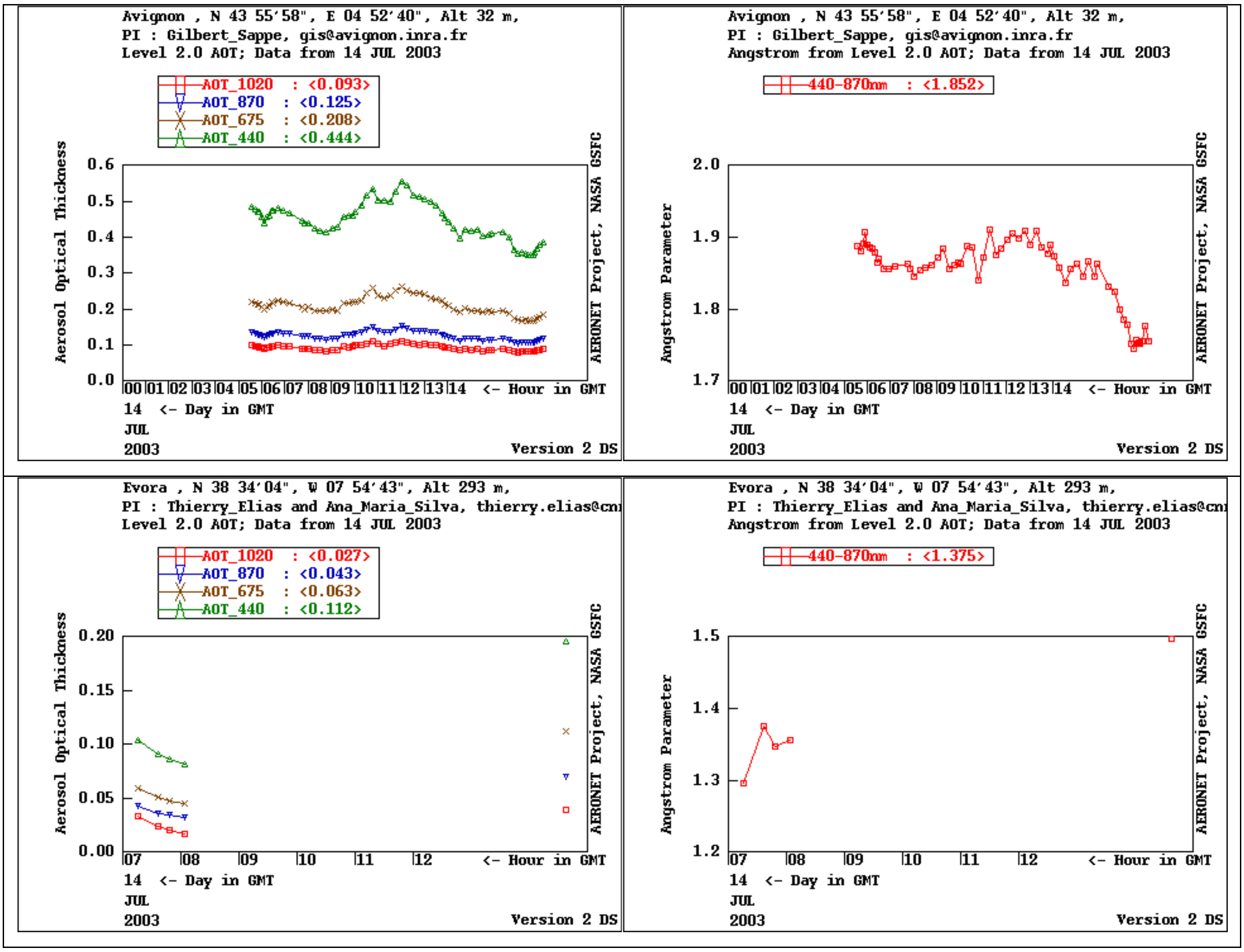

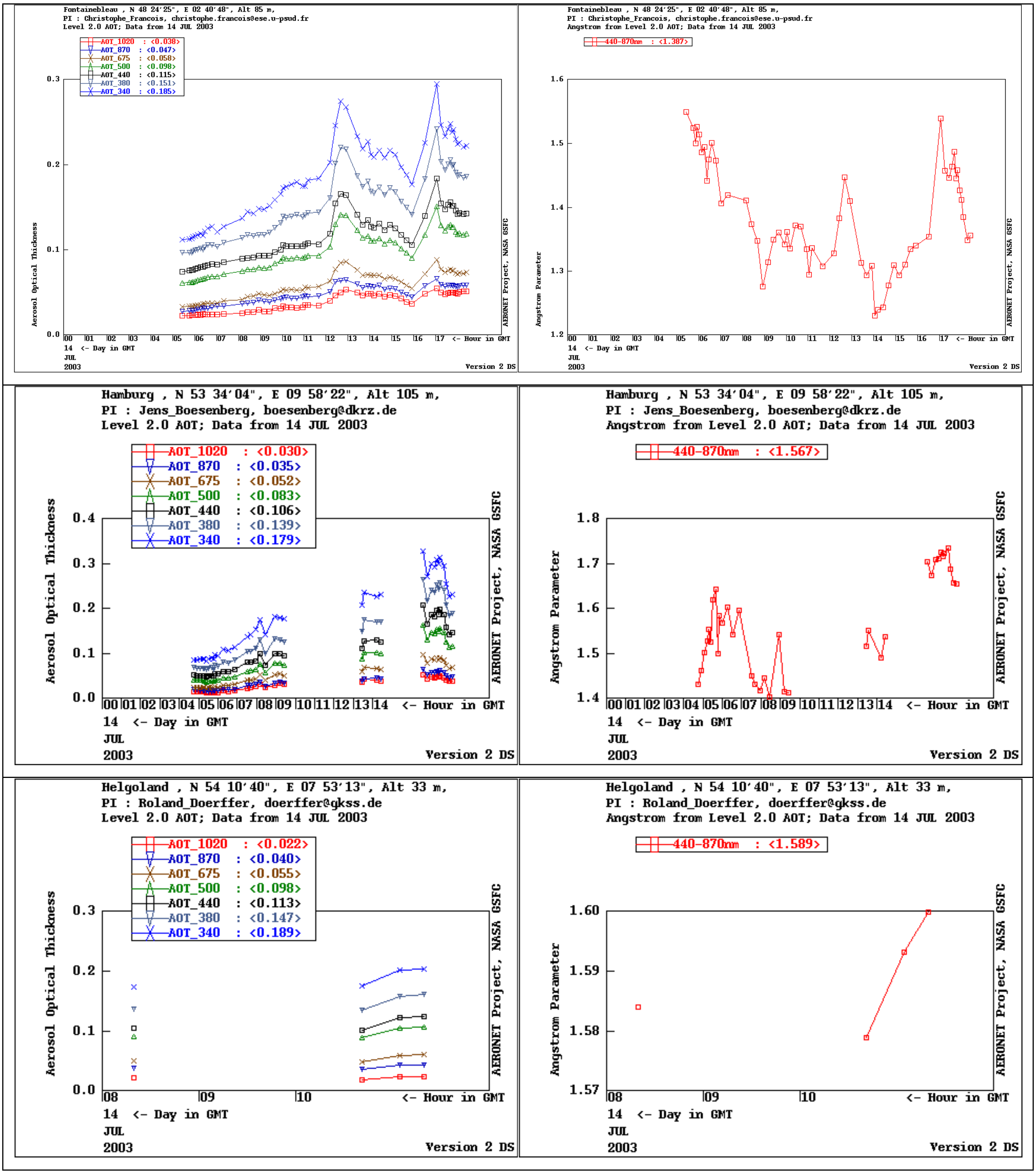

Fontainebleau , N 48 24'25", E 02 40'48", Alt 85 m,
PI : Christophe_Francois, christophe.francois@ese.u-psud.fr
Level 2.0 AOT; Data from 14 JUL 2003
AOT_1020 : <0.038>
AOT_870 : <0.047>
AOT_675 : <0.058>
AOT_500 : <0.098>
AOT_440 : <0.115>
AOT_380 : <0.151>
AOT_340 : <0.185>
Aerosol Optical Thickness
<- Hour in GMT
14 <- Day in GMT
JUL
2003
AERONET Project, NASA GSFC
Version 2 DS
Fontainebleau , N 48 24'25", E 02 40'48", Alt 85 m,
PI : Christophe_Francois, christophe.francois@ese.u-psud.fr
Angstrom from Level 2.0 AOT; Data from 14 JUL 2003
440-870nm : <1.387>
Angstrom Parameter
Hamburg , N 53 34'04", E 09 58'22", Alt 105 m,
PI : Jens_Boesenberg, boesenberg@dkrz.de
Level 2.0 AOT; Data from 14 JUL 2003
AOT_1020 : <0.030>
AOT_870 : <0.035>
AOT_675 : <0.052>
AOT_500 : <0.083>
AOT_440 : <0.106>
AOT_380 : <0.139>
AOT_340 : <0.179>
Hamburg , N 53 34'04", E 09 58'22", Alt 105 m,
PI : Jens_Boesenberg, boesenberg@dkrz.de
Angstrom from Level 2.0 AOT; Data from 14 JUL 2003
440-870nm : <1.567>
Helgoland , N 54 10'40", E 07 53'13", Alt 33 m,
PI : Roland_Doerffer, doerffer@gkss.de
Level 2.0 AOT; Data from 14 JUL 2003
AOT_1020 : <0.022>
AOT_870 : <0.040>
AOT_675 : <0.055>
AOT_500 : <0.098>
AOT_440 : <0.113>
AOT_380 : <0.147>
AOT_340 : <0.189>
Helgoland , N 54 10'40", E 07 53'13", Alt 33 m,
PI : Roland_Doerffer, doerffer@gkss.de
Angstrom from Level 2.0 AOT; Data from 14 JUL 2003
440-870nm : <1.589>

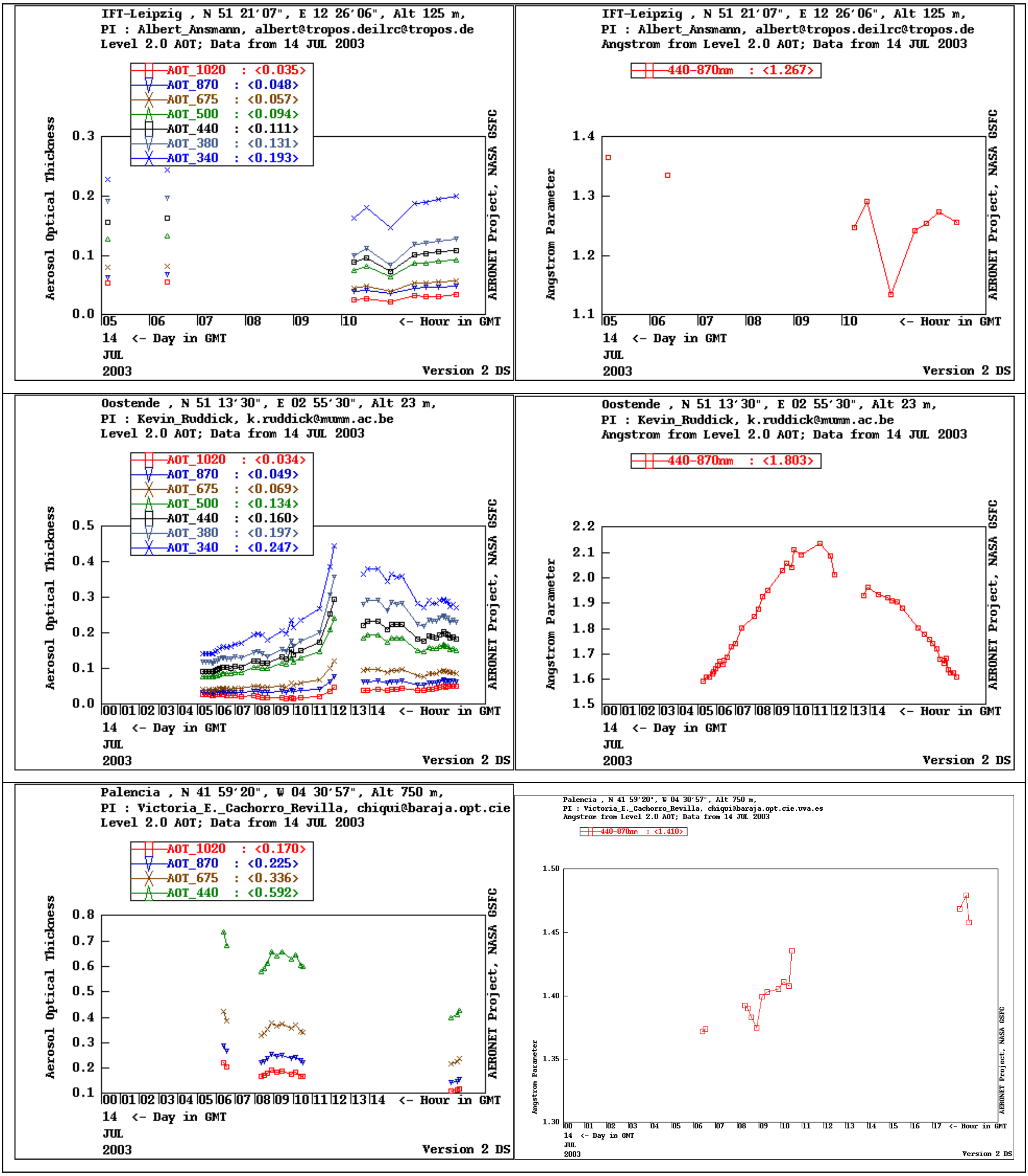

IFT-Leipzig , N 51 21'07", E 12 26'06", Alt 125 m,
PI : Albert_Ansmann, albert@tropos.deilrc@tropos.de
Level 2.0 AOT; Data from 14 JUL 2003
AOT_1020 : <0.035>
AOT_870 : <0.048>
AOT_675 : <0.057>
AOT_500 : <0.094>
AOT_440 : <0.111>
AOT_380 : <0.131>
AOT_340 : <0.193>
Aerosol Optical Thickness
<- Hour in GMT
14 <- Day in GMT
JUL
2003
AERONET Project, NASA GSFC
Version 2 DS
IFT-Leipzig , N 51 21'07", E 12 26'06", Alt 125 m,
PI : Albert_Ansmann, albert@tropos.deilrc@tropos.de
Angstrom from Level 2.0 AOT; Data from 14 JUL 2003
440-870nm : <1.267>
Angstrom Parameter
Oostende , N 51 13'30", E 02 55'30", Alt 23 m,
PI : Kevin_Ruddick, k.ruddick@mumm.ac.be
Level 2.0 AOT; Data from 14 JUL 2003
AOT_1020 : <0.034>
AOT_870 : <0.049>
AOT_675 : <0.069>
AOT_500 : <0.134>
AOT_440 : <0.160>
AOT_380 : <0.197>
AOT_340 : <0.247>
Oostende , N 51 13'30", E 02 55'30", Alt 23 m,
PI : Kevin_Ruddick, k.ruddick@mumm.ac.be
Angstrom from Level 2.0 AOT; Data from 14 JUL 2003
440-870nm : <1.803>
Palencia , N 41 59'20", W 04 30'57", Alt 750 m,
PI : Victoria_E._Cachorro_Revilla, chiqui@baraja.opt.cie
Level 2.0 AOT; Data from 14 JUL 2003
AOT_1020 : <0.170>
AOT_870 : <0.225>
AOT_675 : <0.336>
AOT_440 : <0.592>
Palencia , N 41 59'20", W 04 30'57", Alt 750 m,
PI : Victoria_E._Cachorro_Revilla, chiqui@baraja.opt.cie.uva.es
Angstrom from Level 2.0 AOT; Data from 14 JUL 2003
440-870nm : <1.410>

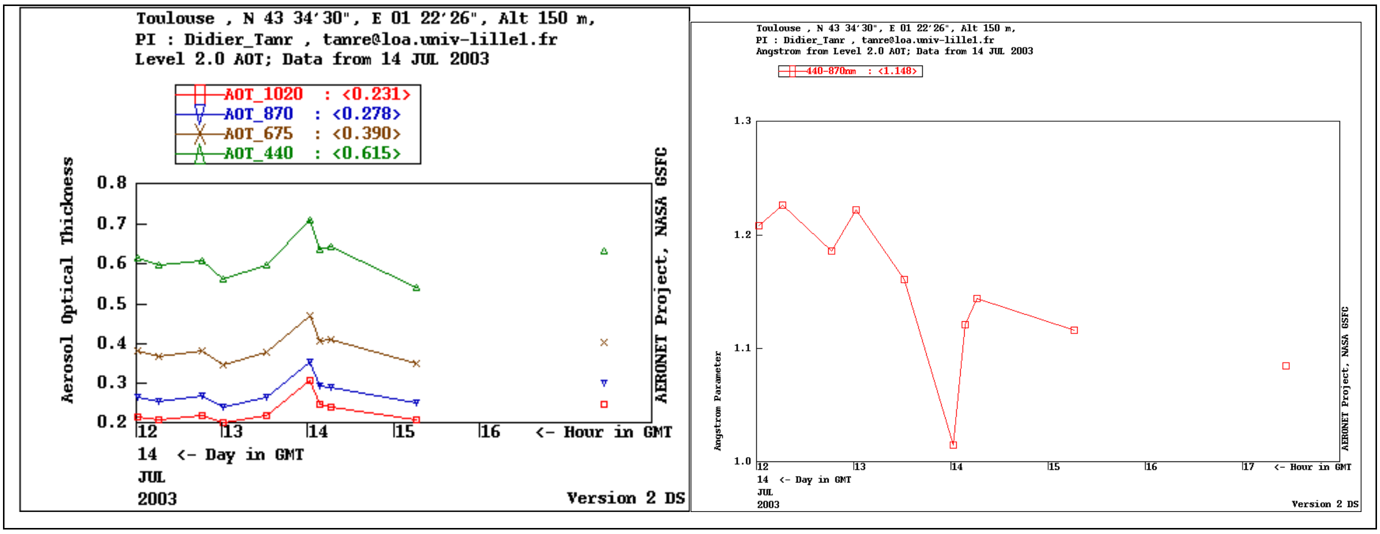

At the time of the acquisition, the values of the AOT at are written on the image.

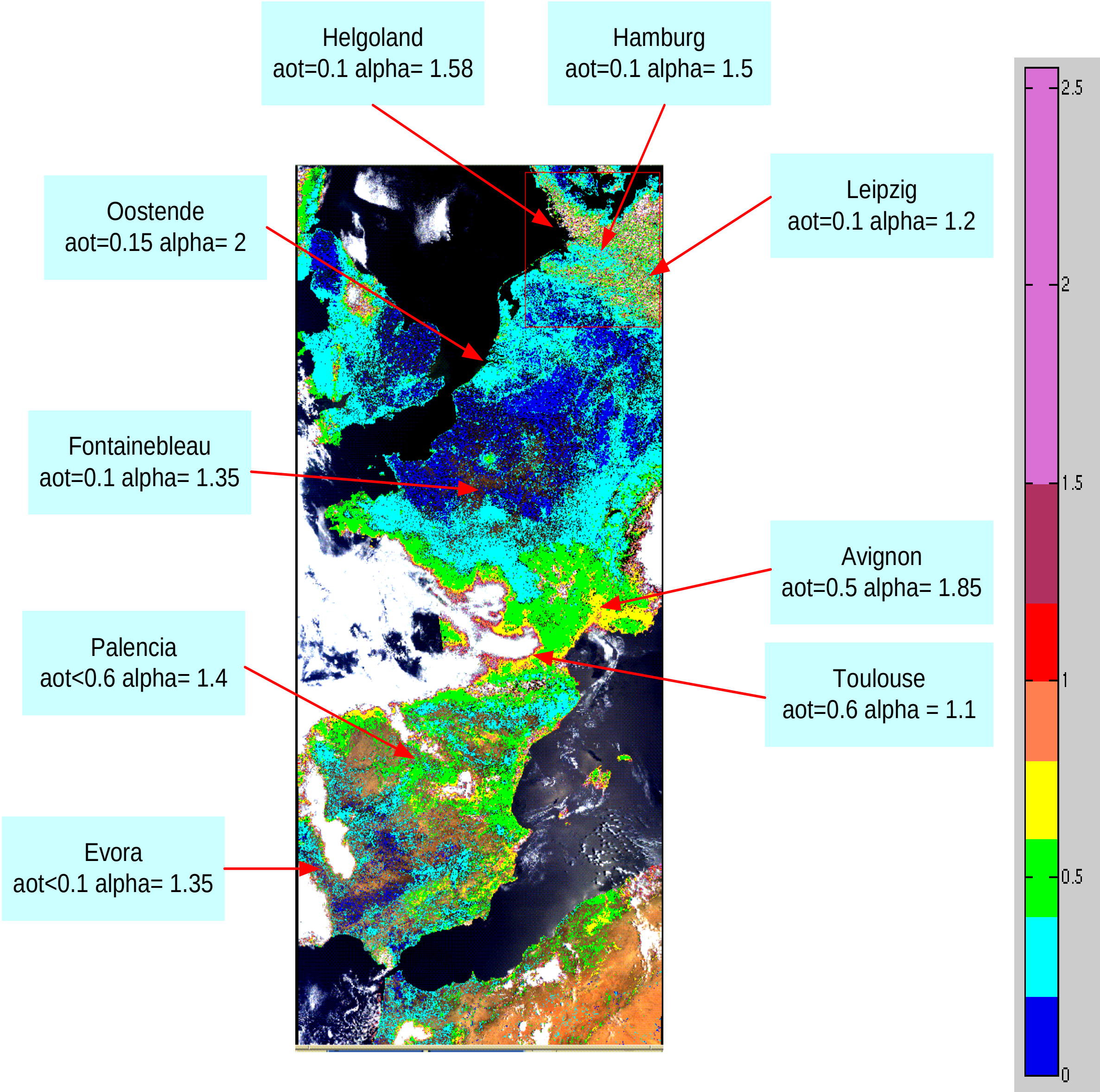

Figure 30: BAER AOT at 440° nm. The values of the sunphotometer are written in the image.

The spatial consistency of the BAER output with the AERONET data is highlighted with this figure. Low and higher values are observed by both estimations.

4.4.2. Comparison between BAER outputs and AERONET measurements

Figure 31 presents the comparisons between AERONET AOTs at 440, 670 and 870 and BAER AOTs at respectively 440, 665 and 865 nm. The BAER AOT has been estimated on the pixel the nearest of the location of the AERONET station. Each plot colour corresponds to one validation site.

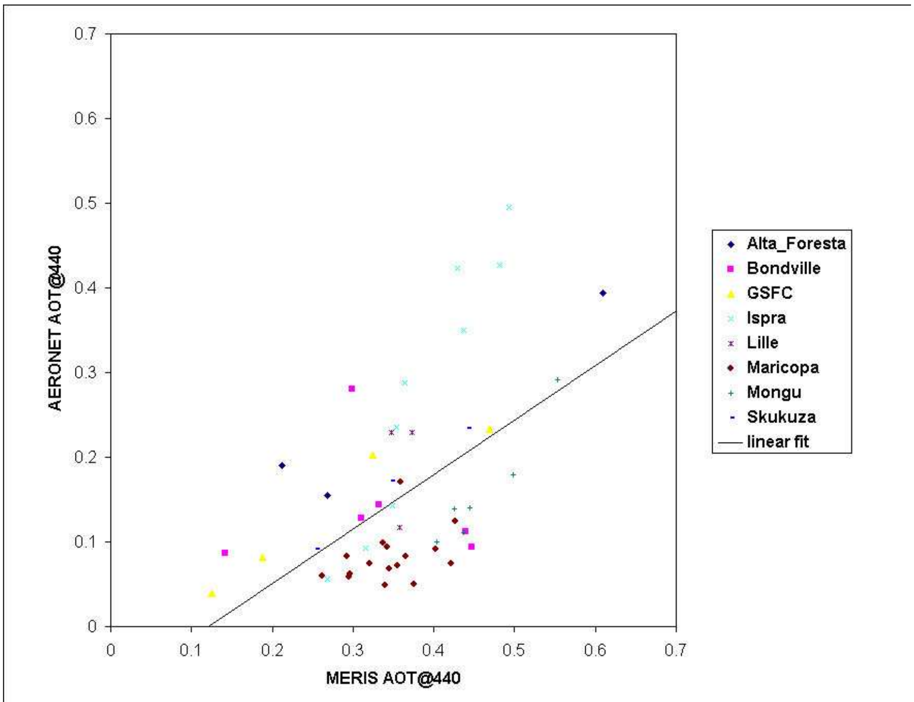

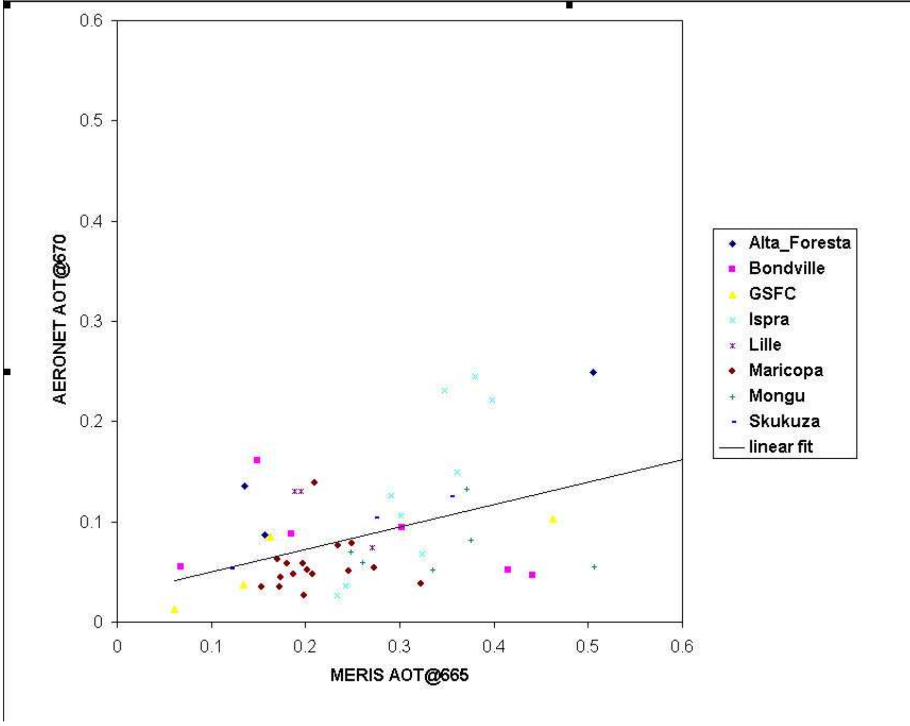

Figure 31: Comparisons between AERONET AOT at 440, 670 and 870 nm and BAER AOT at 440, 665 and 865 nm over several validation sites

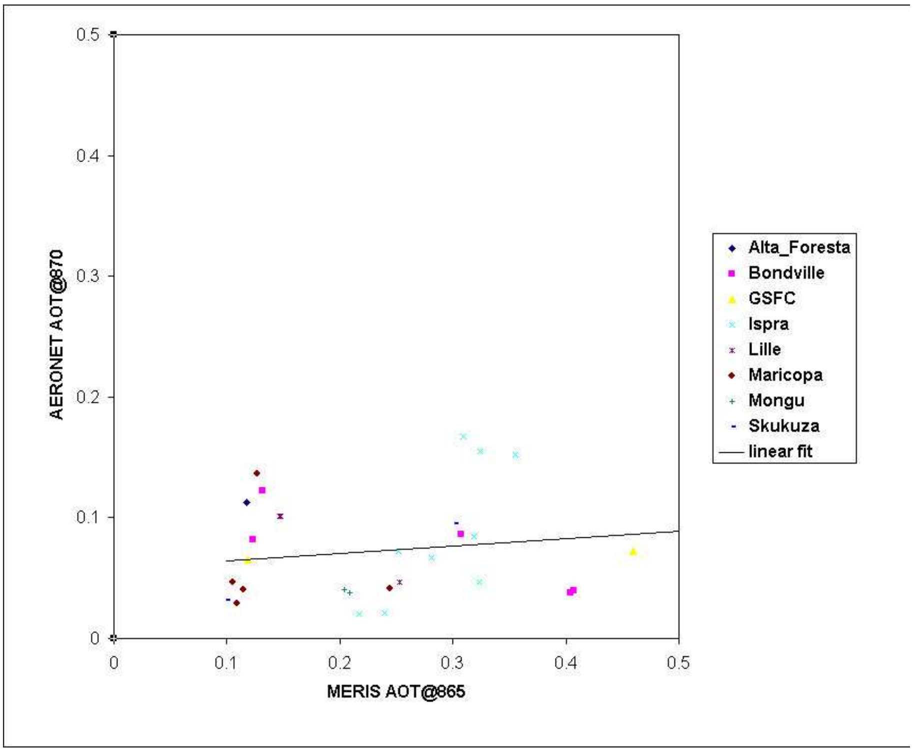

We can remark that:

- The best trend is obtained for the 440 nm band; no correlation is obtained at 870 nm.
- as in the frame of the comparison between BAER AOT and MODIS AOT, a small offset is observed at 440 nm
- the BAER AOT values are usually larger than AERONET AOT values

4.5. Analysis and Conclusions

The validation activities of the BAER outputs have been led by intercomparisons with two independent products MODIS products, AERONET measurements and one derived from MERIS available over DDV pixels. At this stage of the validation activities, we have noted:

- The good spatial consistency of the BAER AOT
- The best accuracy and correlation of the AOT retrieval are obtained in short wavelength 412, 440 and 550 nm.
- A small offset is observed at the shortest wavelength
- BAER AOT values are usually larger than measured MODIS, AERONET and DDV AOTs.

4.6. Sensitivity study

In order to assess the impact of different factors and parameters used in the modelling, a sensitivity study is made, aiming at testing several hypotheses, of which the choice of predefined static input parameters. Five cases are analysed to determine the weight of initial value. The equations in which these parameters are used are reprinted from the ATBD hereafter.

1. The equation allowing the separation of surface effects and atmosphere effects are written hereafter

   $$\rho_{Surf,i=0}^{Mixing}(\lambda) = C_{Veg} \cdot \rho_{Veg}(\lambda) + SF \cdot (1 - C_{Veg}) \cdot \rho_{Soil}(\lambda) \qquad \text{(eq.7 of the ATBD)}$$

   Where ρ_{veg} and ρ_{soil} are the reference spectra of vegetation and bare soil respectively

   C_{veg} is a linear function of NDVI

   SF is a weight given to the bare soil spectra to increase the impact of bare soil.

   The case 2, 3, 5 of the sensitivity study relate to the analysis of this factor

2. The equation allowing to adapt the level of the surface reflectance to that required with the scene

   $$\rho_{Surf}(\lambda) = F \cdot \rho_{Surf,i=0}^{Mixing}(\lambda) \qquad \text{(eq.8 of the ATBD)}$$

   The case 1 of the sensitivity study relates to the analysis of this factor.

3. The relationship between AOT and aerosol reflectance is given by :

   $$\delta AerGuess = f(\rho_{AOTguess}) \qquad \text{(eq.20 of the ATBD)}$$

   The case 4 of the sensitivity study relates to the analysis of this factor.

4.6.1. Case1 : Impact of the scaling factor F

The surface reflectance model used for the separation of surface effects from atmospheric effects is adapted by two parameters to the conditions within the individual pixel: a linearly mixed spectrum of surface reflectance, and a scaling factor *F* to adapt the linearly mixed spectrum to the reflectance conditions.

The impact of this scaling factor F is assessed through a change of its value by a 20% factor.

In this case, F is set to a higher value F=1.2 instead 1.

4.6.2. Case 2 : NDVI weighting

In the reference case, the vegetation cover is estimated from the NDVI. The NDVI value is weighted by a 0.9 factor.

In the sensitivity case, no weight is applied. C_{scal} factor is set to 1.

4.6.3. Case 3 : Soil spectrum weighting

The linearly mixed spectrum of surface reflectance ($\rho_{Surf,i=0}(\lambda)$) is given by a weighted mixing of spectra from 'green vegetation' and 'bare soil'. In the reference case, the soil reference surface reflectance is weighted by a 1.3 factor to increase its account.

In this case, the 1.3 factor is removed.

4.6.4. Case 4 : Impact of the AEROSOL type

The reference case is made for one type of aerosol. The Look Up Table has been precomputed for the results of the LACE 98 campaign, allowing the defined a Look Up Table linking the aerosol optical thickness at all wavelengths of MERIS channel, and the aerosol reflectance.

In this case, another LUT is used, based on continental aerosol type taken from OPAC continental aerosol database

4.6.5. Case 5 (1 to 7) : Impact of reference vegetation and soil spectra

In the case, the full impact of the reference spectra used both for vegetation and soil are assessed. The reference surface reflectance is estimated by a combination of vegetation spectrum and soil spectrum. These spectrums are represented in the following graphs. The LACE_MAPLE and Casi 1 are used as reference, and depending on the brightness of the soil, the KARNIELI 1 is used (automatically) for desert cases.

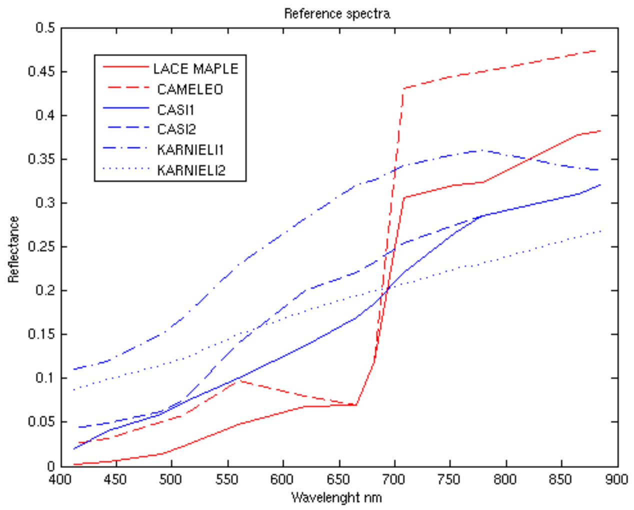

Figure 32: Soil and vegetation reference spectrum used in the sensitivity study.

In the sensitivity study, we still used the same vegetation spectra, but test the impact of the soil spectra. Four new spectra are tested (Karnieli 2A to 2D), which corresponds to more or less bright bare soil. They are represented in the next figure.

The soil spectra used for the sensitivity study are artificial soil spectra, taken from Karnieli 2 spectra and increased by a 0.05 value to keep the same spectral variations (slope) but with an absolute level value higher.

The Karnieli 2A corresponds to Karnieli 2 spectrum with the offset increased by 0.05 (red line)

The Karnieli 2B corresponds to Karnieli 2 spectrum with the offset increased by 0.1 (green line)

The Karnieli 2C corresponds to Karnieli 2 spectrum with the offset increased by 0.15 (pink line)

The Karnieli 2D corresponds to first value of Karnieli 2 and last value of Karnieli 2C (black line)

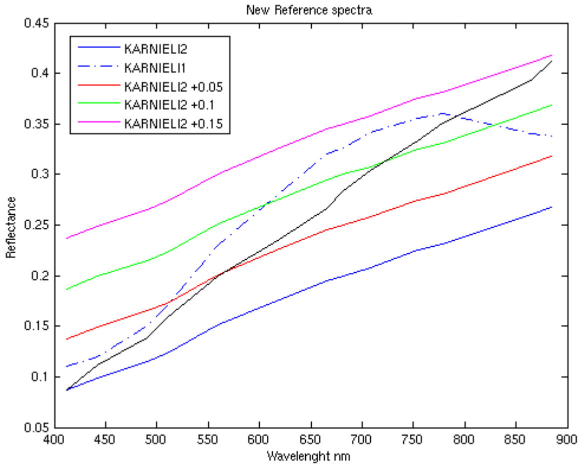

Figure 33: Soil reference spectrum used in the sensitivity study.

The combinations of vegetation and bare soil spectra are given by Table 6.

Table 5: combination of reference soil spectra used in the sensitivity study

Reference of the test	Vegetation spectrum used	Soil spectrum used	Soil spectrum used when desert soil is detected
Cas5_1	LACE+MAPLE	CASI_1	KARNIELI2
Cas5_2	LACE+MAPLE	KARNIELI	KARNIELI2
Cas5_3	LACE+MAPLE	KARNIELI2	KARNIELI2
Cas5_4	LACE+MAPLE	KARNIELI2A	KARNIELI2
Cas5_5	LACE+MAPLE	KARNIELI2B	KARNIELI2
Cas5_6	LACE+MAPLE	KARNIELI2C	KARNIELI2
Cas5_7	LACE+MAPLE	KARNIELI2D	KARNIELI2

4.6.6. Position of the sensitive parameters in the modelling

The different factors which have an impact on different phases of the processing are indicated in Figure 34. They modify:

- The initialisation phase (determination of the first guess)
- The separation of surface and atmosphere contribution phase
- The parameter of radiative transfer

In order to provide synthetic results, the totality of the results (obtained for all the images and all dates) is reported in the annexe of this document.

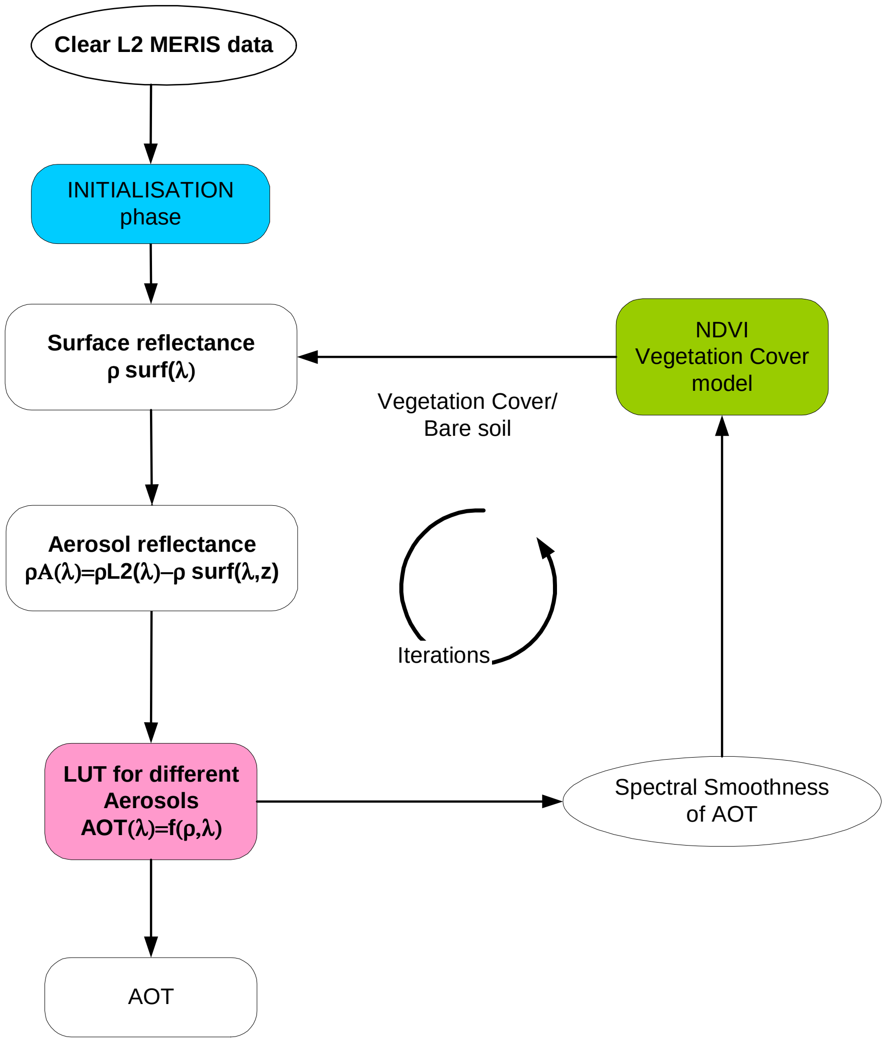

Figure 34: Scheme of the retrieval procedure for the aerosol optical thickness over land. Case 1, 2, 3 impact on the green box. Case 4 impacts on the pink box. Case 5 impacts on the initialisation phase, blue box.

4.6.7. Analysis

The sensitivity studies allows to highlight the impact of different factors used in the modelling, and to hierarchy them, by order of importance.

The changes have been made at different levels of the processing to estimate

- the impact of the guess of the AOT and surface reflectance retrieval,
- the robustness of the retrieval if an uncertainty is introduced in the knowledge of the aerosol type,
- the strength of the iterative method if the initial tuning factors and weighting factors (F, NDVI and SF) are far from their optimal values,

4.6.7.1. Impact of reference soil and vegetation spectra on the AOT guess

It has been seen in the ATBD that the heart of the BAER method results on the decoupling of the surface effects from the atmosphere effects. The assumptions made for the separation of the effects are based on the fact that the surface reflectance is a weighting function of both vegetation and bare soil reflectances, with a weight SF given to the bare soil reflectance reference to increase its contribution. Out to these factors, the weight given itself to the spectral variation of the reference spectra has been examined by the Cases 5 (1 to 7) of the sensitivity study. Seven combinations of mixed reference spectra have been tested on the AOT retrieval.

The case of the AltaForesta site is examined in details. For the reference case, the results obtained for the aot estimation at 560 nm (in comparison with the ddv):

	date	Nb pixel	Offset	Slope	r^2	rmse	Mean baer	Mean ddv	Sdt baer	Sdt ddv

Reference Case5-1	25072003	15388	0.1321	0.5404	0.7527	0.0831	0.2028	0.1309	0.0565	0.0908
	30042003	160959	0.1166	0.7408	0.6619	0.0845	0.2123	0.1292	0.0537	0.0590

Case5-2	25072003	13124	0.1105	0.6206	0.8047	0.0645	0.2013	0.1463	0.0616	0.0890
	30042003	158658	0.1088	0.7501	0.6595	0.0777	0.2062	0.1299	0.0545	0.0590

The Karnieli1 soil spectrum used in this case has a level of reflectance higher than the CASI 1 reflectance spectrum. The rmse is little bit better, and the results are better correlated than in case 5-1.

Case5-3	25072003	13125	0.1075	0.6316	0.8164	0.0629	0.1998	0.1462	0.0623	0.0891
	30042003	158492	0.1073	0.7541	0.6668	0.0768	0.2053	0.1300	0.0545	0.0590

The Karnieli 2 soil spectrum has higher reflectance in the visible channel and lower reflectance in near Infra red channel than the CASI-1.Results are also improved.

Case5-4	25072003	12508	0.0909	0.6911	0.8488	0.0521	0.1950	0.1507	0.0664	0.0885
	30042003	155831	0.1018	0.7640	0.6654	0.0723	0.2016	0.1307	0.0552	0.0589

The Karniel2A soil spectrum has a reflectance level higher by a constant 0.05 factor. The correlation is also better than in the other cases, the offset of the relation has decreased, and the rmse is 0.01 lower .

Case5-5	25072003	12521	0.0770	0.7427	0.8767	0.0448	0.1882	0.1497	0.0708	0.0892
	30042003	153186	0.0971	0.7735	0.6614	0.0686	0.1988	0.1315	0.0560	0.0589

The Karniel2B soil spectrum has a reflectance level higher by a constant 0.1 factor. The correlation is improved, with the accuracy of the regression.

Case5-6	25072003	12559	0.0671	0.7781	0.8957	0.0395	0.1829	0.1488	0.0738	0.0898
	30042003	150777	0.0930	0.7818	0.6584	0.0655	0.1964	0.1322	0.0567	0.0588

The Karniel2C soil spectrum has a reflectance level higher by a constant 0.1 factor. The correlation is improved, with the accuracy of the regression. The offsets decrease too.

Case5-7	25072003	13689	0.1123	0.6151	0.8105	0.0671	0.1998	0.1422	0.0612	0.0896
	30042003	159351	0.1088	0.7560	0.6702	0.0784	0.2068	0.1297	0.0545	0.0590

The Karniel2D soil spectrum has a low reflectance level in the blue channel which increases linearly to a high level in the near infrared channel. The correlation and the accuracy of the results in this case decrease.

Moreover, depending on the reference spectra chosen, the number of pixels for which the retrieval is possible varies at the maximum of 18 % for the first date, 6% for the second which has 10 times more valid pixels.

The results details here are reproduced with the other sites. The use of case 5-5 and 6 (Karnieli 2B and Karnieli 2C) provides the best results whereas the use of the other reference soil spectra does not improve significantly the accuracy of the retrieval.

The results show that the impact of the soil reference spectra shape is important against the vegetation reference spectrum chosen. Indeed, to be able to simulate the linear mixed spectrum of surface reflectance, the two spectra have to cover a large variation of possible reflectance in both the short wave length and near infrared wavelength. The vegetation reference spectrum (LACE MAPLE) has very low values of reflectance (less than 5 %) in the visible channels. When the soil reference spectrum has also low value in the same spectral range, the Cveg factor which estimates the vegetation cover fails in the fitting of Eq 7 of the ATBD. This is the same effect in the near infra red part of the solar spectrum covered by MERIS channels. This is the reason why the KARNIELI 2C and 2D provide the best results.

As these Karnieli2A to D spectra have no reality, the spectra used to represent the vegetation and the soil are CAMELEO and Casi 2 (Nominal case, section 4.2.1). Their variations are around 0.1 in the visible MERIS channels and near infrared channels.

These two spectra are kept as nominal reference spectra for the data processing.

4.6.7.2. Impact of the NDVI weighting factor

The linear mixing of the vegetation and ground surface spectral reflectance is tuned by the Vegetation Cover factor (Cveg), which is proportional to the NDVI. The proportionality factor C_{Scal} is equal to 0.9 NDVI. When the weighting factor is set to 1, no real differences are seen with the reference case.

4.6.7.3. Impact on the soil reference spectrum weighting

In order to increase the bare soil effect in the estimation of the mixing reflectance, the bare soil spectrum is weighted by a 1.3 factor in the reference case. In this case, the weighting factor is removed (set to 1) and the case 3 of the sensitivity study allows to estimate its impact on the retrieval. As seen on the results, the SF factor change has no impact on the retrieval accuracy.

This factor has the same impact than the use of a Karnieli2 A, B, C, or D spectrum, which increases linearly the soil reflectance and increase the variation with the vegetation reference spectrum.

4.6.7.4. Impact of the scaling factor F

F scaling factor allows to adapt the surface reflectance level retrieved by the processing to the one obtained by the linear mixing of reference spectra. It means that at the first iteration, the surface reflectances are equal to the surface reflectance obtained by the mixing of reference spectra and the NDVI. If the F factor changes, the surface reflectance is equal to 1.2 times the reflectance mixing surface reflectance.

The impact of the F factor change is low. F scaling is set to 1 in the processing.

4.6.7.5. Impact of the uncertainty in the aerosol type knowledge

The aerosol type is considered in the BAER processing as an a priori knowledge. Its influence is studied here through the use of the LUT which link the aerosol reflectance to the aerosol optical thickness. Three LUT are available in the processing: LACE 98, OPAC average continental and OPAC clean continental. They are related to the aerosol type, and single scattering albedo. The slope linking both variables is higher for continental aerosol type than for the LACE.

In this study, the reference case uses the LACE-98 aerosol type as input. The studied case uses the OPAC-Continental. The differences of the LUT are seen on the next figure, mainly in the backscattering direction.

The results are illustrated for the alta foresta site for the estimation of the AOT at 560 nm.

date	Nb pixel	Offset	Slope	r^2	rmse	Mean baer	Mean ddv	Sdt baer	Sdt ddv
5072003	5147	0.2404	1.1550	0.5548	0.2559	0.3537	0.0981	0.1193	0.0770
30042003	82484	0.2901	1.4889	0.3389	0.3501	0.4713	0.1217	0.1038	0.0406

The rmse is poor, where the correlation decreases from 80% for the reference case to 55 and 35%. The relation is highly biased. The offset of the relation is increased by a two factor.

As results of the sensitivity study, we see that the accuracy of the retrieval decreases with the change of aerosol type prior information. The coefficient of determination (r^2) does not decrease too much, but the offset of the relationship changes providing increasing of the rmse.

4.7. Conclusion

The retrieval of both aerosol optical thickness and angstrom coefficient has been made over more than 50 MERIS L2 images. The validation of the results has been made by intercomparing the BAER products with other satellite products, MERIS official products over ddv and daily MODIS atmosphere products. The comparison has been made at three channels, 412 nm, 560 nm and 865 nm. We can see that the results in the channel 1 are good, and decrease with the increase of the wavelength. However, the results are highly dependant on the cloud presence and filtering, and to the colour of the soil.

As it has been written in the ATBD, there are at least two interests for the AOT retrieval. The first one concerns the environmental study, and the second one deals with the use of the AOT product in the atmospheric correction scheme. The objectives behind the atmospheric correction processing being to estimation the biophysical variables such as LAI and fapar, which are highly depending on the red, green, and near infra red reflectance levels. The level of the minimum accuracy to have to perform the atmospheric correction is about 0.05 at 550 nm. This level is reached using the BAER processor when extreme conditions of cloudiness and soil brightness are discarded from the processing.

A sensitivity study allows to confirm the choice of the input parameter of the IBAER processor in term of aerosol characterisation. All studied factors have statistically a low impact on the results, except the prior knowledge of aerosol, which is an input of the processing. This is the reason why the choice of the parameter is let to the user and to his prior knowledge of the studied area.

4.8. Possible ways to improve the algorithm

The improvement concerns the smoothing of the AOT map. These maps have used as input of the atmospheric correction processor. When the retrieval has failed, the pixel is declared invalid, so that no surface reflectances are computed. These invalid AOTs prevent consequently the use of the processors dedicated to the estimation of biophysical products from the surface reflectances. A way to circumvent this effect could be to degrade the spatial resolution of the AOT maps using an acceptable NxN window smoothing, N to be defined, between 5 and 10 km, in order to fill a maximum of pixels, without create information.

5. Validation of surface reflectances

5.1. Introduction

The surface reflectance product results from atmospheric correction of the top of the aerosol reflectance in the 13 land bands. It is required as input for studies on Land cover/change, fire, vegetation biophysical properties (LAI, FPAR)... The accuracy of the Surface Reflectance product is mostly driven by the knowledge of the AOT. Vermote et al. 1996, report that the uncertainty on the AOT estimation involve an uncertainty on surface reflectances which varies between 0.003 and 0.008 for AOT at 550 nm of 0.1 and 0.004 to 0.18 for AOT at 550 nm of 0.5.

BAER algorithm provides aerosol estimates with good rmse over areas with dense, dark vegetation. The objectives of the study is to compare the surface reflectances obtained by the two methods integrated in BAER, by using the aerosol optical thickness estimated in the previous step. These are:

- The SMAC method, which is used for a large number of data processing, and reprocessing, in an operational mode or not (for instance, the atmospheric correction for the VEGETATION sensor re made using the SMAC method; the reprocessing of data for the CYCLOPES project (Baret et al; 2003) for AVHRR, VEGETATION is also made using SMAC, and MODIS monthly data in input.
- The UBAC method which is linked to the BAER processor because the surface reflectances are computed at each iteration until reaching the convergence of the processes. In this case, the aerosol reflectance is computed with the last aerosol optical thickness in each MERIS channel and removed from the level 2 MERIS data, according to the equations described in the ATBD.

The surface reflectance validation is a difficult exercise, because it is difficult to compare a mean directional value of surface reflectance with a reflectance measured at ground level by an instrument. The pixel heterogeneity (1 km) prevents to compare both measurements.

Within this paragraph, we compared the surface reflectances estimated with both methods in four channels: Channel 1, 5, 7 and 13.

5.2. Results

5.2.1. Presentation

The results are represented for each selected image and for channels 2, 5 7 and 13:

Table 6:Table showing how the results are summarised.

<u>Surface reflectance in channel 2, 5, 7 or 13 estimated using SMAC</u>	<u>Surface reflectance in channel 2, 5, 7 or 13 estimated using UBAC</u>
<u>Surface reflectance difference</u> SMAC minus UBAC	<u>Histogram of surface reflectance difference.</u> The title of this image provide with the date of

	acquisition, the channel number, the mean of the difference, and the standard deviation of the difference.
<u>AOT map at 550 nm</u>	<u>Histogram of AOT at 550 nm</u>

An example of image acquired over South of France and Italy is given hereafter.

For all channels, we can see that the SMAC method provides higher values of surface reflectances. The mean of the difference is about 0.02 for the three first channels, whereas it is 0.04 in the near infrared channel. Where the AOT at 550 is less than 0.2, the results are equivalent, whereas when the AOT increases (due to higher value or non clear pixel), the UBAC value are very low, or provide negative values which are set to 0, with an flag declared as invalid.

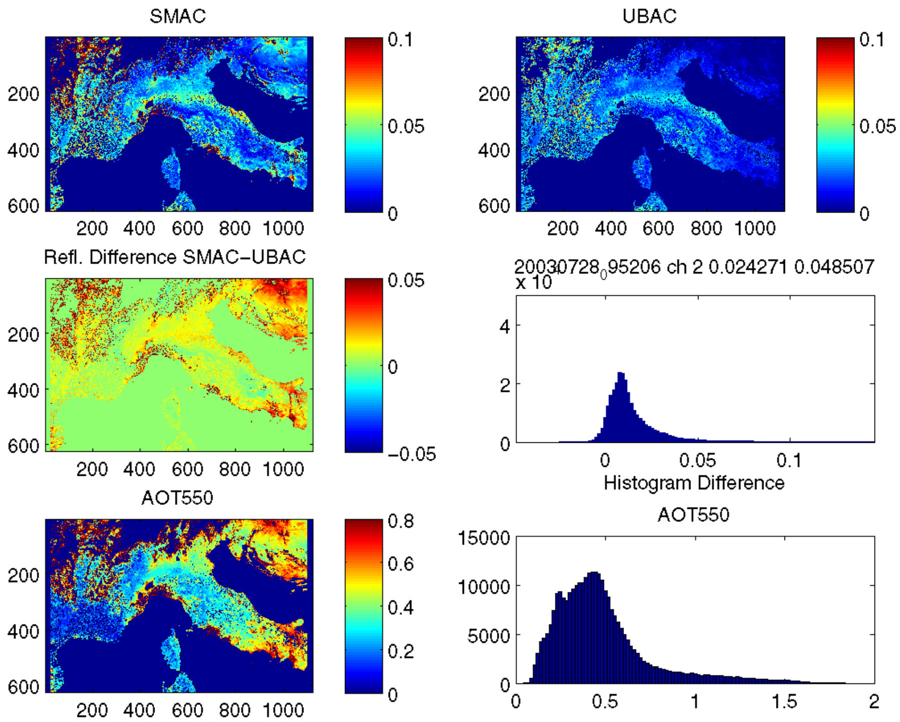

Figure 35: Results for channel 2

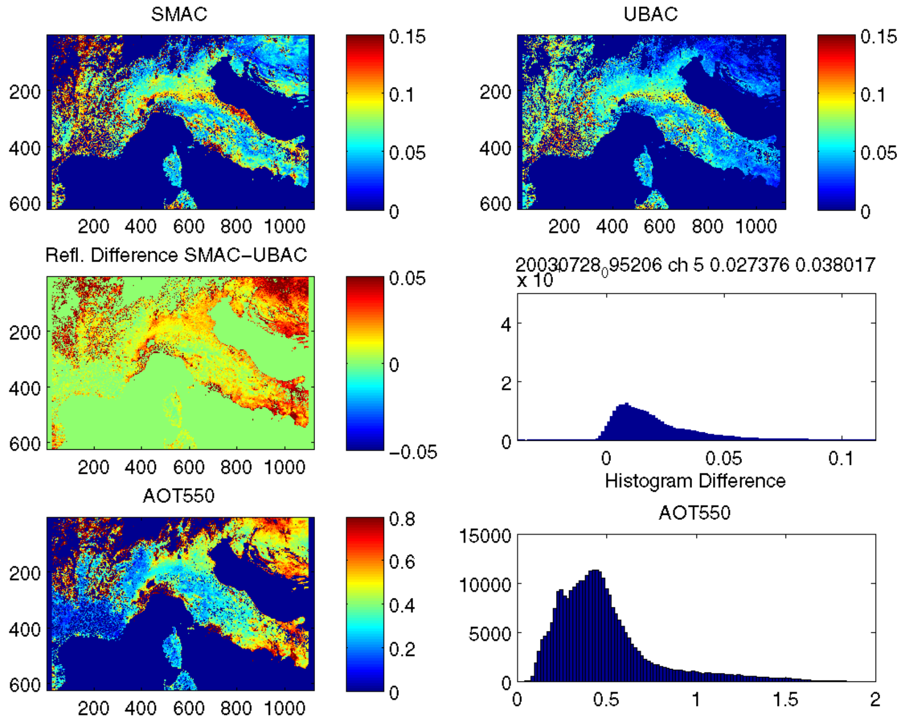

Figure 36: Results for channel 5

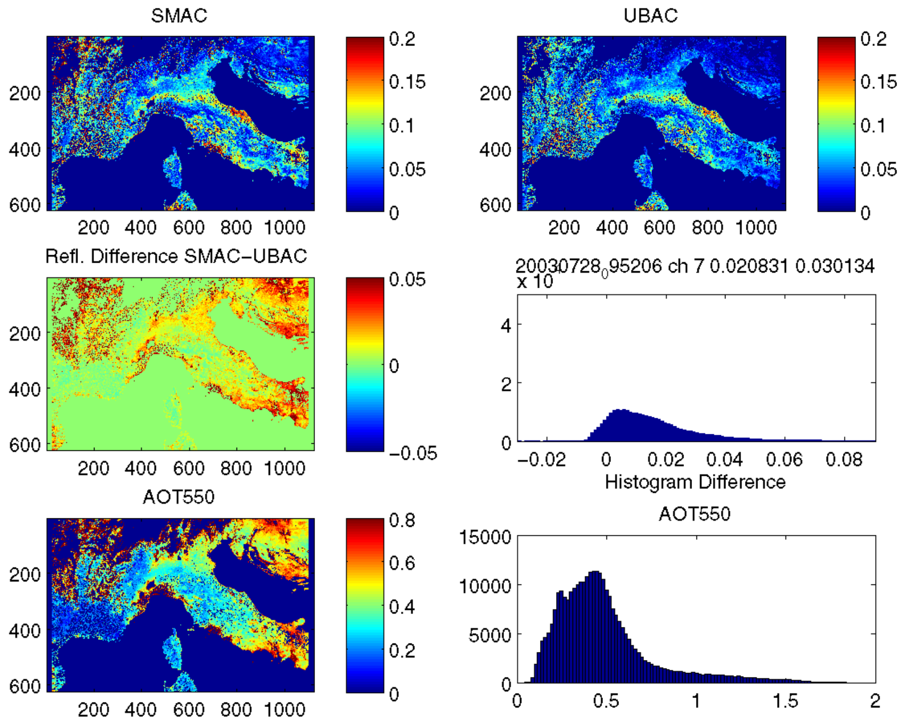

Figure 37: Results for channel 7

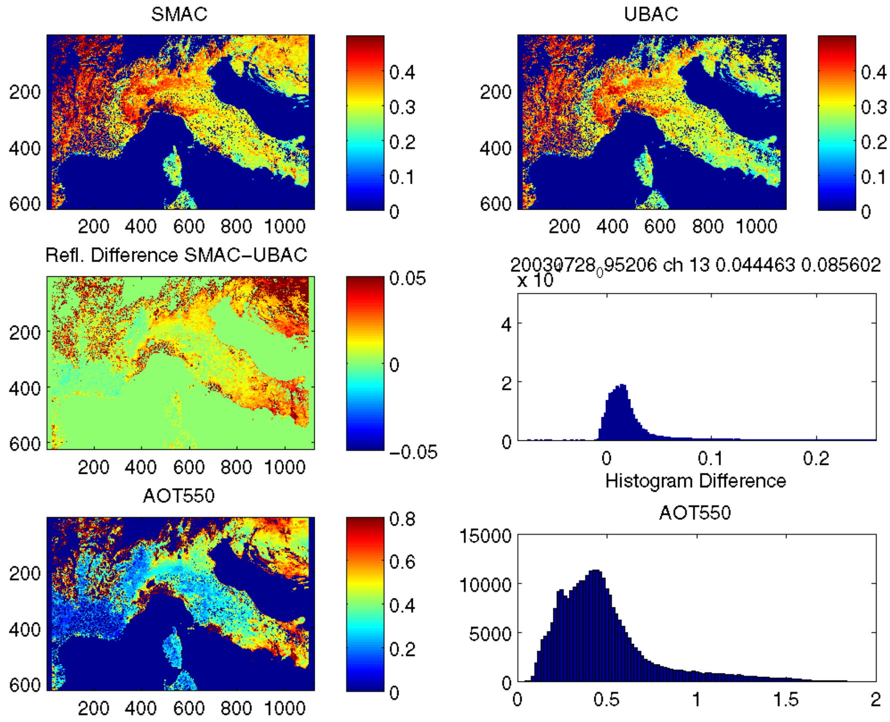

Figure 38: Results for channel 13

5.2.2. Summary of the differences for the other images

The following table provides the statistical results obtained for all images.

Table 7: results of the difference of surface reflectances SMAC – UBAC for the MERIS dataset.

Date	Mean difference	Standard deviation of the difference
Channel 2 -22/03	0.0295	0.0328
Ch 5	0.025	0.028
Ch 7	0.020	0.024
Ch 13	0.011	0.026
Ch.2 – 30/04	0.0099	0.026
Ch 5	0.0085	0.022
Ch 7	0.005	0.018
Ch 13	0.006	0.038
Ch2- 23/05	0.027	0.069
Ch 5	0.024	0.057
Ch 7	0.019	0.05
Ch 13	0.027	0.081
Ch2- 01/06	0.034	0.064

Date	Mean difference	Standard deviation of the difference
Ch 5	0.035	0.051
Ch 7	0.028	0.042
Ch 13	0.043	0.076
Ch2-16/06	0.017	0.043
Ch 5	0.016	0.036
Ch 7	0.010	0.028
Ch 13	0.021	0.07
Ch2- 21/06	0.016	0.046
Ch 5	0.014	0.038
Ch 7	0.008	0.03
Ch 13	0.039	0.1099
Ch2 – 11/07	0.014	0.033
Ch 5	0.016	0.028
Ch 7	0.012	0.022
Ch 13	0.023	0.082
Ch2- 28/07	0.024	0.048
Ch 5	0.027	0.038
Ch 7	0.020	0.030
Ch 13	0.044	0.085
Ch2-02/08	0.008	0.023
Ch 5	0.010	0.019
Ch 7	0.0076	0.016
Ch 13	0.008	0.025
Ch2-25/08	0.0334	0.067
Ch 5	0.034	0.051
Ch 7	0.028	0.042
Ch 13	0.028	0.051
Ch2-15/09	0.014	0.0314
Ch 5	0.014	0.025
Ch 7	0.011	0.021
Ch 13	0.0103	0.034
Ch2-15/09	0.009	0.028
Ch 5	0.014	0.024
Ch 7	0.013	0.023
Ch 13	0.012	0.034

Date	Mean difference	Standard deviation of the difference
Ch2-18/11	0.012	0.04
Ch 5	0.013	0.033
Ch 7	0.011	0.028
Ch 13	0.013	0.032
Ch2-21/11	0.03	0.065
Ch 5	0.02	0.057
Ch 7	0.018	0.052
Ch 13	0.027	0.096

The mean of the difference is about 1 or 2%, except on the channel 13 on area where the AOT is high (for the date 28/7 and 21/06). In this case, the standard deviation of the reflectance difference is higher than in the other channels. The standard deviation is a good indicator of cloudy pixel presence which is not detected by the filtering. For these pixels, the AOT is high, and clouds or sub pixels clouds are assimilated to clear pixels and processed as if they were valid.

Over clear area, the mean difference is about 1%.

5.3. Conclusion

The comparison of surface reflectance between the two methods shows the same trends as shown previously on all the images. The aerosol reflectance computed by UBAC is higher than the one computed by SMAC. This leads to have SMAC surface reflectance higher than UBAC surface reflectances in the four channels. The impact of the differences is not the same in the red visible channel than in the NIR channels. The study trends to conclude that the difference is low, about in mean 1 to 2%.

5.4. Possible ways to validate the surface reflectance results

To complete the validation process, ground measurement of the surface reflectance could be compared to results obtained using full resolution of MERIS data. The use of the Barrax database acquired during the SPARC measurement campaign is a possibility.

6. Conclusion

The processor developed in the frame work of the study has been developed to be integrated to the BEAM software, whose aim is to facilitate the utilisation, the viewing and processing of ESA MERIS, data. The IBAER developed will complement the collection of existing executable tools. Its use has a great interest because it allows to achieve the processing of the Level 2 MERIS by removing the aerosol signal, providing both aerosol optical thickness and surface reflectances in the thirteen MERIS channels.

In this study, we have presented the results of the validation of both atmosphere products (aerosol optical thickness and angstrom exponent), and surface reflectances. The validation has been performed in an indirect way (using satellite data) and by direct way, by comparing the results to in situ sun photometer measurements of the AERONET network.

The correlation between products varies with the channel. It is good at 412 nm, and 550 nm. The accuracy of the retrieval against the ddv is less than 0.1 at 550 nm, with better value when the land cover is not very bright. The method provides more results than the one which is in the operational ESA processor. It is not applicable only over dark target, but can be extended to almost most surface type. The case of bright surface provides however results with less accuracy.

Once the AOT estimated, the atmospheric process can be applied. Two methods are compared in this report. They provided results with a few difference in the visible channels (in the order of 1 to 2 %).

We note at this time, that the cloud filtering which has been assessed in dedicated section is not reliable enough to remove all clouds. This provides high value of Aerosol optical thickness, and inaccurate surface reflectances. SMAC seems more resistant to these high values where UBAC provides negatives values of surface reflectances.

The validation has been performed on more than 50 MERIS images. All the results are summarised in the annexe report, referred by NOV-3341-NT-3292.

7. Annex 1 : List of the selected MERIS products

Alta_Foresta:

- MER_RR__2PP01R20030430_132600_000001072016_00024_06090_0001.N1
- MER_RR__2PP01R20030709_132602_000001072018_00024_07092_0001.N1
- MER_RR__2PP01R20030725_132315_000001102018_00253_07321_0001.N1
- MER_RR__2PP01R20030810_132026_000001102018_00482_07550_0001.N1

Bondville

- MER_RR__2PP01R20030323_162735_000001072014_00484_05548_0001.N1
- MER_RR__2PP01R20030401_164427_000001072015_00112_05677_0001.N1
- MER_RR__2PP01R20030620_163016_000001102017_00255_06822_0001.N1
- MER_RR__2PP01R20030621_155918_000001102017_00269_06836_0001.N1
- MER_RR__2PP01R20030920_163857_000001072020_00069_08139_0001.N1
- MER_RR__2PP01R20030924_161333_000001102020_00126_08196_0001.N1
- MER_RR__2PP01R20031022_163309_000001102021_00026_08597_0001.N1
- MER_RR__2PP01R20031120_162159_000001102021_00441_09012_0001.N1
- MER_RR__2PP01R20031129_163852_000001102022_00069_09141_0001.N1

Bordeaux

- MER_RR__2PP01R20030619_101753_000001102017_00237_06804_0001.N1
- MER_RR__2PP01R20030711_102624_000001072018_00051_07119_0001.N1
- MER_RR__2PP01R20030802_103459_000001102018_00366_07434_0001.N1
- MER_RR__2PP01R20030825_101253_000001072019_00194_07763_0001.N1
- MER_RR__2PP01R20030915_105232_000001102019_00495_08064_0001.N1

GSFC

- MER_RR__2PP01R20030324_155531_000001072014_00498_05562_0001.N1
- MER_RR__2PP01R20030325_152423_000001072015_00011_05576_0001.N1
- MER_RR__2PP01R20031030_154125_000001072021_00140_08711_0001.N1
- MER_RR__2PP01R20031121_154959_000001072021_00455_09026_0001.N1

HOWLAND

- MER_RR__2PP01R20030616_151327_000001102017_00197_06764_0001.N1

ISPRA

- MER_RR__2PP01R20030620_094622_000001072017_00251_06818_0001.N1
- MER_RR__2PP01R20030706_094331_000001102017_00480_07047_0001.N1
- MER_RR__2PP01R20030722_094006_000001072018_00208_07276_0001.N1
- MER_RR__2PP01R20030725_094625_000001102018_00251_07319_0001.N1
- MER_RR__2PP01R20030728_095206_000001102018_00294_07362_0001.N1
- MER_RR__2PP01R20030804_093123_000001102018_00394_07462_0001.N1
- MER_RR__2PP01R20030810_094352_000001072018_00480_07548_0001.N1
- MER_RR__2PP01R20030813_094931_000001102019_00022_07591_0001.N1
- MER_RR__2PP01R20030823_093507_000001072019_00165_07734_0001.N1

LAMPEDUSA

- MER_RR__2PP01R20030601_094456_000001072016_00480_06546_0001.N1
- MER_RR__2PP01R20030611_093044_000001102017_00122_06689_0001.N1
- MER_RR__2PP01R20030722_094215_000001072018_00208_07276_0001.N1

LILLE

- MER_RR__2PP01R20030322_101214_000001102014_00466_05530_0001.N1
- MER_RR__2PP01R20030322_101236_000001072014_00466_05530_0001.N1
- MER_RR__2PP01R20030616_101043_000001102017_00194_06761_0001.N1
- MER_RR__2PP01R20030714_102954_000001102018_00094_07162_0001.N1

MARICOPA

- MER_RR__2PP01R20030116_174256_000001072013_00041_04604_0001.N1
- MER_RR__2PP01R20030119_174836_000001072013_00084_04647_0001.N1
- MER_RR__2PP01R20030129_173427_000001072013_00227_04790_0001.N1
- MER_RR__2PP01R20030204_174545_000001102013_00313_04876_0001.N1
- MER_RR__2PP01R20030311_174615_000001072014_00313_05377_0001.N1
- MER_RR__2PP01R20030330_174838_000001072015_00084_05649_0001.N1
- MER_RR__2PP01R20030330_174917_000001072015_00084_05649_0001.N1
- MER_RR__2PP01R20030504_174917_000001072016_00084_06150_0001.N1
- MER_RR__2PP01R20030510_180035_000001072016_00170_06236_0001.N1
- MER_RR__2PP01R20030621_174047_000001102017_00270_06837_0001.N1
- MER_RR__2PP01R20030707_173722_000001072017_00499_07066_0001.N1
- MER_RR__2PP01R20030710_174329_000001102018_00041_07109_0001.N1
- MER_RR__2PP01R20030713_174843_000001072018_00084_07152_0001.N1
- MER_RR__2PP01R20030713_174911_000001072018_00084_07152_0001.N1
- MER_RR__2PP01R20030912_173149_000001072019_00456_08025_0001.N1
- MER_RR__2PP01R20030912_173225_000001072019_00456_08025_0001.N1
- MER_RR__2PP01R20030915_173728_000001102019_00499_08068_0001.N1
- MER_RR__2PP01R20030915_173807_000001072019_00499_08068_0001.N1
- MER_RR__2PP01R20030918_174337_000001072020_00041_08111_0001.N1
- MER_RR__2PP01R20030921_174916_000001072020_00084_08154_0001.N1
- MER_RR__2PP01R20030928_172931_000001072020_00184_08254_0001.N1
- MER_RR__2PP01R20030928_172948_000001072020_00184_08254_0001.N1
- MER_RR__2PP01R20031017_173212_000001102020_00456_08526_0001.N1
- MER_RR__2PP01R20031020_173800_000001102020_00499_08569_0001.N1
- MER_RR__2PP01R20031023_174331_000001102021_00041_08612_0001.N1
- MER_RR__2PP01R20031026_174920_000001102021_00084_08655_0001.N1
- MER_RR__2PP01R20031105_173431_000001102021_00227_08798_0001.N1
- MER_RR__2PP01R20031121_173142_000001102021_00456_09027_0001.N1
- MER_RR__2PP01R20031127_174332_000001102022_00041_09113_0001.N1

MONGU

- MER_RR__2PP01R20030421_080806_000001102015_00393_05958_0001.N1
- MER_RR__2PP01R20030507_080515_000001072016_00121_06187_0001.N1
- MER_RR__2PP01R20030523_080222_000001072016_00350_06416_0001.N1
- MER_RR__2PP01R20030614_081057_000001072017_00164_06731_0001.N1
- MER_RR__2PP01R20030709_082507_000001102018_00021_07089_0001.N1
- MER_RR__2PP01R20030807_081352_000001102018_00436_07504_0001.N1

SKUKUZA

- MER_RR__2PP01R20030429_071914_000001072016_00006_06072_0001.N1
- MER_RR__2PP01R20030524_073317_000001102016_00364_06430_0001.N1
- MER_RR__2PP01R20031109_072206_000001072021_00278_08849_0001.N1
- MER_RR__2PP01R20031118_073905_000001072021_00407_08978_0001.N1

8. Annexe 2 : Overview of the Input/Ouput data of the IBAER processor

8.1. Input Data

Top of aerosol reflectances

- L2 Top of aerosol reflectance Channel 1
- L2 Top of aerosol reflectance Channel 2
- L2 Top of aerosol reflectance Channel 3
- L2 Top of aerosol reflectance Channel 4
- L2 Top of aerosol reflectance Channel 5
- L2 Top of aerosol reflectance Channel 6
- L2 Top of aerosol reflectance Channel 7
- L2 Top of aerosol reflectance Channel 8
- L2 Top of aerosol reflectance Channel 9
- L2 Top of aerosol reflectance Channel 10
- L2 Top of aerosol reflectance Channel 12
- L2 Top of aerosol reflectance Channel 13
- L2 Top of aerosol reflectance Channel 14

L2_Flags

Pressure

Tie-point information

- Solar and satellite zenith angles
- Solar and satellite azimuth angles
- Geographical coordinates

8.2. Products

The outputs of the processor are

CLOUD products

Cloud mask

ATMOSPHERE products

- The angstrom exponent ALPHA
- The Aerosol Optical Thickness at 412nm
- The Aerosol Optical Thickness AOT at 440 nm

- The Aerosol Optical Thickness AOT at 550 nm

SURFACE REFLECTANCE products

- L2 Surface reflectance Channel 1
- L2 Surface reflectance Channel 2
- L2 Surface reflectance Channel 3
- L2 Surface reflectance Channel 4
- L2 Surface reflectance Channel 5
- L2 Surface reflectance Channel 6
- L2 Surface reflectance Channel 7
- L2 Surface reflectance Channel 8
- L2 Surface reflectance Channel 9
- L2 Surface reflectance Channel 10
- L2 Surface reflectance Channel 12
- L2 Surface reflectance Channel 13
- L2 Surface reflectance Channel 14

Quality indicator (Flag channel)

The quality indicator contains seven fields which qualify the quality of the input and the quality of the output. The value of the flag channel is the sum of the fields which are activated (true).

Flag denomination	Value if true	Valid if false
Invalid	1	0
Invalid_Input	2	0
Cloud_input	8	0
ALPHA_OUT_OF_RANGE	16	0
AOT_OUT_OF_RANGE	32	0
Invalid_output	64	0
Smac_correction	128	0

9. Annexe 3: Extensive cloud detection assessment on L2 MERIS data

The following images represents the IBAER cloud mask over the coloured composition Of MERIS surface reflectance products. The blue values indicate the Level 2 cloud mask. The red values are the pixels that are detected by the BAER.

AltaForesta

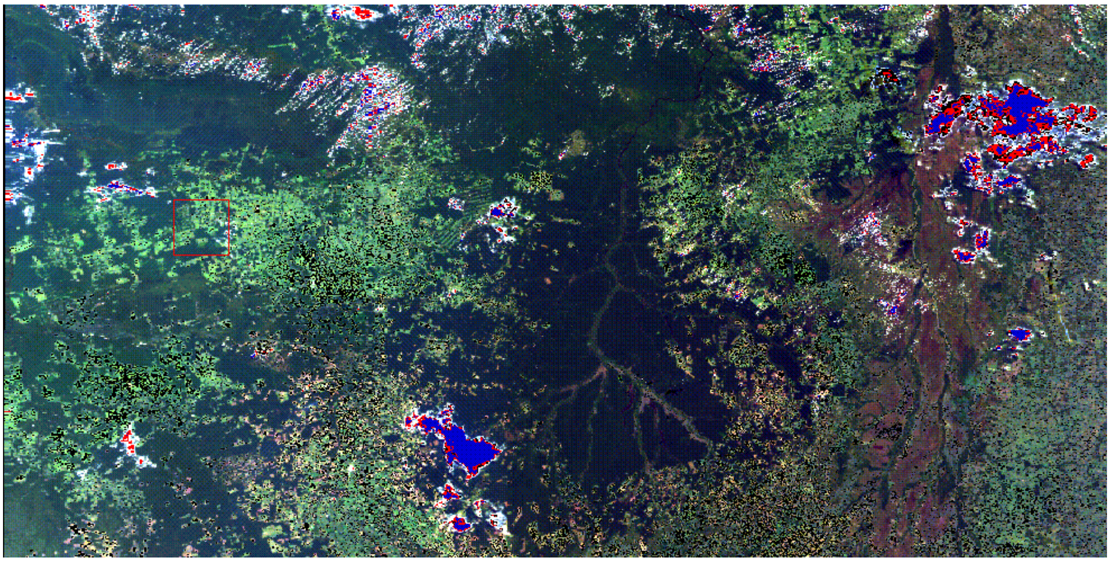

Bondville

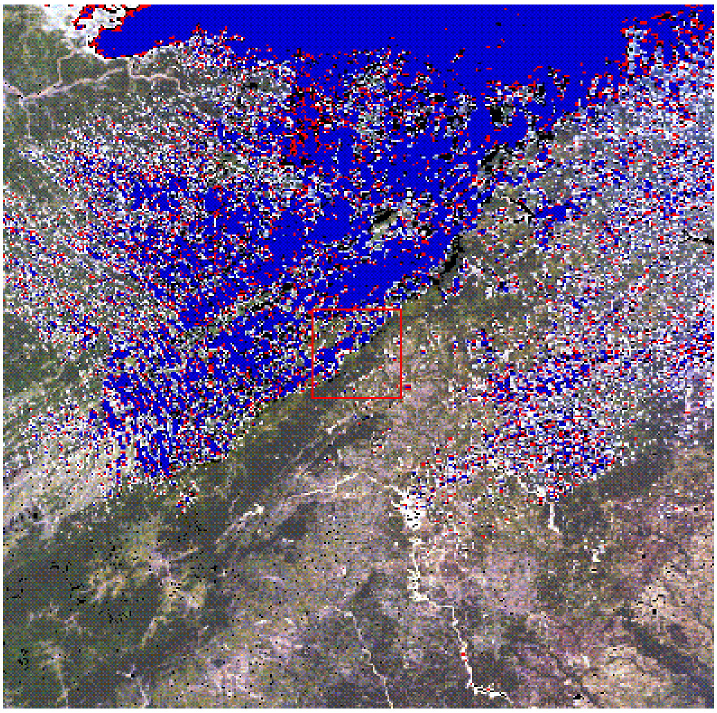

Bordeaux-

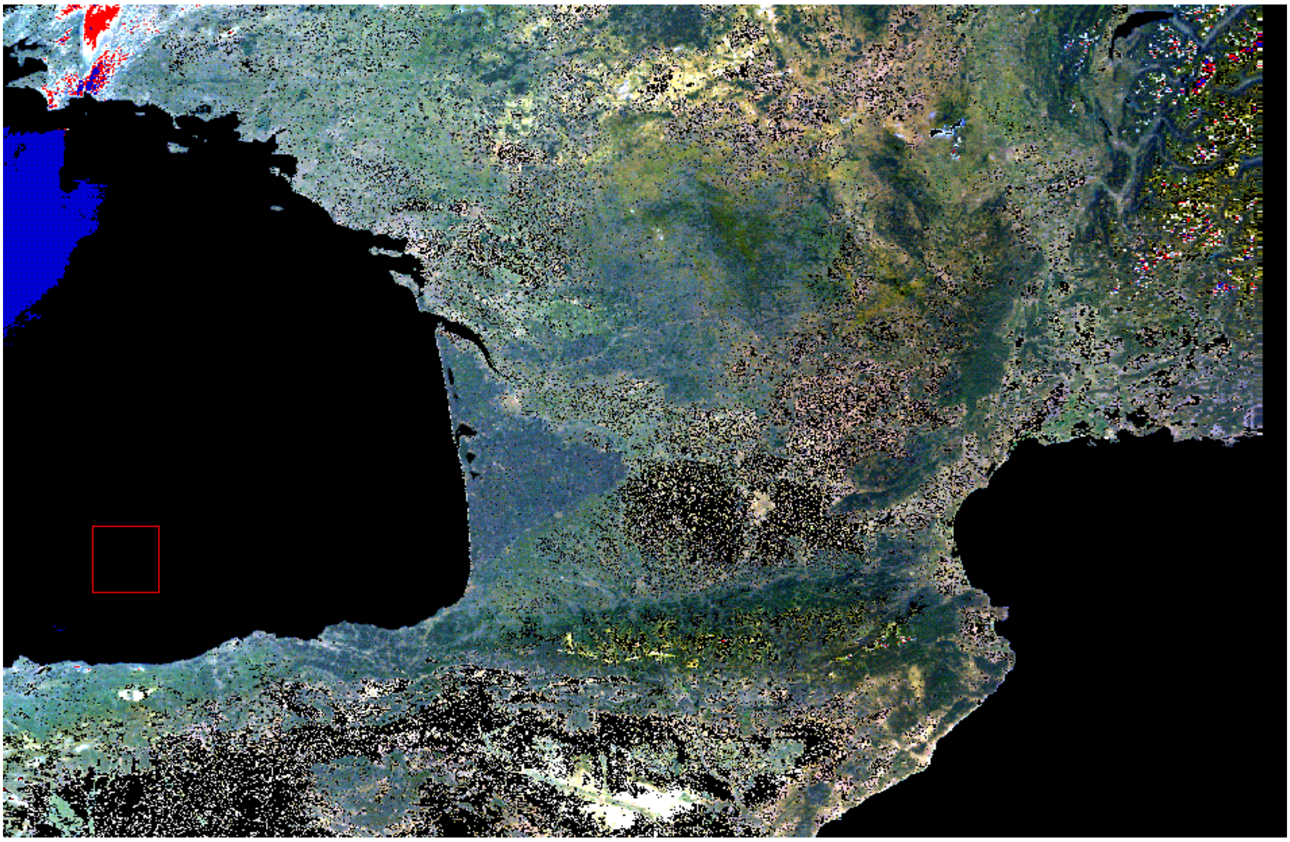

BORDEAUX

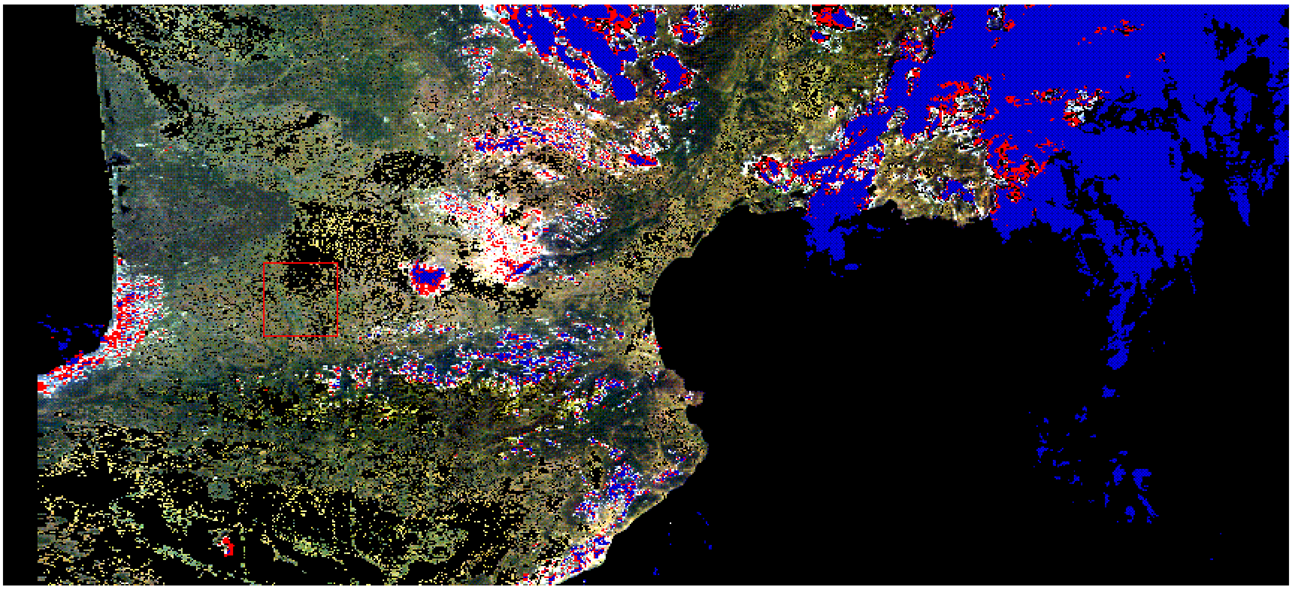

BORDEAUX

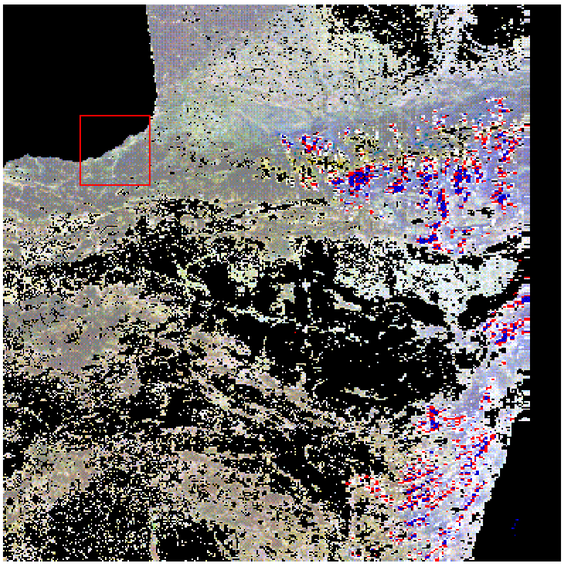

South of France

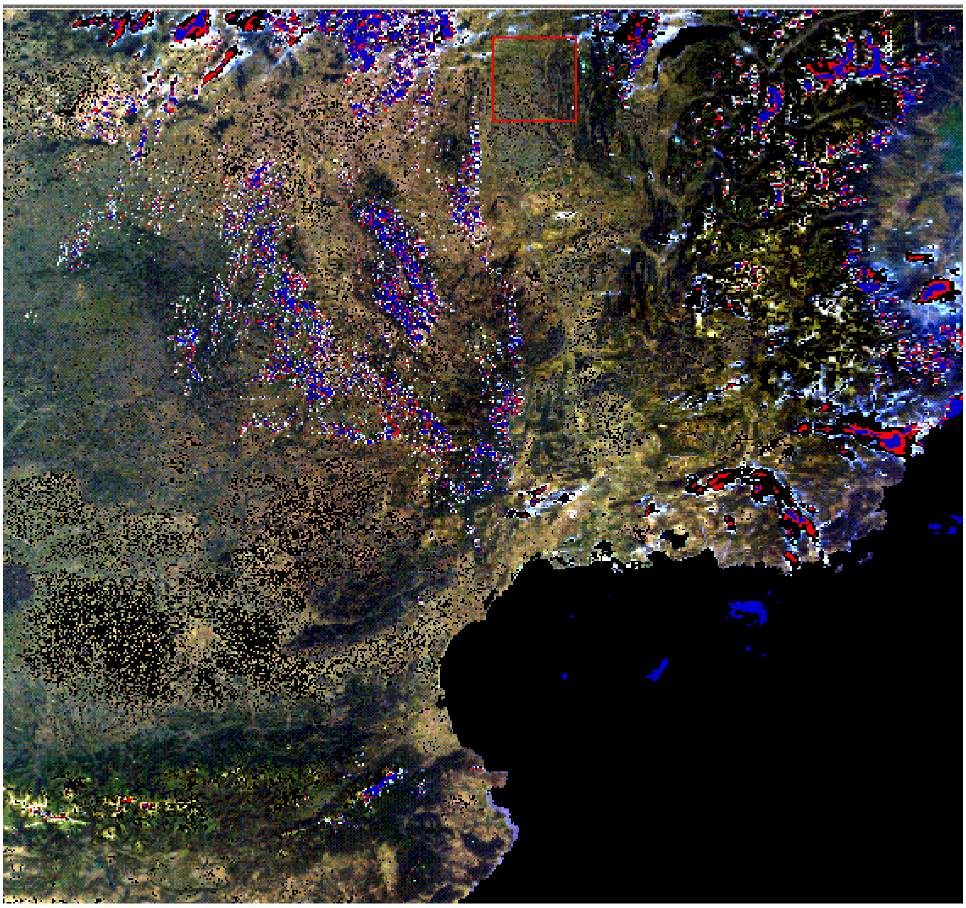

Lande forest

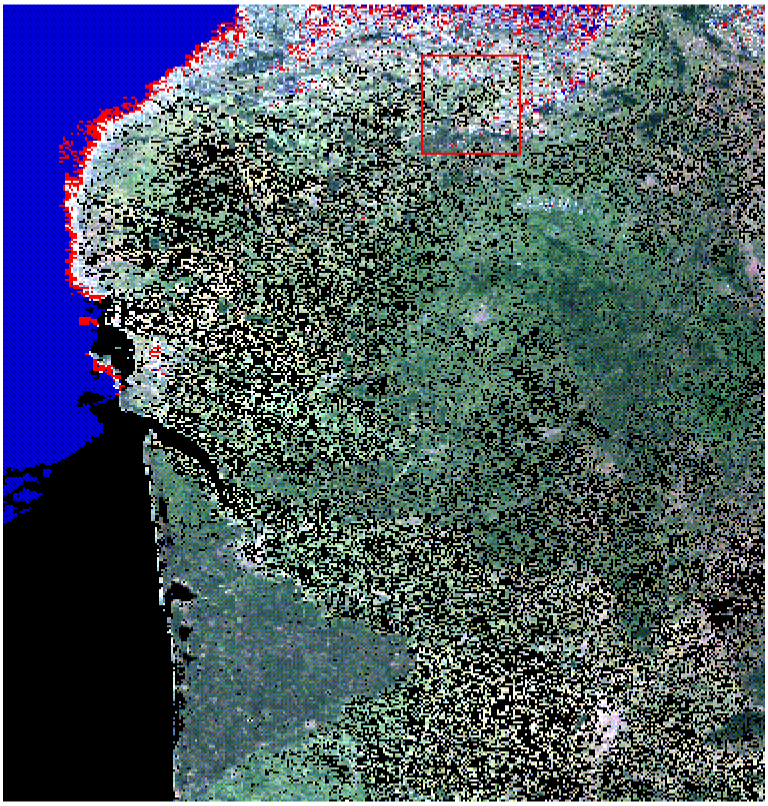

GFSC

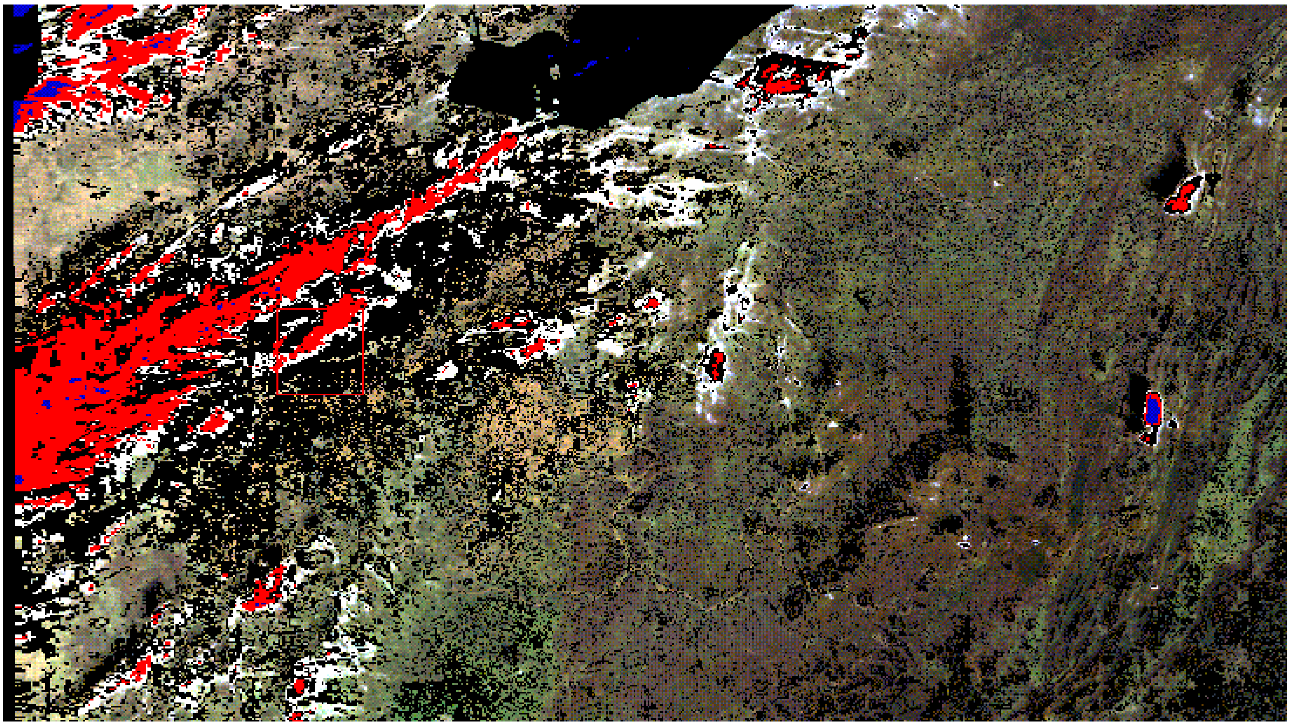

Howkland

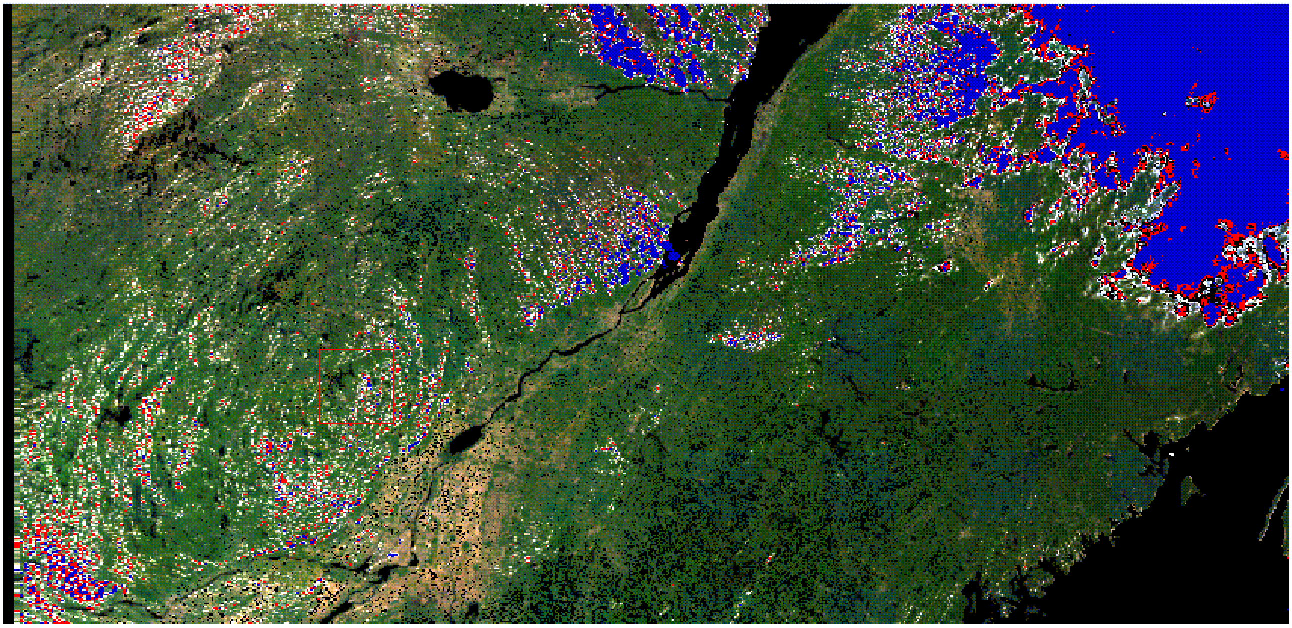

Ispra

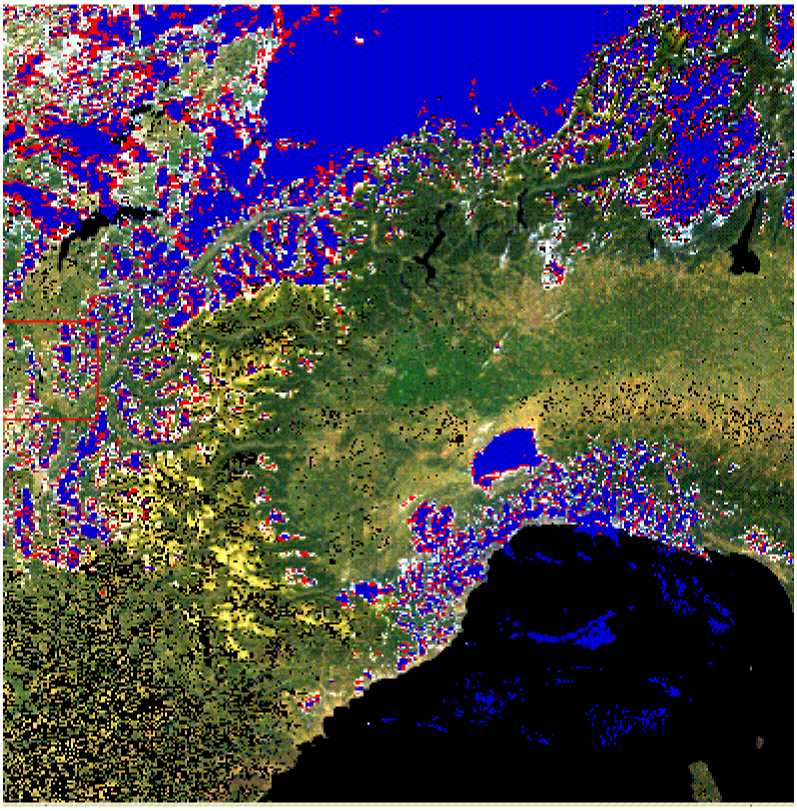

Lampedusa

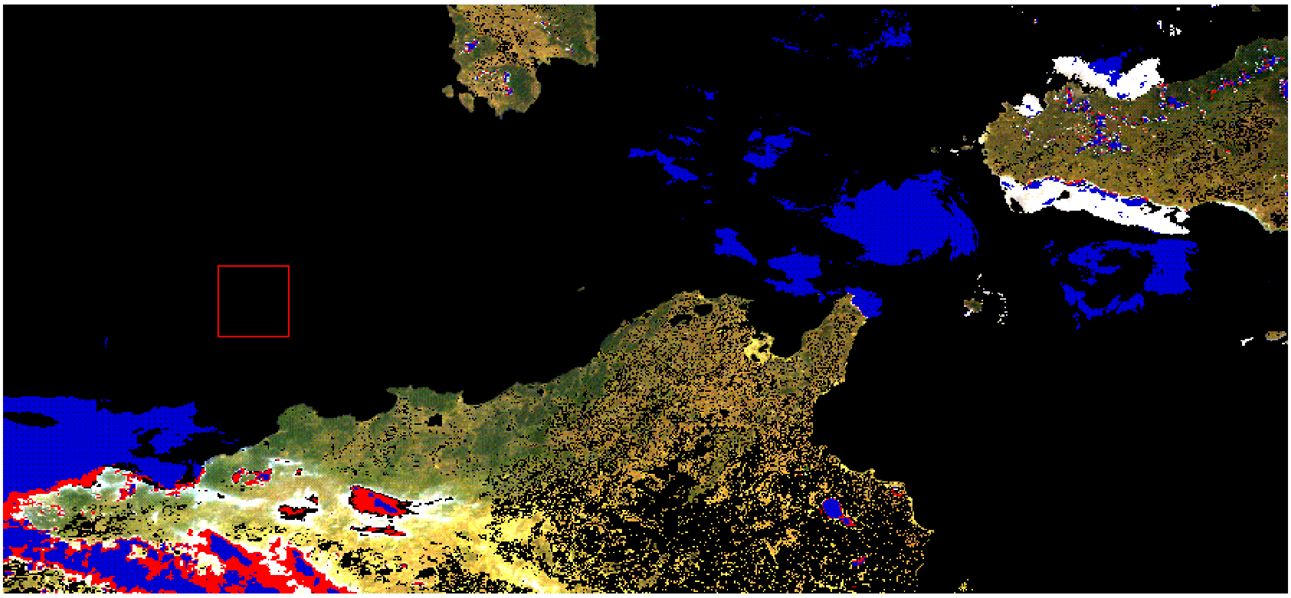

Lille

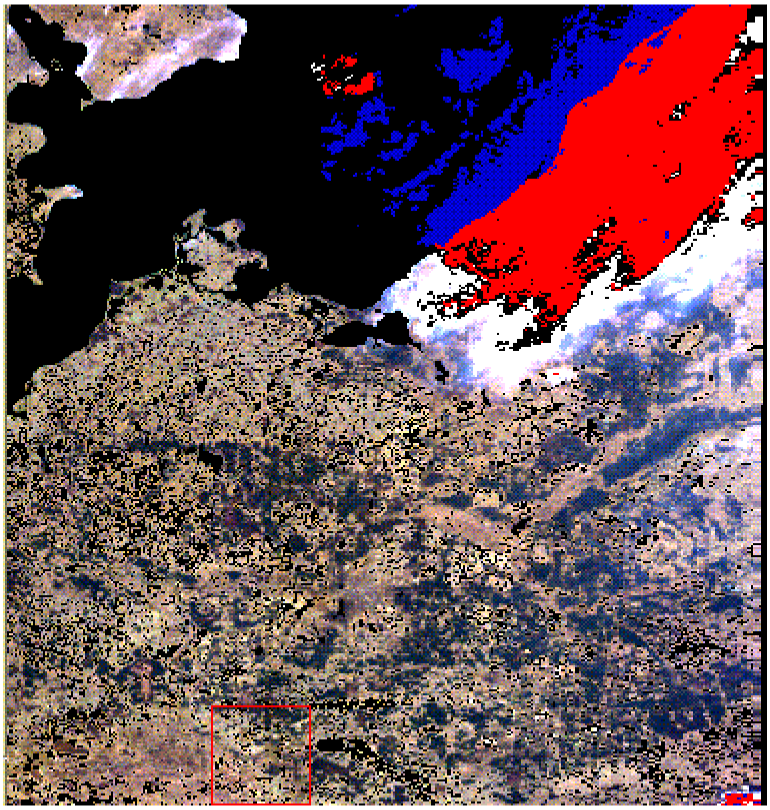

Maricopa

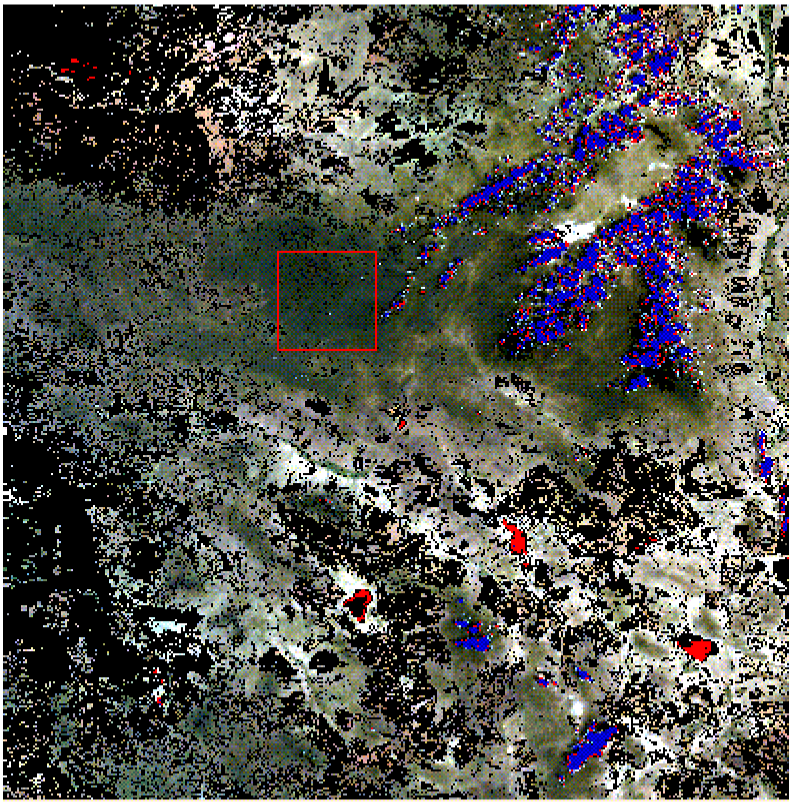

Mongu

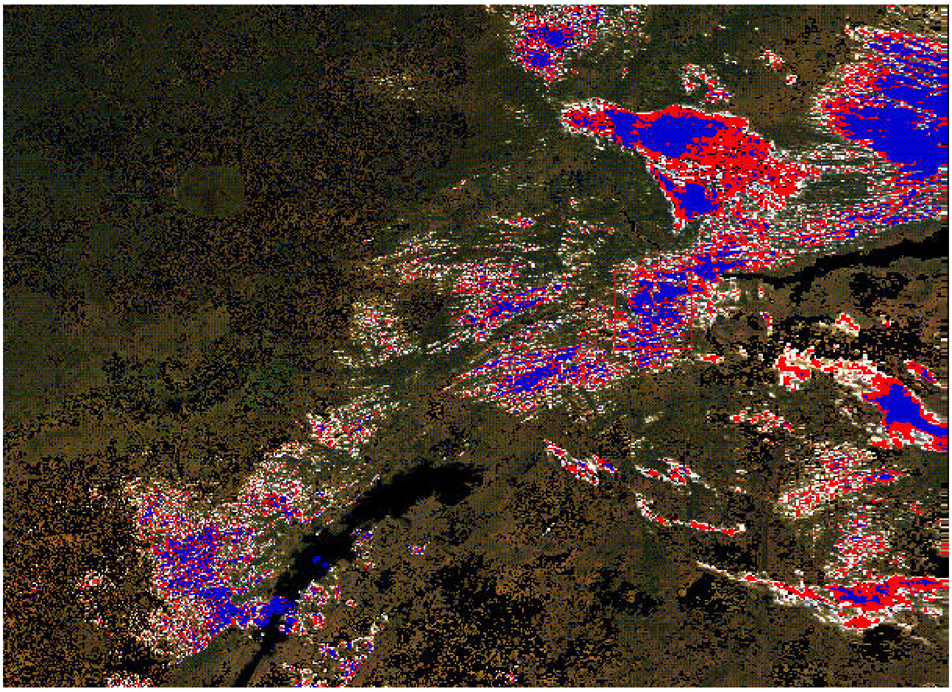

SKUKUZA -

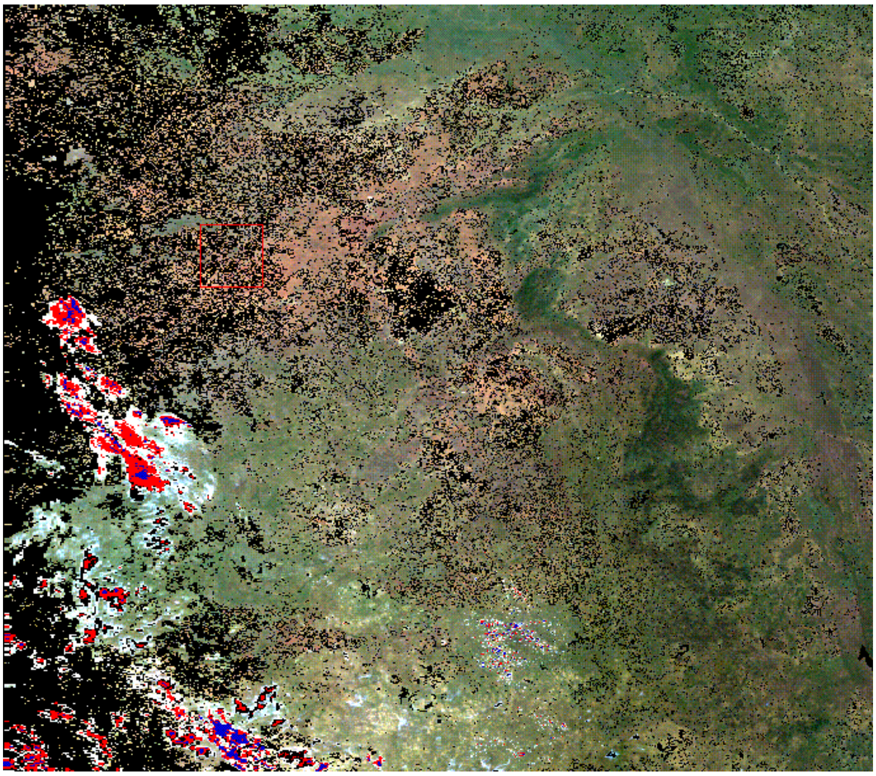

10. Annexe 4 : results of the comparison between BAER AOT and AOT over DDV

The results are summarised in tables containing

Column (1) is the site

Column (2) is the acquisition date of the analysed image

Column (3) is the acquisition hour of the analysed image

Column (4) is the variable analysed in the regression (baer versus ddv)

Column (5) is the number of pixels used in the analysis

Column (6) is the offset of the linear regression

Column (7) is the slope of the linear regression

Column (8) is the determination coefficient (r^2)

Column (9) is the root mean square error (rmse)

Column (10) is the mean baer

Column (11) is the mean ddv

Column (12) is the standard deviation baer

Column (13) is the standard deviation ddv

10.1. Alta Foresta

Site	date	hour	variable	Nb pixel	Offset	Slope	R2	rmse	Mean baer	Mean ddv	Sdt baer	Sdt ddv
Alta_Foresta	25072003	132315	alpha	14007	0.5631	0.1459	0.0268	0.4572	0.6245	0.4212	0.4277	0.4795
Alta_Foresta	30042003	132600	alpha	158811	0.5675	-0.0262	0.0023	0.3914	0.5557	0.4518	0.1996	0.3678
Alta_Foresta	09072003	132602	alpha	141599	0.7935	-0.0570	0.0063	0.4890	0.7704	0.4048	0.2212	0.3073
Alta_Foresta	10082003	132026	alpha	134590	0.5228	0.1323	0.0451	0.2967	0.5740	0.3875	0.1656	0.2660
Alta_Foresta	25072003	132315	aot412	14007	0.1219	0.7376	0.9571	0.0869	0.2308	0.1475	0.0721	0.0956
Alta_Foresta	30042003	132600	aot412	158811	0.1220	0.8680	0.8903	0.1030	0.2493	0.1467	0.0609	0.0662
Alta_Foresta	09072003	132602	aot412	141599	0.0881	0.9419	0.9453	0.0710	0.3704	0.2997	0.1228	0.1267
Alta_Foresta	10082003	132026	aot412	134590	0.0571	1.0694	0.9327	0.0768	0.3545	0.2782	0.1336	0.1207
Alta_Foresta	25072003	132315	aot560	14007	0.0868	0.7021	0.8465	0.0533	0.1834	0.1376	0.0699	0.0917
Alta_Foresta	30042003	132600	aot560	158811	0.1044	0.7403	0.6781	0.0724	0.2003	0.1296	0.0532	0.0592
Alta_Foresta	09072003	132602	aot560	141599	0.0821	0.7742	0.8260	0.0326	0.2878	0.2657	0.0905	0.1063
Alta_Foresta	10082003	132026	aot560	134590	0.0514	0.9633	0.8659	0.0425	0.2889	0.2465	0.1028	0.0993
Alta_Foresta	25072003	132315	aot860	14007	0.0891	0.5043	0.6382	0.0507	0.1526	0.1258	0.0548	0.0868
Alta_Foresta	30042003	132600	aot860	158811	0.1176	0.4336	0.3552	0.0628	0.1653	0.1100	0.0383	0.0527
Alta_Foresta	09072003	132602	aot860	141599	0.1091	0.4243	0.4862	0.0532	0.2047	0.2255	0.0518	0.0851
Alta_Foresta	10082003	132026	aot860	134590	0.0856	0.6760	0.6370	0.0307	0.2269	0.2089	0.0653	0.0771

10.2. BONDVILLE

Site	date	hour	variable	Nb pixel	Offset	Slope	R2	rmse	Mean baer	Mean ddv	Sdt baer	Sdt ddv
BONDVILLE	21062003	155918	alpha	134338	0.8588	0.0760	0.0062	0.5287	0.8982	0.5187	0.3845	0.3984
BONDVILLE	24092003	161333	alpha	123198	0.5964	-0.0010	0.0000	0.4824	0.5957	0.8062	0.3698	0.4336
BONDVILLE	20112003	162159	alpha	29	1.3927	-0.1237	0.0187	0.7471	1.2707	0.9862	0.5661	0.6256
BONDVILLE	23032003	162735	alpha	16194	0.4131	0.0599	0.0092	0.4095	0.4512	0.6349	0.2435	0.3893
BONDVILLE	20062003	163016	alpha	99119	0.7807	0.0690	0.0071	0.4287	0.8178	0.5370	0.2850	0.3480
BONDVILLE	22102003	163309	alpha	817	0.5573	0.0006	0.0000	0.8733	0.5580	1.1337	0.3877	0.6574
BONDVILLE	20092003	163857	alpha	46328	0.6764	-0.0292	0.0014	0.4653	0.6530	0.8011	0.3367	0.4285
BONDVILLE	01042003	164427	alpha	84	0.4685	0.0484	0.0022	0.4674	0.4929	0.5038	0.5065	0.4939
BONDVILLE	21062003	155918	aot412	134338	0.0786	1.0381	0.9373	0.0915	0.4214	0.3303	0.2376	0.2216
BONDVILLE	24092003	161333	aot412	123198	0.1044	1.1901	0.8988	0.1363	0.2940	0.1594	0.1407	0.1121
BONDVILLE	20112003	162159	aot412	29	0.1247	0.6328	0.3544	0.1149	0.1417	0.0269	0.0168	0.0158
BONDVILLE	23032003	162735	aot412	16194	0.1014	1.0459	0.8793	0.1175	0.4601	0.3429	0.1957	0.1754
BONDVILLE	20062003	163016	aot412	99119	0.1087	0.8623	0.9182	0.0632	0.4679	0.4166	0.2413	0.2682
BONDVILLE	22102003	163309	aot412	817	0.1617	0.6998	0.7293	0.1245	0.2537	0.1314	0.0643	0.0784
BONDVILLE	20092003	163857	aot412	46328	0.1165	1.0557	0.9395	0.1273	0.3161	0.1891	0.1719	0.1578
BONDVILLE	01042003	164427	aot412	84	0.1520	0.6555	0.8787	0.0838	0.3005	0.2265	0.0801	0.1146
BONDVILLE	21062003	155918	aot560	134338	0.0515	0.9430	0.8138	0.0372	0.3135	0.2778	0.1901	0.1818
BONDVILLE	24092003	161333	aot560	123198	0.0947	1.0898	0.7838	0.1065	0.2333	0.1272	0.1115	0.0906

Site	date	hour	variable	Nb pixel	Offset	Slope	R2	rmse	Mean baer	Mean ddv	Sdt baer	Sdt ddv
BONDVILLE	20112003	162159	aot560	29	0.0864	0.3209	0.0175	0.0730	0.0930	0.0206	0.0347	0.0143
BONDVILLE	23032003	162735	aot560	16194	0.1536	0.8151	0.7988	0.1041	0.3905	0.2906	0.1448	0.1588
BONDVILLE	20062003	163016	aot560	99119	0.0534	0.8496	0.8613	0.0320	0.3490	0.3480	0.1949	0.2129
BONDVILLE	22102003	163309	aot560	817	0.1496	0.5791	0.4711	0.1113	0.2089	0.1025	0.0654	0.0776
BONDVILLE	20092003	163857	aot560	46328	0.1053	0.9251	0.8597	0.0945	0.2451	0.1511	0.1260	0.1263
BONDVILLE	01042003	164427	aot560	84	0.1104	0.6276	0.6992	0.0553	0.2389	0.2048	0.0884	0.1177
BONDVILLE	21062003	155918	aot860	134338	0.0698	0.6759	0.7129	0.0465	0.2193	0.2212	0.1147	0.1433
BONDVILLE	24092003	161333	aot860	123198	0.1132	0.8089	0.5606	0.0961	0.1894	0.0942	0.0761	0.0704
BONDVILLE	20112003	162159	aot860	29	0.0590	0.1979	0.0062	0.0482	0.0620	0.0150	0.0333	0.0133
BONDVILLE	23032003	162735	aot860	16194	0.1921	0.5397	0.6989	0.1073	0.3180	0.2333	0.0924	0.1432
BONDVILLE	20062003	163016	aot860	99119	0.0749	0.6597	0.7715	0.0576	0.2553	0.2735	0.1208	0.1608
BONDVILLE	22102003	163309	aot860	817	0.1414	0.4444	0.3344	0.1075	0.1755	0.0768	0.0589	0.0766
BONDVILLE	20092003	163857	aot860	46328	0.1147	0.6244	0.7125	0.0810	0.1842	0.1114	0.0697	0.0942
BONDVILLE	01042003	164427	aot860	84	0.1416	0.4466	0.4254	0.0781	0.2224	0.1810	0.0824	0.1203

10.3. BORDEAUX

Site	date	hour	variable	Nb pixel	Offset	Slope	R2	rmse	Mean baer	Mean ddv	Sdt baer	Sdt ddv
BORDEAUX	19062003	101753	alpha		0.0436	0.7396	0.0021	0.4666	0.7638	0.5527	0.4105	0.4352
BORDEAUX	11072003	102624	alpha		-0.0649	0.8765	0.0073	0.4374	0.8330	0.6713	0.2890	0.3817
BORDEAUX	02082003	103459	alpha		0.0150	0.8095	0.0003	0.4808	0.8201	0.7017	0.4213	0.4731
BORDEAUX	25082003	101253	alpha		0.0074	0.5437	0.0001	0.5258	0.5507	0.9427	0.3334	0.3530
BORDEAUX	15092003	105232	alpha		-0.0244	0.4637	0.0016	0.5387	0.4483	0.6305	0.3043	0.4949
BORDEAUX	19062003	101753	aot412		1.0013	0.0995	0.8794	0.0999	0.3658	0.2660	0.1943	0.1820
BORDEAUX	11072003	102624	aot412		1.0604	0.0995	0.8051	0.1202	0.4567	0.3368	0.1877	0.1588
BORDEAUX	02082003	103459	aot412		0.8831	0.1401	0.7046	0.1177	0.3125	0.1953	0.0933	0.0887
BORDEAUX	25082003	101253	aot412		1.0312	0.1238	0.8879	0.1313	0.3678	0.2366	0.1097	0.1003
BORDEAUX	15092003	105232	aot412	27017	0.7974	0.1361	0.6425	0.1032	0.2696	0.1674	0.0710	0.0714
BORDEAUX	19062003	101753	aot560		0.8218	0.0888	0.7623	0.0558	0.2773	0.2294	0.1515	0.1609
BORDEAUX	11072003	102624	aot560		0.9890	0.0688	0.7054	0.0658	0.3422	0.2764	0.1567	0.1331
BORDEAUX	02082003	103459	aot560		0.7943	0.0966	0.4810	0.0654	0.2258	0.1626	0.0941	0.0822
BORDEAUX	25082003	101253	aot560		0.9440	0.1302	0.7300	0.1202	0.2999	0.1798	0.0897	0.0812
BORDEAUX	15092003	105232	aot560	27017	0.5575	0.1423	0.3865	0.0845	0.2224	0.1437	0.0624	0.0696
BORDEAUX	19062003	101753	aot860		0.5602	0.1015	0.6382	0.0649	0.2076	0.1894	0.0992	0.1415
BORDEAUX	11072003	102624	aot860		0.6480	0.1131	0.5039	0.0544	0.2504	0.2118	0.0994	0.1089
BORDEAUX	02082003	103459	aot860		0.5652	0.1090	0.3004	0.0627	0.1815	0.1283	0.0785	0.0761
BORDEAUX	25082003	101253	aot860		0.6601	0.1642	0.4469	0.1241	0.2456	0.1233	0.0619	0.0627
BORDEAUX	15092003	105232	aot860	27017	0.2538	0.1647	0.1370	0.0921	0.1948	0.1186	0.0476	0.0693

10.4. GSFC

Site	date	hour	variable	Nb pixel	Offset	Slope	R2	rmse	Mean baer	Mean ddv	Sdt baer	Sdt ddv
GSFC	24032003	155531	alpha	3135	0.3686	0.2357	0.3235	0.4543	0.5714	0.8602	0.1901	0.4588
GSFC	25032003	152423	alpha	8115	0.3545	0.0652	0.0115	0.5847	0.4026	0.7378	0.3112	0.5126
GSFC	21112003	154959	alpha	773	0.2997	0.0334	0.0073	0.8676	0.3338	1.0202	0.2156	0.5495
GSFC	30102003	154125	alpha	391	0.4732	-0.0177	0.0026	0.8612	0.4533	1.1227	0.1835	0.5332
GSFC	24032003	155531	aot412	3135	0.2867	0.4491	0.5804	0.1230	0.4266	0.3115	0.0464	0.0786
GSFC	25032003	152423	aot412	8115	0.2021	0.4854	0.5569	0.0962	0.3049	0.2118	0.0302	0.0465
GSFC	21112003	154959	aot412	773	0.0971	0.8517	0.5073	0.0902	0.1372	0.0470	0.0235	0.0196
GSFC	30102003	154125	aot412	391	0.1242	0.7232	0.7602	0.1080	0.1683	0.0609	0.0351	0.0423
GSFC	24032003	155531	aot560	3135	0.2543	0.4121	0.5612	0.1202	0.3568	0.2489	0.0494	0.0899
GSFC	25032003	152423	aot560	8115	0.2053	0.3336	0.2156	0.0967	0.2639	0.1756	0.0426	0.0593
GSFC	21112003	154959	aot560	773	0.1043	0.5881	0.1914	0.0899	0.1253	0.0357	0.0237	0.0176
GSFC	30102003	154125	aot560	391	0.1242	0.5201	0.5178	0.1040	0.1481	0.0459	0.0290	0.0402
GSFC	24032003	155531	aot860	3135	0.2037	0.4277	0.5900	0.1120	0.2830	0.1855	0.0536	0.0963
GSFC	25032003	152423	aot860	8115	0.1810	0.3706	0.2222	0.1034	0.2324	0.1389	0.0549	0.0699
GSFC	21112003	154959	aot860	773	0.1028	0.1875	0.0225	0.0834	0.1076	0.0253	0.0210	0.0168
GSFC	30102003	154125	aot860	391	0.1090	0.3555	0.2925	0.0916	0.1204	0.0322	0.0251	0.0382

10.5. HOWLAND

Site	date	hour	variable	Nb pixel	Offset	Slope	R2	rmse	Mean baer	Mean ddv	Sdt baer	Sdt ddv
HOWLAND	16062003	151327	alpha	113048	0.7799	-0.0830	0.0053	0.4554	0.7272	0.6342	0.4675	0.4116
HOWLAND	16062003	151327	aot412	113048	0.0976	0.8832	0.9394	0.0725	0.3044	0.2341	0.1394	0.1529
HOWLAND	16062003	151327	aot560	113048	0.0744	0.8228	0.7852	0.0460	0.2350	0.1952	0.1209	0.1302
HOWLAND	16062003	151327	aot860	113048	0.0873	0.6584	0.6040	0.0507	0.1883	0.1534	0.0915	0.1080

10.6. ISPRA

Site	date	hour	variable	Nb pixel	Offset	Slope	R2	rmse	Mean baer	Mean ddv	Sdt baer	Sdt ddv
ISPRA	04082003	093123	alpha	208437	0.6930	0.0827	0.0117	0.3314	0.7619	0.8337	0.2695	0.3527
ISPRA	23082003	093507	alpha	87527	0.7397	0.1098	0.0151	0.2815	0.8350	0.8686	0.2808	0.3139
ISPRA	22072003	094006	alpha	145500	0.7398	-0.0264	0.0012	0.3809	0.7228	0.6430	0.2745	0.3629
ISPRA	06072003	094331	alpha	80196	0.6529	0.1219	0.0206	0.3382	0.7308	0.6392	0.3152	0.3708
ISPRA	10082003	094352	alpha	47796	0.6134	0.0945	0.0127	0.3144	0.6879	0.7881	0.2757	0.3291
ISPRA	20062003	094622	alpha	66205	0.7927	0.0490	0.0027	0.4637	0.8189	0.5340	0.3634	0.3847
ISPRA	25072003	094625	alpha	59688	0.6979	0.0586	0.0047	0.3694	0.7365	0.6577	0.3264	0.3834
ISPRA	13082003	094931	alpha	53482	0.7393	0.0294	0.0015	0.3161	0.7635	0.8244	0.2427	0.3196
ISPRA	28072003	095206	alpha	68159	0.7540	0.0697	0.0076	0.3355	0.7986	0.6405	0.2545	0.3181
ISPRA	04082003	093123	aot412	208437	0.1366	0.9861	0.8514	0.1316	0.4927	0.3611	0.1647	0.1541

Site	date	hour	variable	Nb pixel	Offset	Slope	R2	rmse	Mean baer	Mean ddv	Sdt baer	Sdt ddv
ISPRA	23082003	093507	aot412	87527	0.0581	1.3184	0.8920	0.1900	0.5699	0.3882	0.2434	0.1744
ISPRA	22072003	094006	aot412	145500	0.1435	0.8948	0.8836	0.1096	0.4426	0.3342	0.1465	0.1539
ISPRA	06072003	094331	aot412	80196	0.0917	1.0515	0.8669	0.1097	0.4530	0.3436	0.1869	0.1655
ISPRA	10082003	094352	aot412	47796	0.0591	1.3106	0.8080	0.1723	0.5168	0.3492	0.1888	0.1295
ISPRA	20062003	094622	aot412	66205	0.1071	0.9917	0.8765	0.1048	0.3824	0.2776	0.1628	0.1537
ISPRA	25072003	094625	aot412	59688	0.0943	1.1381	0.9056	0.1407	0.4575	0.3192	0.2220	0.1857
ISPRA	13082003	094931	aot412	53482	0.1634	0.9664	0.7663	0.1515	0.5070	0.3555	0.1281	0.1160
ISPRA	28072003	095206	aot412	68159	0.1045	1.0537	0.8850	0.1264	0.5266	0.4006	0.1885	0.1683
ISPRA	04082003	093123	aot560	208437	0.1614	0.7888	0.7011	0.1050	0.3860	0.2847	0.1226	0.1302
ISPRA	23082003	093507	aot560	87527	0.1067	1.0979	0.7769	0.1368	0.4364	0.3003	0.1714	0.1376
ISPRA	22072003	094006	aot560	145500	0.1243	0.7722	0.7144	0.0680	0.3397	0.2789	0.1229	0.1345
ISPRA	06072003	094331	aot560	80196	0.0950	0.8888	0.7040	0.0652	0.3486	0.2853	0.1496	0.1412
ISPRA	10082003	094352	aot560	47796	0.1380	0.9773	0.6480	0.1318	0.4092	0.2775	0.1304	0.1074
ISPRA	20062003	094622	aot560	66205	0.0748	0.8645	0.7340	0.0463	0.2811	0.2386	0.1366	0.1353
ISPRA	25072003	094625	aot560	59688	0.0754	1.0345	0.7797	0.0846	0.3467	0.2623	0.1767	0.1508
ISPRA	13082003	094931	aot560	53482	0.1923	0.7304	0.6084	0.1198	0.3968	0.2801	0.0933	0.0996
ISPRA	28072003	095206	aot560	68159	0.1025	0.9064	0.7352	0.0728	0.4022	0.3306	0.1486	0.1406
ISPRA	04082003	093123	aot860	208437	0.1791	0.4716	0.4762	0.0898	0.2760	0.2055	0.0720	0.1053
ISPRA	23082003	093507	aot860	87527	0.1638	0.6317	0.5277	0.0941	0.2968	0.2105	0.0887	0.1020

Site	date	hour	variable	Nb pixel	Offset	Slope	R2	rmse	Mean baer	Mean ddv	Sdt baer	Sdt ddv
ISPRA	22072003	094006	aot860	145500	0.1636	0.4380	0.4103	0.0767	0.2593	0.2186	0.0791	0.1157
ISPRA	06072003	094331	aot860	80196	0.1368	0.5690	0.5047	0.0656	0.2634	0.2224	0.0953	0.1190
ISPRA	10082003	094352	aot860	47796	0.2066	0.4743	0.3373	0.1103	0.3027	0.2025	0.0717	0.0878
ISPRA	20062003	094622	aot860	66205	0.1005	0.5822	0.5356	0.0529	0.2143	0.1955	0.0943	0.1185
ISPRA	25072003	094625	aot860	59688	0.1265	0.6780	0.5611	0.0723	0.2629	0.2013	0.1061	0.1172
ISPRA	13082003	094931	aot860	53482	0.2055	0.3990	0.3140	0.0982	0.2859	0.2017	0.0598	0.0840
ISPRA	28072003	095206	aot860	68159	0.1529	0.5300	0.4719	0.0635	0.2878	0.2544	0.0886	0.1149

10.7. LAMPEDUSA

Site	date	hour	variable	Nb pixel	Offset	Slope	R2	rmse	Mean baer	Mean ddv	Sdt baer	Sdt ddv
LAMPEDUSA	11062003	093044	alpha	8540	0.7994	0.0134	0.0003	0.3872	0.8083	0.6655	0.2704	0.3648
LAMPEDUSA	22072003	094215	alpha	2673	0.9029	-0.0602	0.0267	0.5502	0.8584	0.7379	0.1867	0.5064
LAMPEDUSA	01062003	094456	alpha	6239	0.8469	0.0305	0.0017	0.3663	0.8694	0.7365	0.2599	0.3521
LAMPEDUSA	11062003	093044	aot412	8540	0.1167	0.9878	0.8634	0.1127	0.4449	0.3322	0.1327	0.1248
LAMPEDUSA	22072003	094215	aot412	2673	0.1768	0.9062	0.7698	0.1525	0.4152	0.2630	0.1176	0.1138
LAMPEDUSA	01062003	094456	aot412	6239	0.0842	1.1145	0.8554	0.1329	0.5469	0.4151	0.1809	0.1501
LAMPEDUSA	11062003	093044	aot560	8540	0.0999	0.8393	0.6577	0.0586	0.3298	0.2738	0.1131	0.1093

LAMPEDUSA	22072003	094215	aot560	2673	0.1753	0.6267	0.4976	0.1021	0.3115	0.2174	0.0945	0.1064
LAMPEDUSA	01062003	094456	aot560	6239	0.1108	0.9056	0.6634	0.0800	0.4160	0.3370	0.1470	0.1322
LAMPEDUSA	11062003	093044	aot860	8540	0.1456	0.4723	0.4189	0.0618	0.2455	0.2115	0.0713	0.0977
LAMPEDUSA	22072003	094215	aot860	2673	0.1735	0.2742	0.2083	0.0885	0.2202	0.1705	0.0606	0.1009
LAMPEDUSA	01062003	094456	aot860	6239	0.1590	0.5065	0.4624	0.0663	0.2876	0.2540	0.0863	0.1158

10.8. LILLE

Site	date	hour	variable	Nb pixel	Offset	Slope	R2	rmse	Mean baer	Mean ddv	Sdt baer	Sdt ddv
LILLE	16062003	101043	alpha	201671	0.4985	0.3357	0.1240	0.2573	0.6669	0.5014	0.2829	0.2967
LILLE	22032003	101214	alpha	1188	0.3004	0.1857	0.0899	0.3431	0.3871	0.4670	0.2539	0.4099
LILLE	22032003	101236	alpha	1986	0.3030	0.1322	0.0667	0.4147	0.3701	0.5073	0.2310	0.4511
LILLE	14072003	102954	alpha	49870	0.6846	-0.0295	0.0010	0.4835	0.6682	0.5540	0.4326	0.4563
LILLE	16062003	101043	aot412	201671	0.0421	1.1135	0.8421	0.0934	0.5240	0.4327	0.2157	0.1778
LILLE	22032003	101214	aot412	1188	0.2010	0.6433	0.5651	0.0727	0.4624	0.4062	0.1108	0.1295
LILLE	22032003	101236	aot412	1986	0.2150	0.6007	0.6057	0.0785	0.4482	0.3882	0.0978	0.1267
LILLE	14072003	102954	aot412	49870	0.1220	0.8830	0.9207	0.0953	0.3338	0.2400	0.1289	0.1401
LILLE	16062003	101043	aot560	201671	0.0440	0.9804	0.7398	0.0368	0.4076	0.3709	0.1709	0.1499
LILLE	22032003	101214	aot560	1188	0.2327	0.4767	0.5006	0.0851	0.4059	0.3632	0.0948	0.1407
LILLE	22032003	101236	aot560	1986	0.2416	0.4482	0.5455	0.0921	0.3964	0.3455	0.0844	0.1391

LILLE	14072003	102954	aot560	49870	0.0816	0.8468	0.7339	0.0532	0.2583	0.2087	0.1232	0.1246
LILLE	16062003	101043	aot860	201671	0.1178	0.6552	0.6083	0.0454	0.3150	0.3009	0.1053	0.1253
LILLE	22032003	101214	aot860	1188	0.2436	0.3323	0.4958	0.1081	0.3483	0.3152	0.0727	0.1541
LILLE	22032003	101236	aot860	1986	0.2454	0.3244	0.5464	0.1116	0.3421	0.2984	0.0667	0.1519
LILLE	14072003	102954	aot860	49870	0.0980	0.6725	0.5138	0.0545	0.2151	0.1741	0.1028	0.1095

10.9. MARICOPA

Site	date	hour	variable	Nb pixel	Offset	Slope	R2	rmse	Mean baer	Mean ddv	Sdt baer	Sdt ddv
MARICOPA	28092003	172931	alpha	546	0.8132	0.2442	0.0299	0.4821	0.9649	0.6212	0.6326	0.4478
MARICOPA	28092003	172948	alpha	943	0.8316	-0.0779	0.0039	0.5386	0.7682	0.8144	0.6179	0.4981
MARICOPA	21112003	173142	alpha	76	0.9624	-0.1159	0.0064	0.5803	0.8552	0.9256	0.7504	0.5197
MARICOPA	12092003	173149	alpha	569	0.8926	0.0034	0.0000	0.5472	0.8947	0.6303	0.4044	0.4812
MARICOPA	17102003	173212	alpha	21	1.0919	0.1872	0.0213	0.6013	1.2267	0.7201	0.5242	0.4084
MARICOPA	12092003	173225	alpha	576	0.8901	0.0206	0.0007	0.5221	0.9046	0.7023	0.3883	0.4919
MARICOPA	29012003	173427	alpha	317	0.3410	0.2684	0.0733	0.4078	0.5347	0.7213	0.4922	0.4964
MARICOPA	05112003	173431	alpha	36	0.6147	-0.0039	0.0000	0.6292	0.6113	0.8950	0.5678	0.5673
MARICOPA	07072003	173722	alpha	495	0.5506	0.2660	0.0712	0.4271	0.7838	0.8767	0.5667	0.5685
MARICOPA	15092003	173728	alpha	942	0.6785	0.1918	0.0187	0.4392	0.7815	0.5367	0.6337	0.4514
MARICOPA	20102003	173800	alpha	22	1.0839	0.0528	0.0021	0.6172	1.1219	0.7197	0.5893	0.5059
MARICOPA	15092003	173807	alpha	609	0.9375	0.0025	0.0000	0.5534	0.9393	0.7334	0.5762	0.5153

Site	date	hour	variable	Nb pixel	Offset	Slope	R2	rmse	Mean baer	Mean ddv	Sdt baer	Sdt ddv
MARICOPA	21062003	174047	alpha	24	1.0045	-0.0948	0.0100	0.7416	0.9260	0.8278	0.6516	0.6858
MARICOPA	16012003	174256	alpha	456	0.3703	0.0479	0.0034	0.3232	0.3937	0.4884	0.2654	0.3249
MARICOPA	10072003	174329	alpha	75	0.5712	0.1589	0.0569	0.5198	0.7284	0.9892	0.3584	0.5381
MARICOPA	23102003	174331	alpha	5	0.2322	0.0634	0.1643	0.7875	0.2912	0.9298	0.0860	0.5500
MARICOPA	27112003	174332	alpha	28	0.1493	0.1722	0.1511	0.6179	0.2669	0.6831	0.2488	0.5618
MARICOPA	18092003	174337	alpha	190	0.9966	-0.1212	0.0088	0.6144	0.9264	0.5784	0.5844	0.4527
MARICOPA	04022003	174545	alpha	77	0.5079	-0.1418	0.0590	0.6358	0.4268	0.5719	0.3184	0.5457
MARICOPA	11032003	174615	alpha	2925	0.9994	-0.0934	0.0050	0.6167	0.9477	0.5534	0.5719	0.4338
MARICOPA	19012003	174836	alpha	349	0.4664	0.0740	0.0066	0.4091	0.5082	0.5646	0.3976	0.4382
MARICOPA	30032003	174838	alpha	829	1.0810	0.1129	0.0054	0.7339	1.1366	0.4926	0.6076	0.3970
MARICOPA	13072003	174843	alpha	1080	0.8234	0.0850	0.0154	0.4212	0.9053	0.9640	0.3120	0.4560
MARICOPA	13072003	174911	alpha	197	0.7050	0.1580	0.0428	0.3607	0.8482	0.9063	0.3237	0.4239
MARICOPA	21092003	174916	alpha	65	0.7114	0.0103	0.0001	0.5379	0.7182	0.6605	0.5195	0.5446
MARICOPA	30032003	174917	alpha	1326	1.0854	-0.0072	0.0000	0.6977	1.0814	0.5526	0.6390	0.4519
MARICOPA	26102003	174920	alpha	31	0.6179	0.2146	0.0753	0.5263	0.8960	1.2957	0.3466	0.4432
MARICOPA	10052003	180035	alpha	6010	0.6525	-0.0179	0.0001	0.3553	0.6427	0.5507	0.5484	0.3372
MARICOPA	28092003	172931	aot412	546	0.1635	1.5189	0.9866	0.2385	0.3635	0.1317	0.1655	0.1082
MARICOPA	28092003	172948	aot412	943	0.1102	1.4788	0.7016	0.1537	0.2387	0.0869	0.0903	0.0512
MARICOPA	21112003	173142	aot412	76	0.1935	1.1200	0.8728	0.2105	0.3494	0.1392	0.1059	0.0883

Site	date	hour	variable	Nb pixel	Offset	Slope	R2	rmse	Mean baer	Mean ddv	Sdt baer	Sdt ddv
MARICOPA	12092003	173149	aot412	569	0.1431	1.8384	0.8175	0.1983	0.2600	0.0636	0.0663	0.0326
MARICOPA	17102003	173212	aot412	21	0.2204	0.5063	0.6444	0.1858	0.2574	0.0731	0.0306	0.0485
MARICOPA	12092003	173225	aot412	576	0.1953	0.8145	0.7180	0.1824	0.2526	0.0703	0.0301	0.0313
MARICOPA	29012003	173427	aot412	317	0.2202	0.9334	0.8023	0.2047	0.4410	0.2365	0.1374	0.1319
MARICOPA	05112003	173431	aot412	36	0.2340	0.9173	0.8830	0.2177	0.4194	0.2021	0.1536	0.1573
MARICOPA	07072003	173722	aot412	495	0.2596	1.0783	0.6857	0.2717	0.4242	0.1527	0.1554	0.1193
MARICOPA	15092003	173728	aot412	942	0.1698	1.5281	0.9052	0.2217	0.3146	0.0948	0.0865	0.0538
MARICOPA	20102003	173800	aot412	22	0.1499	1.3455	0.8365	0.1960	0.3185	0.1253	0.1455	0.0989
MARICOPA	15092003	173807	aot412	609	0.2035	0.8518	0.5884	0.1917	0.2715	0.0798	0.0363	0.0327
MARICOPA	21062003	174047	aot412	24	0.3045	0.3441	0.3988	0.2191	0.3547	0.1459	0.0565	0.1037
MARICOPA	16012003	174256	aot412	456	0.1877	1.0498	0.8705	0.2082	0.6168	0.4088	0.1879	0.1670
MARICOPA	10072003	174329	aot412	75	0.1728	1.6284	0.7928	0.3489	0.5867	0.2542	0.3094	0.1692
MARICOPA	23102003	174331	aot412	5	0.4851	0.1533	0.1312	0.2704	0.5252	0.2615	0.0335	0.0792
MARICOPA	27112003	174332	aot412	28	0.2817	0.6055	0.7498	0.1815	0.4420	0.2649	0.0714	0.1021
MARICOPA	18092003	174337	aot412	190	0.1969	0.8475	0.6696	0.1867	0.2540	0.0674	0.0285	0.0276
MARICOPA	04022003	174545	aot412	77	0.3272	0.8903	0.6351	0.2857	0.6687	0.3836	0.1813	0.1623
MARICOPA	11032003	174615	aot412	2925	0.1718	0.8656	0.7749	0.1459	0.3400	0.1944	0.0627	0.0638
MARICOPA	19012003	174836	aot412	349	0.1272	1.2312	0.9439	0.2150	0.5693	0.3591	0.2475	0.1953
MARICOPA	30032003	174838	aot412	829	0.1250	1.0995	0.8096	0.1391	0.2794	0.1404	0.0662	0.0542

Site	date	hour	variable	Nb pixel	Offset	Slope	R2	rmse	Mean baer	Mean ddv	Sdt baer	Sdt ddv
MARICOPA	13072003	174843	aot412	1080	0.2005	1.6384	0.6886	0.4214	0.7489	0.3348	0.2409	0.1220
MARICOPA	13072003	174911	aot412	197	0.1528	1.6483	0.7498	0.4088	0.7690	0.3738	0.3078	0.1617
MARICOPA	21092003	174916	aot412	65	0.2185	0.7236	0.5998	0.1923	0.2879	0.0960	0.0380	0.0407
MARICOPA	30032003	174917	aot412	1326	0.1272	1.0760	0.7801	0.1373	0.2694	0.1322	0.0589	0.0484
MARICOPA	26102003	174920	aot412	31	0.1127	1.8753	0.9217	0.4210	0.7276	0.3279	0.2998	0.1535
MARICOPA	10052003	180035	aot412	6010	0.0874	1.0368	0.8993	0.0963	0.3351	0.2389	0.1178	0.1078
MARICOPA	28092003	172931	aot560	546	0.0737	1.7330	0.8400	0.1665	0.2626	0.1090	0.1659	0.0877
MARICOPA	28092003	172948	aot560	943	0.1025	1.0955	0.3978	0.1091	0.1780	0.0689	0.0710	0.0409
MARICOPA	21112003	173142	aot560	76	0.1276	1.2810	0.6228	0.1604	0.2694	0.1107	0.1364	0.0840
MARICOPA	12092003	173149	aot560	569	0.1156	1.5328	0.4198	0.1444	0.1967	0.0529	0.0595	0.0252
MARICOPA	17102003	173212	aot560	21	0.1840	-0.0788	0.0049	0.1275	0.1791	0.0612	0.0517	0.0459
MARICOPA	12092003	173225	aot560	576	0.1578	0.5177	0.1167	0.1309	0.1872	0.0568	0.0358	0.0236
MARICOPA	29012003	173427	aot560	317	0.1581	1.0142	0.6410	0.1610	0.3626	0.2017	0.1638	0.1293
MARICOPA	05112003	173431	aot560	36	0.2172	0.7765	0.5695	0.1830	0.3480	0.1684	0.1661	0.1614
MARICOPA	07072003	173722	aot560	495	0.2261	0.7347	0.4049	0.1961	0.3154	0.1215	0.1272	0.1101
MARICOPA	15092003	173728	aot560	942	0.1189	1.9618	0.3079	0.2045	0.2811	0.0827	0.1813	0.0513
MARICOPA	20102003	173800	aot560	22	0.0651	1.5819	0.6904	0.1328	0.2274	0.1026	0.1523	0.0800
MARICOPA	15092003	173807	aot560	609	0.0979	2.0665	0.1409	0.1691	0.2310	0.0644	0.1509	0.0274
MARICOPA	21062003	174047	aot560	24	0.2578	-0.1223	0.0792	0.1643	0.2425	0.1245	0.0452	0.1040

Site	date	hour	variable	Nb pixel	Offset	Slope	R2	rmse	Mean baer	Mean ddv	Sdt baer	Sdt ddv
MARICOPA	16012003	174256	aot560	456	0.2530	0.7950	0.7828	0.1822	0.5383	0.3589	0.1369	0.1523
MARICOPA	10072003	174329	aot560	75	0.2059	1.2105	0.5914	0.2480	0.4389	0.1925	0.2151	0.1366
MARICOPA	23102003	174331	aot560	5	0.4533	0.1194	0.3329	0.2829	0.4781	0.2078	0.0220	0.1064
MARICOPA	27112003	174332	aot560	28	0.2512	0.6611	0.5519	0.1777	0.4025	0.2289	0.1013	0.1138
MARICOPA	18092003	174337	aot560	190	0.1645	0.4638	0.0507	0.1342	0.1913	0.0578	0.0541	0.0263
MARICOPA	04022003	174545	aot560	77	0.3739	0.6012	0.5099	0.2467	0.5806	0.3439	0.1477	0.1754
MARICOPA	11032003	174615	aot560	2925	0.0817	0.8804	0.3067	0.0621	0.2298	0.1682	0.1026	0.0645
MARICOPA	19012003	174836	aot560	349	0.1513	1.0583	0.8789	0.1701	0.4862	0.3164	0.2071	0.1835
MARICOPA	30032003	174838	aot560	829	0.0754	0.8560	0.3359	0.0582	0.1810	0.1233	0.0783	0.0530
MARICOPA	13072003	174843	aot560	1080	0.2629	1.1465	0.4143	0.3006	0.5546	0.2544	0.1871	0.1050
MARICOPA	13072003	174911	aot560	197	0.2219	1.2089	0.5521	0.2838	0.5719	0.2896	0.2213	0.1360
MARICOPA	21092003	174916	aot560	65	0.1847	0.5591	0.0852	0.1499	0.2299	0.0809	0.0720	0.0376
MARICOPA	30032003	174917	aot560	1326	0.0920	0.8861	0.1473	0.0792	0.1934	0.1144	0.1111	0.0481
MARICOPA	26102003	174920	aot560	31	0.1897	1.5237	0.7781	0.3125	0.5320	0.2246	0.1894	0.1096
MARICOPA	10052003	180035	aot560	6010	0.0587	1.0515	0.5416	0.0694	0.2736	0.2043	0.1371	0.0960
MARICOPA	28092003	172931	aot860	546	0.0504	1.8227	0.6989	0.1326	0.2054	0.0851	0.1478	0.0678
MARICOPA	28092003	172948	aot860	943	0.1054	0.7094	0.1598	0.0911	0.1417	0.0512	0.0599	0.0338
MARICOPA	21112003	173142	aot860	76	0.1287	1.2160	0.4216	0.1476	0.2295	0.0829	0.1482	0.0791
MARICOPA	12092003	173149	aot860	569	0.0933	1.1603	0.1792	0.1001	0.1421	0.0421	0.0596	0.0218

Site	date	hour	variable	Nb pixel	Offset	Slope	R2	rmse	Mean baer	Mean ddv	Sdt baer	Sdt ddv
MARICOPA	17102003	173212	aot860	21	0.0875	0.5055	0.1550	0.0667	0.1120	0.0486	0.0547	0.0426
MARICOPA	12092003	173225	aot860	576	0.0925	1.0059	0.1937	0.0927	0.1361	0.0434	0.0458	0.0200
MARICOPA	29012003	173427	aot860	317	0.1968	0.7919	0.4449	0.1647	0.3270	0.1644	0.1492	0.1256
MARICOPA	05112003	173431	aot860	36	0.2306	0.5317	0.3182	0.1835	0.3030	0.1361	0.1559	0.1654
MARICOPA	07072003	173722	aot860	495	0.2073	0.4192	0.2203	0.1654	0.2459	0.0921	0.0936	0.1048
MARICOPA	15092003	173728	aot860	942	0.0756	1.8586	0.5224	0.1416	0.2048	0.0695	0.1259	0.0490
MARICOPA	20102003	173800	aot860	22	0.0270	1.7776	0.5521	0.0994	0.1670	0.0787	0.1445	0.0604
MARICOPA	15092003	173807	aot860	609	0.0982	1.0886	0.1303	0.1026	0.1518	0.0492	0.0767	0.0254
MARICOPA	21062003	174047	aot860	24	0.2178	-0.2498	0.1164	0.1526	0.1918	0.1039	0.0747	0.1020
MARICOPA	16012003	174256	aot860	456	0.3108	0.4728	0.5898	0.1697	0.4536	0.3019	0.0891	0.1447
MARICOPA	10072003	174329	aot860	75	0.2454	0.5465	0.2923	0.1911	0.3191	0.1348	0.1135	0.1123
MARICOPA	23102003	174331	aot860	5	0.4036	0.1216	0.8509	0.2845	0.4227	0.1575	0.0173	0.1309
MARICOPA	27112003	174332	aot860	28	0.2753	0.5018	0.4680	0.1900	0.3716	0.1919	0.0926	0.1262
MARICOPA	18092003	174337	aot860	190	0.1165	0.4852	0.0466	0.0929	0.1396	0.0476	0.0575	0.0256
MARICOPA	04022003	174545	aot860	77	0.3935	0.3107	0.3300	0.2254	0.4874	0.3020	0.1012	0.1872
MARICOPA	11032003	174615	aot860	2925	0.0902	0.7141	0.2125	0.0538	0.1900	0.1398	0.1037	0.0669
MARICOPA	19012003	174836	aot860	349	0.1915	0.7752	0.7280	0.1368	0.3996	0.2684	0.1569	0.1727
MARICOPA	30032003	174838	aot860	829	0.0635	0.7066	0.1795	0.0363	0.1372	0.1043	0.0877	0.0526
MARICOPA	13072003	174843	aot860	1080	0.2872	0.5505	0.2059	0.2118	0.3844	0.1767	0.1117	0.0921

Site	date	hour	variable	Nb pixel	Offset	Slope	R2	rmse	Mean baer	Mean ddv	Sdt baer	Sdt ddv
MARICOPA	13072003	174911	aot860	197	0.2740	0.5967	0.3342	0.1966	0.3966	0.2054	0.1181	0.1144
MARICOPA	21092003	174916	aot860	65	0.1473	0.5109	0.0906	0.1166	0.1808	0.0656	0.0626	0.0369
MARICOPA	30032003	174917	aot860	1326	0.0803	0.6155	0.1228	0.0475	0.1389	0.0953	0.0858	0.0489
MARICOPA	26102003	174920	aot860	31	0.2250	0.9689	0.5689	0.2209	0.3546	0.1337	0.0910	0.0709
MARICOPA	10052003	180035	aot860	6010	0.0660	0.9963	0.5201	0.0654	0.2311	0.1657	0.1177	0.0852

10.10. MONGU

Site	date	hour	variable	Nb pixel	Offset	Slope	R2	rmse	Mean baer	Mean ddv	Sdt baer	Sdt ddv
MONGU	07052003	080515	alpha	22316	1.2517	-0.4496	0.2441	0.8869	0.6549	1.3276	0.3628	0.3987
MONGU	21042003	080806	alpha	27512	0.7749	-0.2323	0.1216	0.9328	0.4844	1.2503	0.2880	0.4322
MONGU	14062003	081057	alpha	978	0.6691	-0.0446	0.0040	0.9056	0.6070	1.3939	0.3016	0.4292
MONGU	07082003	081352	alpha	288	0.5181	0.3129	0.2146	0.6031	0.9908	1.5109	0.3005	0.4449
MONGU	09072003	082507	alpha	322	0.6275	-0.0474	0.0020	1.1975	0.5465	1.7077	0.2940	0.2798
MONGU	23052003	080222	alpha	5094	0.9347	-0.2100	0.0749	0.8771	0.6463	1.3731	0.3114	0.4058
MONGU	07052003	080515	aot412	22316	0.1628	1.2486	0.9582	0.2399	0.5174	0.2840	0.2851	0.2235
MONGU	21042003	080806	aot412	27512	0.1731	1.1079	0.9058	0.1932	0.3738	0.1812	0.1535	0.1318
MONGU	14062003	081057	aot412	978	0.1545	1.3896	0.8769	0.2597	0.5140	0.2587	0.1824	0.1229

Site	date	hour	variable	Nb pixel	Offset	Slope	R2	rmse	Mean baer	Mean ddv	Sdt baer	Sdt ddv
MONGU	07082003	081352	aot412	288	0.1797	1.6360	0.8443	0.4903	0.9528	0.4726	0.2771	0.1557
MONGU	09072003	082507	aot412	322	0.2562	1.7565	0.6865	0.4762	0.7587	0.2861	0.1635	0.0771
MONGU	23052003	080222	aot412	5094	0.1711	1.2304	0.9201	0.2294	0.4683	0.2416	0.1931	0.1506
MONGU	07052003	080515	aot560	22316	0.1963	1.0249	0.8848	0.2014	0.4037	0.2024	0.1891	0.1736
MONGU	21042003	080806	aot560	27512	0.1806	0.9338	0.7580	0.1721	0.3031	0.1311	0.1136	0.1059
MONGU	14062003	081057	aot560	978	0.1940	1.3399	0.6693	0.2544	0.4249	0.1724	0.1495	0.0913
MONGU	07082003	081352	aot560	288	0.3425	1.1427	0.5368	0.3856	0.6851	0.2998	0.1697	0.1088
MONGU	09072003	082507	aot560	322	0.3807	1.5132	0.3421	0.4690	0.6391	0.1708	0.1292	0.0499
MONGU	23052003	080222	aot560	5094	0.1972	1.0682	0.7980	0.2088	0.3760	0.1674	0.1408	0.1178
MONGU	07052003	080515	aot860	22316	0.2124	0.6691	0.6350	0.1750	0.2974	0.1271	0.1022	0.1218
MONGU	21042003	080806	aot860	27512	0.2105	0.4924	0.3701	0.1722	0.2521	0.0846	0.0633	0.0782
MONGU	14062003	081057	aot860	978	0.2236	1.0889	0.3413	0.2325	0.3316	0.0992	0.1190	0.0638
MONGU	07082003	081352	aot860	288	0.3644	0.4972	0.1753	0.2858	0.4446	0.1613	0.0906	0.0763
MONGU	09072003	082507	aot860	322	0.4555	0.6630	0.0389	0.4277	0.5104	0.0828	0.1017	0.0302
MONGU	23052003	080222	aot860	5094	0.2034	0.8138	0.5349	0.1851	0.2859	0.1015	0.0942	0.0846

10.11. SKUKUZA

Site	date	hour	variable	Nb pixel	Offset	Slope	R2	rmse	Mean baer	Mean ddv	Sdt baer	Sdt ddv
SKUKUZA	29042003	071914	alpha	6810	0.5473	0.0875	0.0096	0.4301	0.6093	0.7082	0.4108	0.4588
SKUKUZA	09112003	072206	alpha	4844	0.7688	-0.3548	0.0898	0.5584	0.5861	0.5151	0.4842	0.4088
SKUKUZA	24052003	073317	alpha	17879	0.5848	-0.1176	0.0384	0.8044	0.4604	1.0582	0.2889	0.4817
SKUKUZA	18112003	073905	alpha	3912	1.0057	-0.1492	0.0228	0.6258	0.9251	0.5400	0.4244	0.4293
SKUKUZA	29042003	071914	aot412	6810	0.1371	0.9336	0.7948	0.1237	0.3289	0.2055	0.1300	0.1241
SKUKUZA	09112003	072206	aot412	4844	0.1753	0.6040	0.4818	0.1090	0.2791	0.1719	0.0439	0.0504
SKUKUZA	24052003	073317	aot412	17879	0.1829	0.6676	0.6814	0.1210	0.3127	0.1945	0.0626	0.0774
SKUKUZA	18112003	073905	aot412	3912	0.1921	0.6609	0.6932	0.1329	0.3134	0.1834	0.0655	0.0825
SKUKUZA	29042003	071914	aot560	6810	0.1330	0.7983	0.6704	0.1009	0.2711	0.1731	0.1141	0.1170
SKUKUZA	09112003	072206	aot560	4844	0.1829	0.1973	0.0225	0.0748	0.2126	0.1502	0.0675	0.0513
SKUKUZA	24052003	073317	aot560	17879	0.2016	0.4504	0.2975	0.1275	0.2678	0.1469	0.0610	0.0739
SKUKUZA	18112003	073905	aot560	3912	0.1288	0.5071	0.3728	0.0642	0.2097	0.1597	0.0677	0.0815
SKUKUZA	29042003	071914	aot860	6810	0.1395	0.5788	0.5112	0.0933	0.2197	0.1385	0.0883	0.1091
SKUKUZA	09112003	072206	aot860	4844	0.2020	-0.0748	0.0037	0.0885	0.1926	0.1262	0.0671	0.0544
SKUKUZA	24052003	073317	aot860	17879	0.2077	0.1821	0.0524	0.1367	0.2262	0.1019	0.0552	0.0694
SKUKUZA	18112003	073905	aot860	3912	0.1240	0.3191	0.1830	0.0647	0.1667	0.1338	0.0610	0.0817

11. Annexe 5 : Surface reflectance map comparison

The following images are the results of the intercomparison of surface reflectances estimated using either SMAC or UBAC methods. For each date, the comparison is represented for 4 channels (channel 2, 5, 7 and 13). The difference between the reflectances is also represented with the histogram of the differences. The AOT map at 550 nm is represented as last map with the histogram of the AOT for the valid pixels.

MER_RR__2PP01R20030322_101214_000001102014_00466_05530_0001.N1.dim

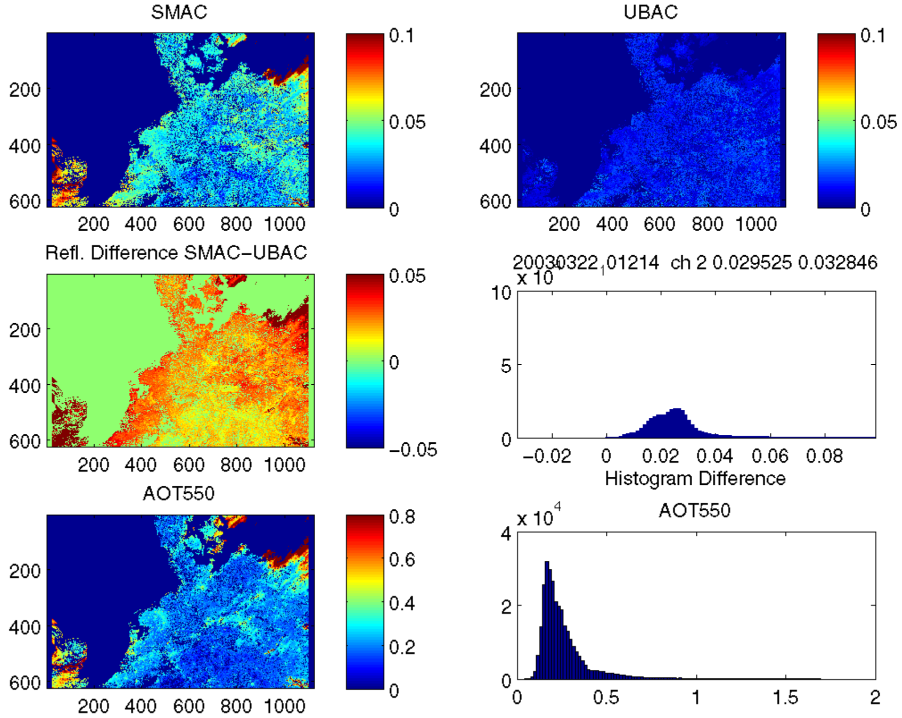

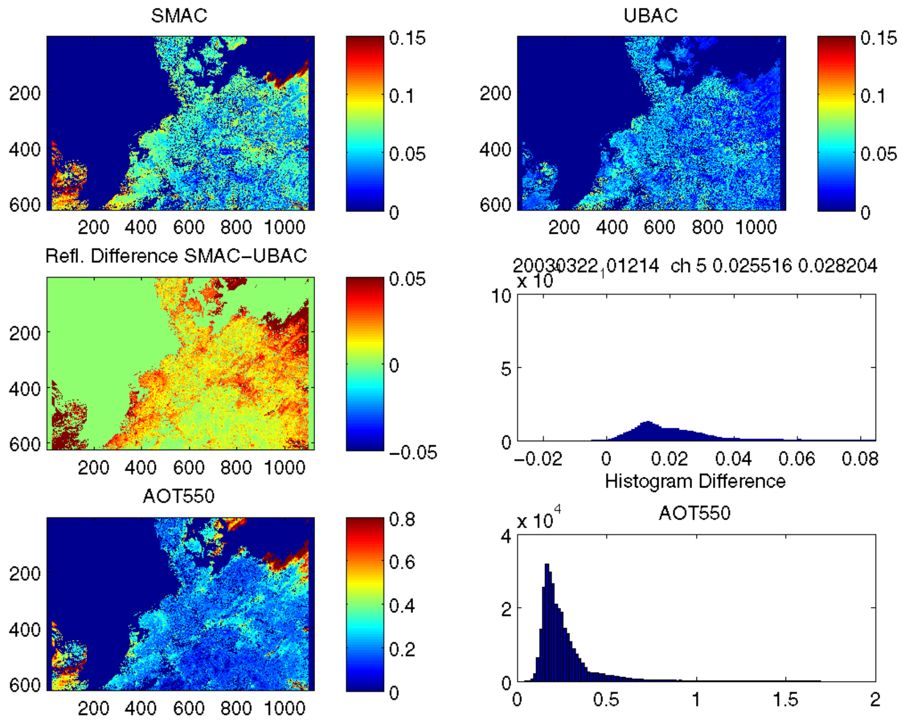

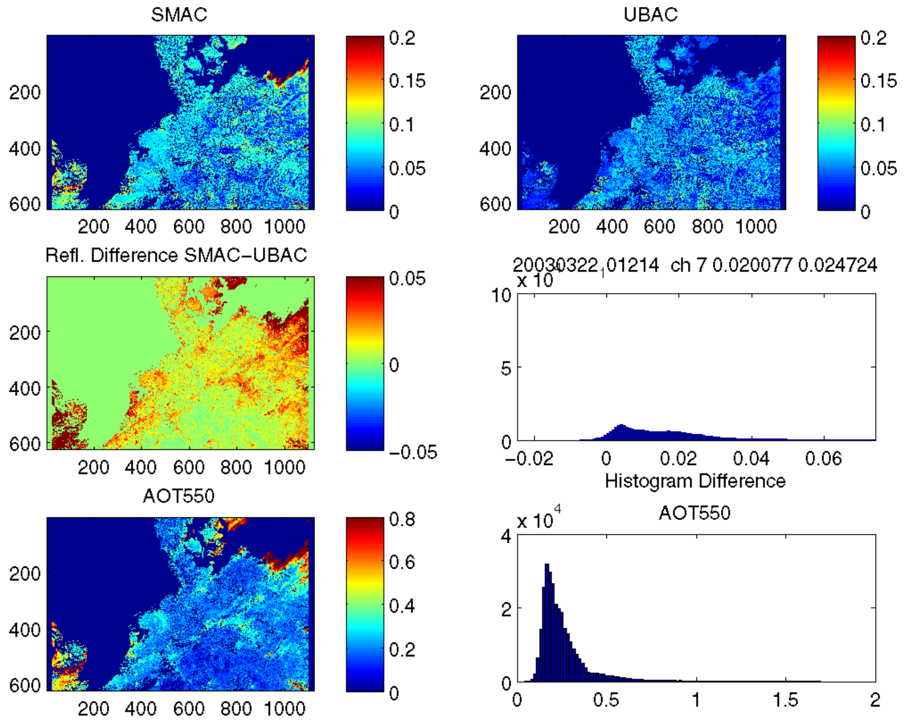
SMAC
UBAC
Refl. Difference SMAC−UBAC
20030322_01214 ch 7 0.020077 0.024724
Histogram Difference
AOT550
AOT550

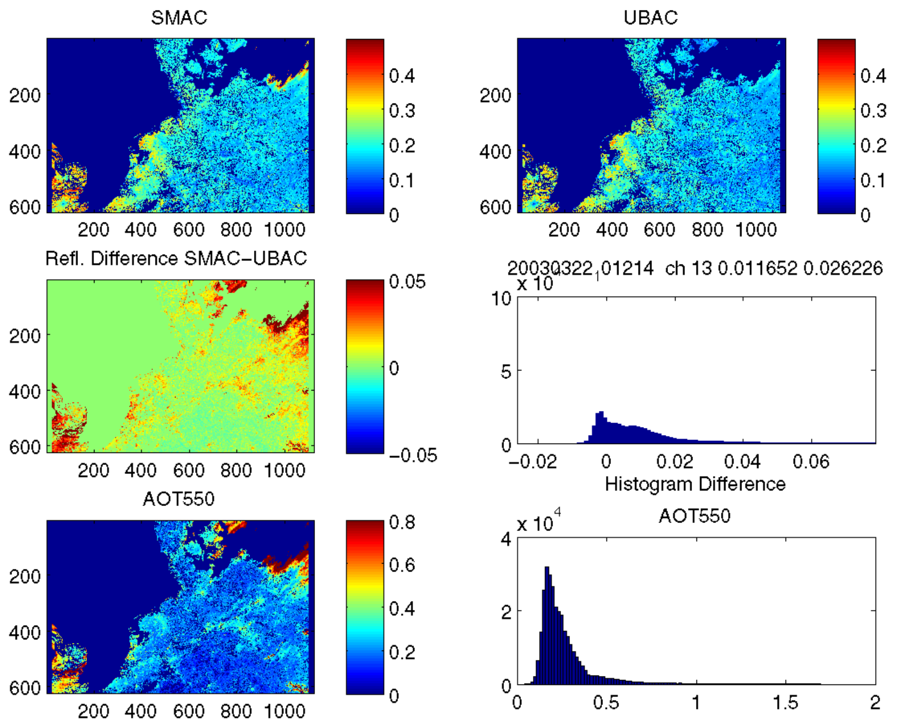
SMAC
UBAC
Refl. Difference SMAC−UBAC
20030322_01214 ch 13 0.011652 0.026226
Histogram Difference
AOT550
AOT550

MER_RR__2PP01R20030430_132600_000001072016_00024_06090_0001.N1.dim

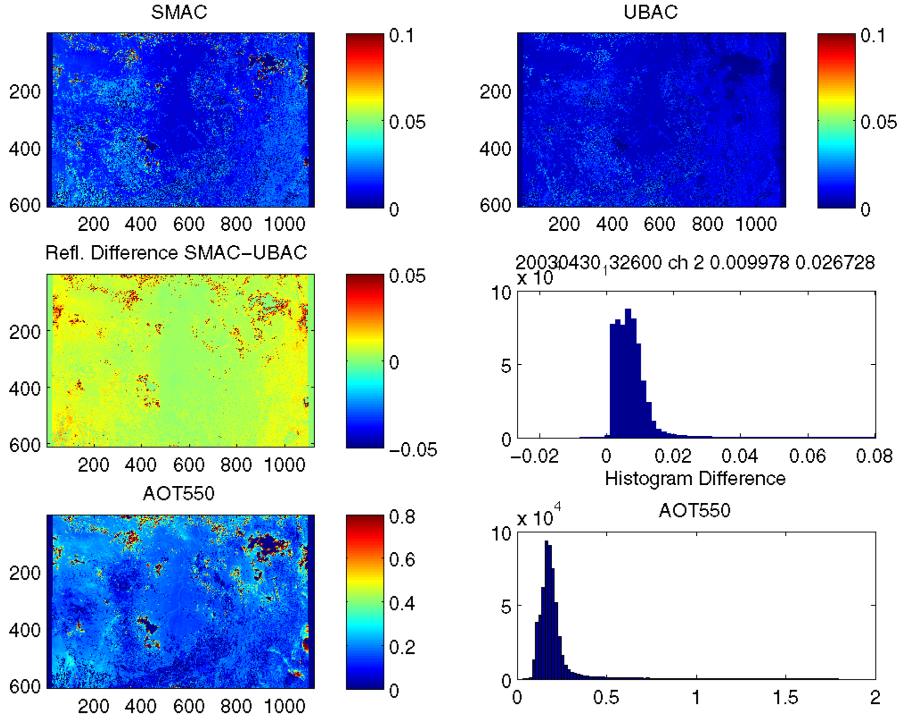

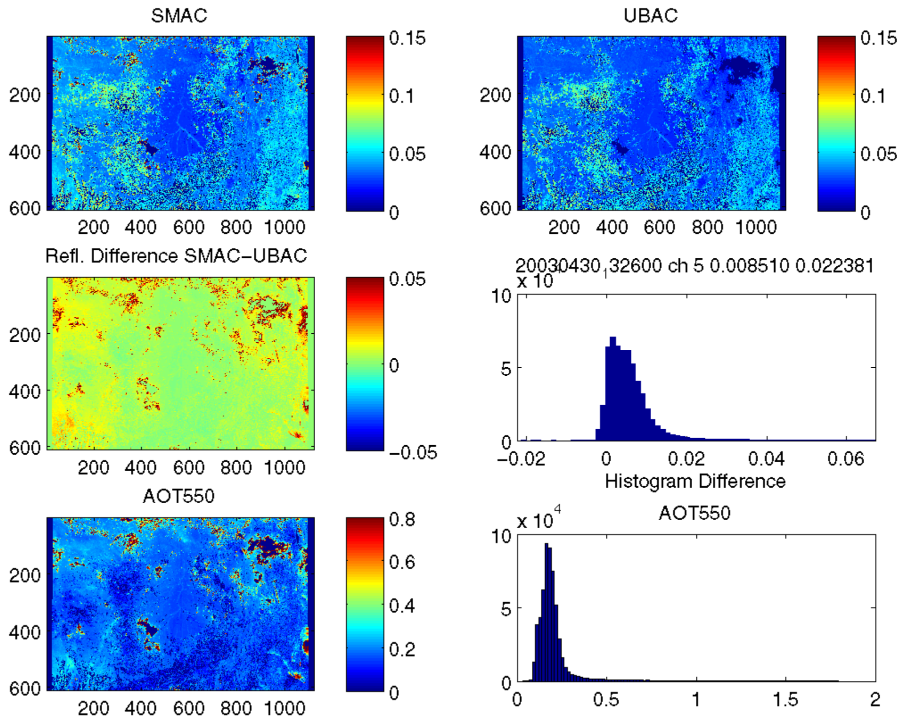

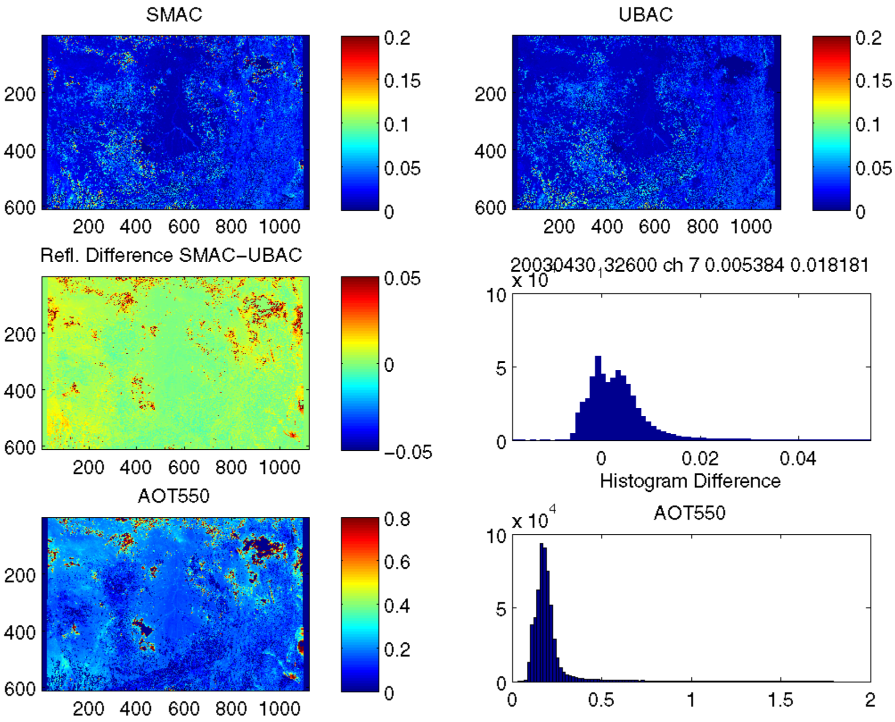
SMAC
UBAC
Refl. Difference SMAC−UBAC
20030430 32600 ch 7 0.005384 0.018181
Histogram Difference
AOT550
AOT550

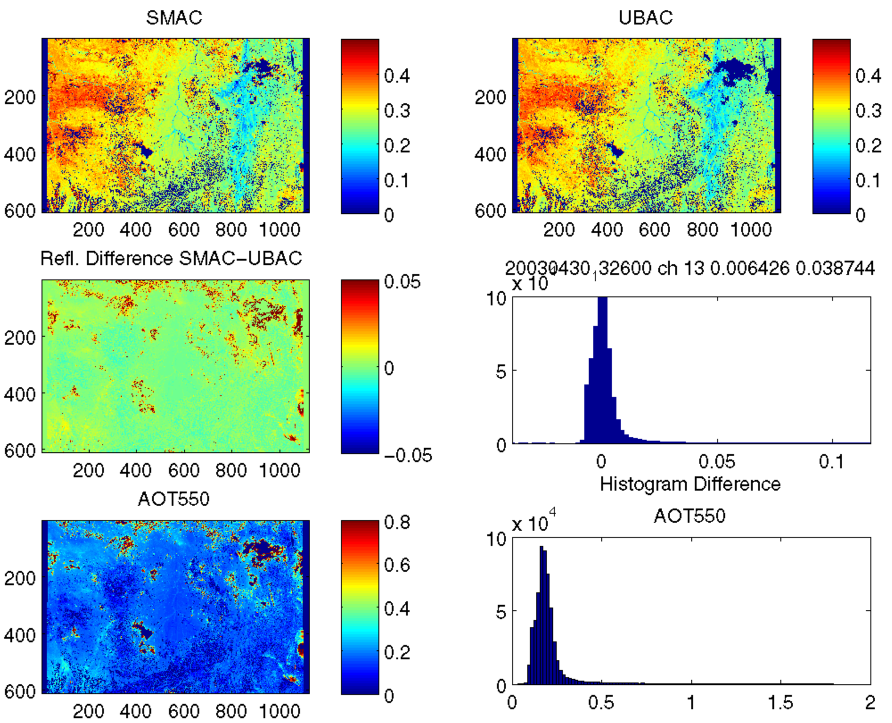
SMAC
UBAC
Refl. Difference SMAC−UBAC
20030430 32600 ch 13 0.006426 0.038744
Histogram Difference
AOT550
AOT550

MER_RR__2PP01R20030523_080222_000001072016_00350_06416_0001.N1.dim

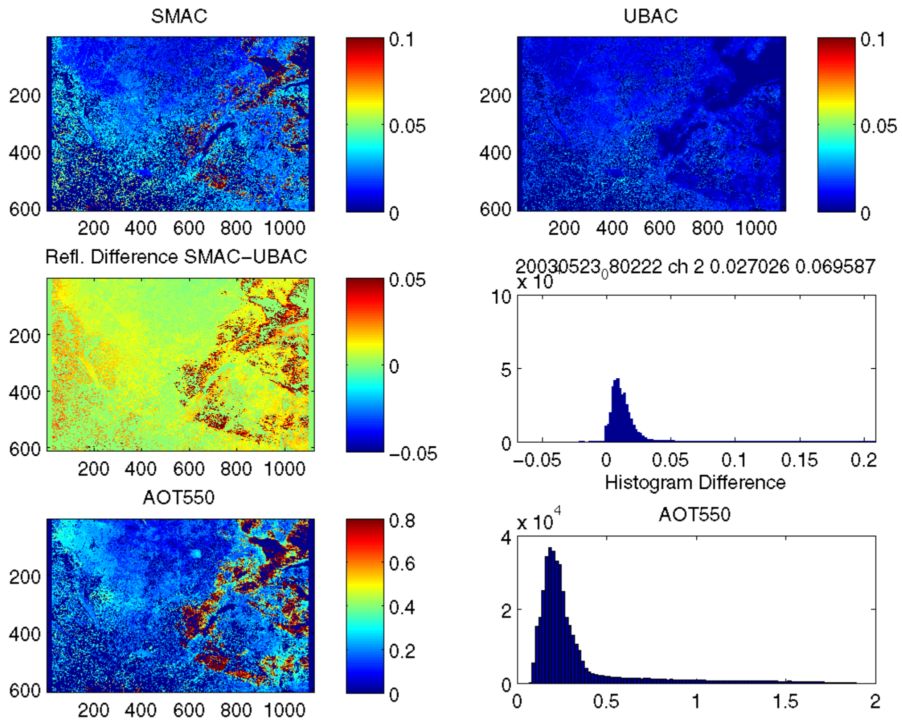

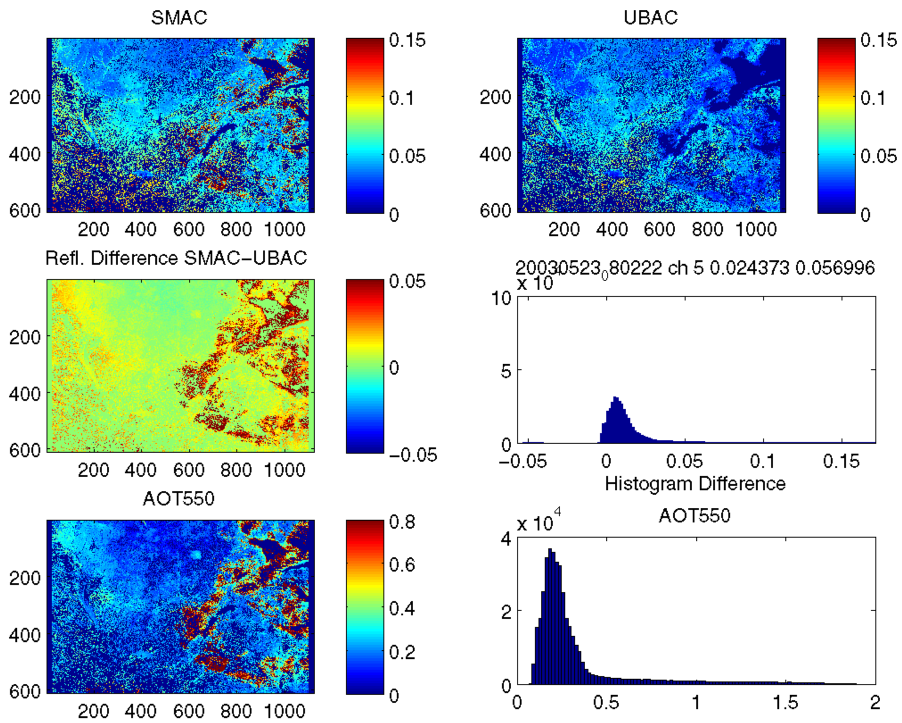

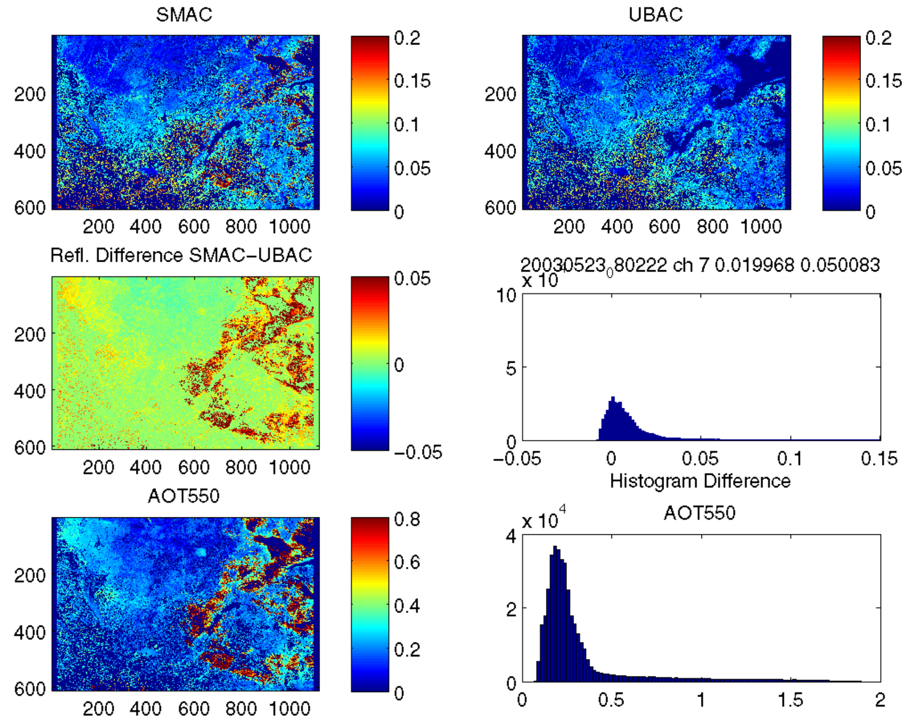
SMAC
UBAC
Refl. Difference SMAC−UBAC
20030523_080222 ch 7 0.019968 0.050083
Histogram Difference
AOT550
AOT550

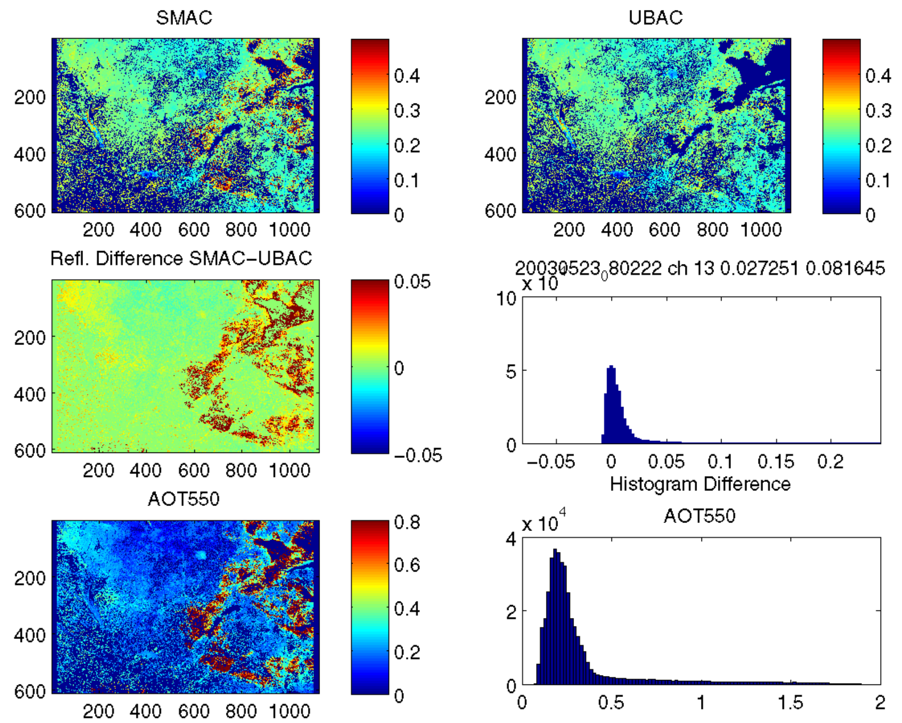
SMAC
UBAC
Refl. Difference SMAC−UBAC
20030523_080222 ch 13 0.027251 0.081645
Histogram Difference
AOT550
AOT550

MER_RR__2PP01R20030601_094456_000001072016_00480_06546_0001.N1.dim

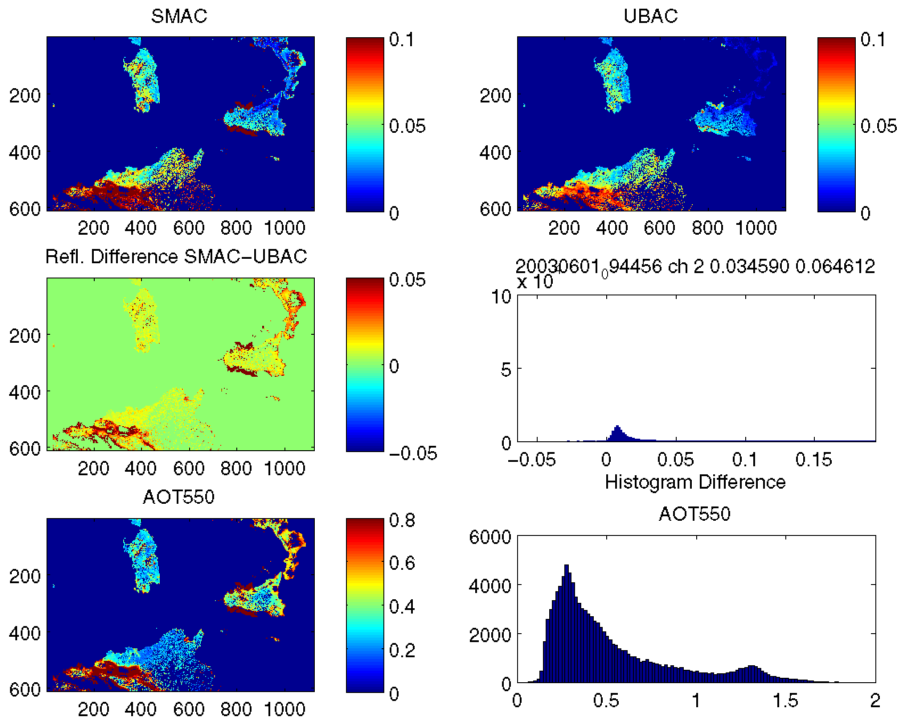

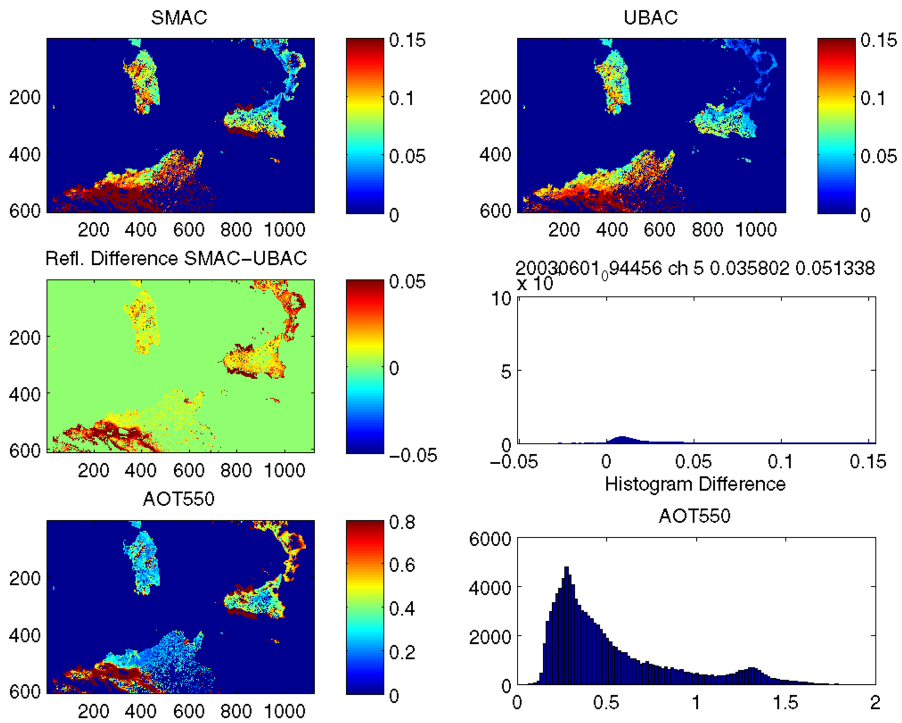

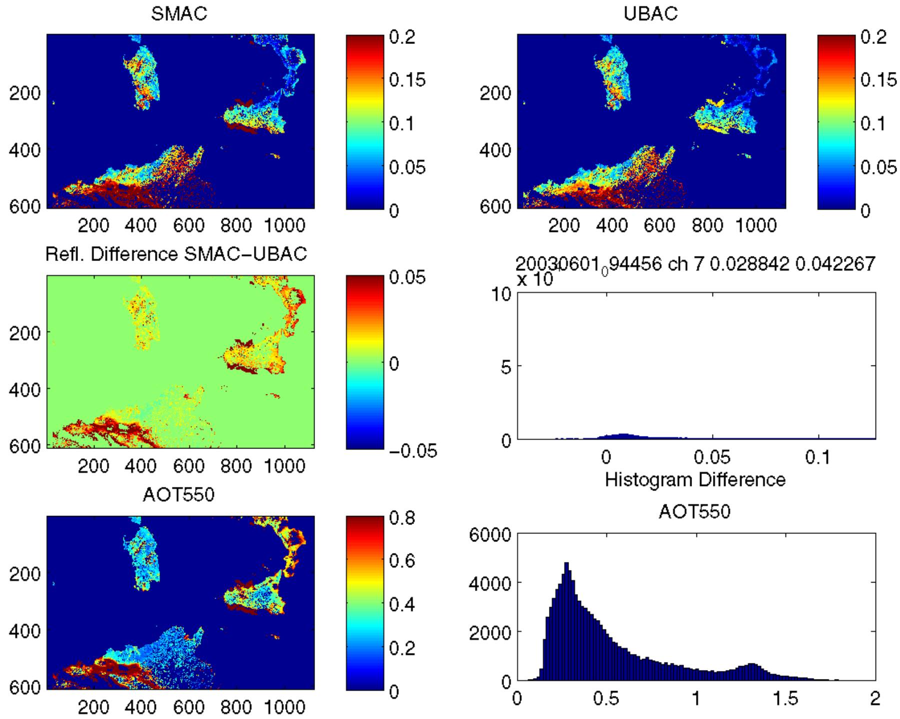

SMAC
UBAC
Refl. Difference SMAC−UBAC
20030601_94456 ch 7 0.028842 0.042267
Histogram Difference
AOT550

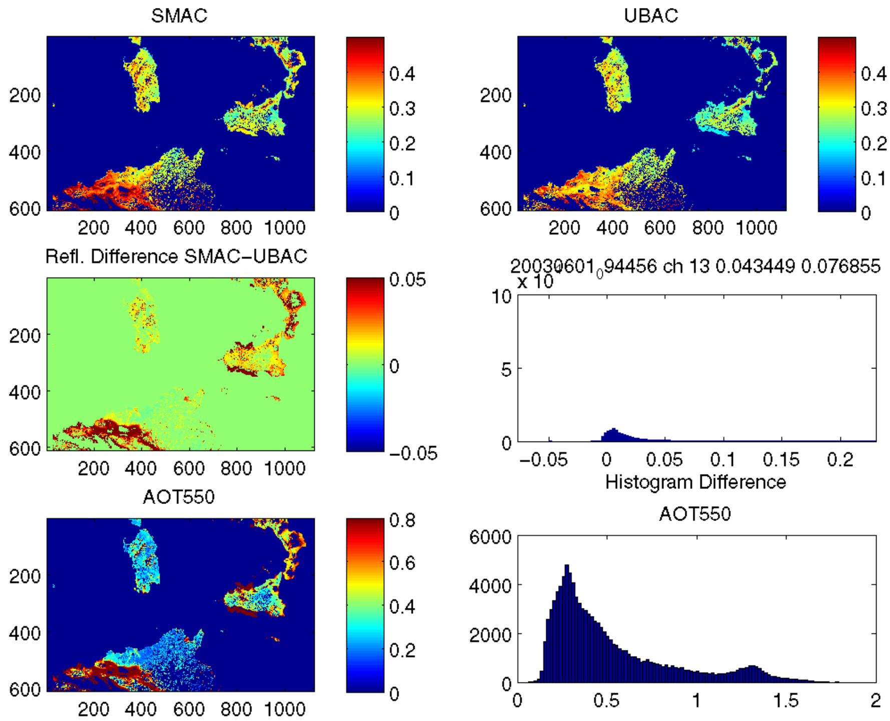

SMAC
UBAC
Refl. Difference SMAC−UBAC
20030601_94456 ch 13 0.043449 0.076855
Histogram Difference
AOT550

MER_RR__2PP01R20030616_151327_000001102017_00197_06764_0001.N1.dim

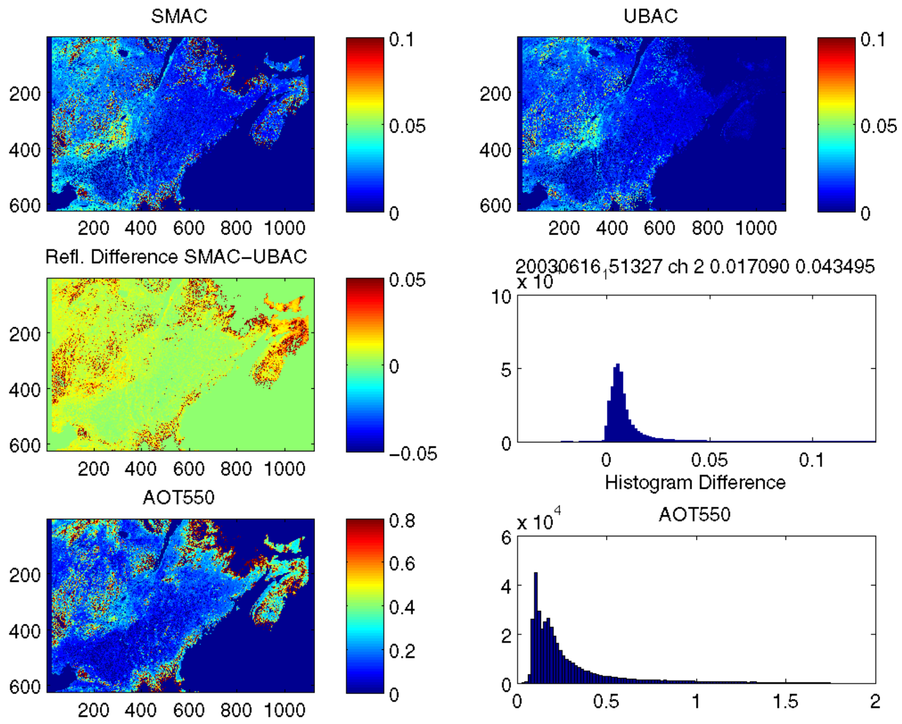

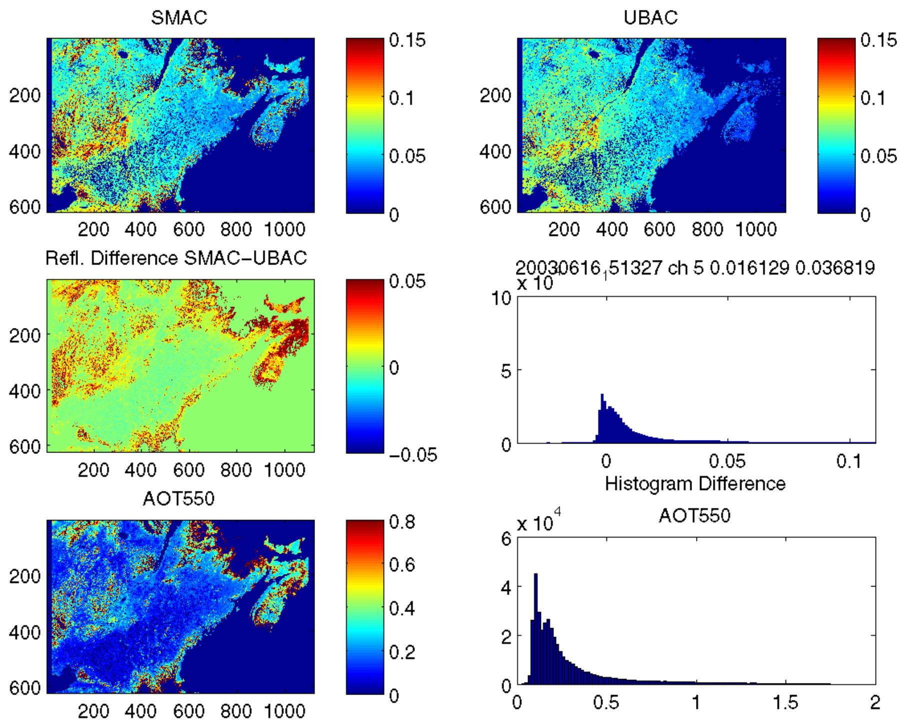

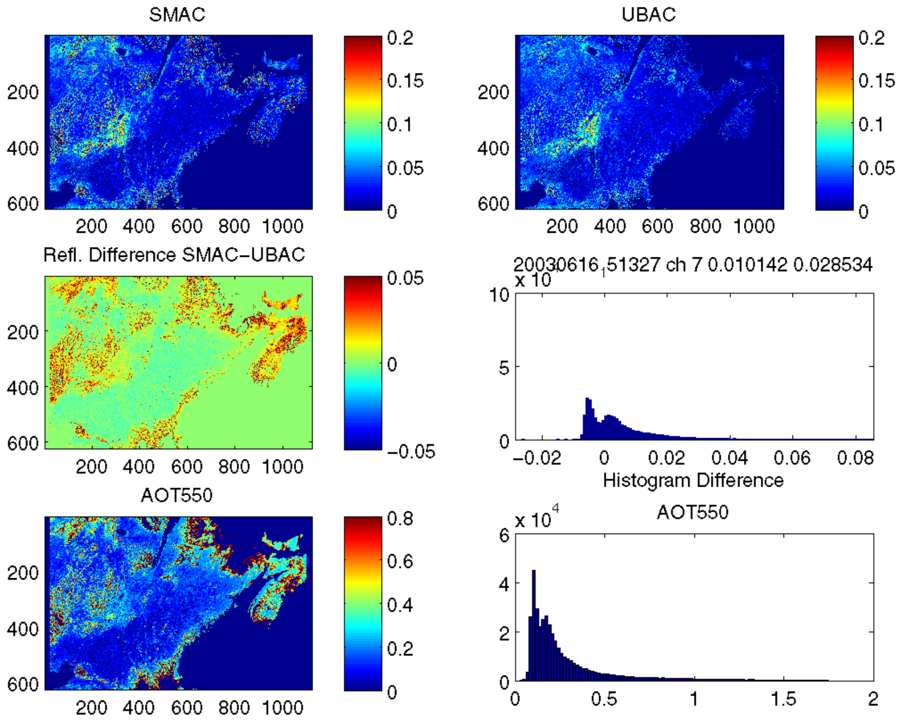

SMAC
UBAC
Refl. Difference SMAC−UBAC
20030616_51327 ch 7 0.010142 0.028534
Histogram Difference
AOT550
AOT550

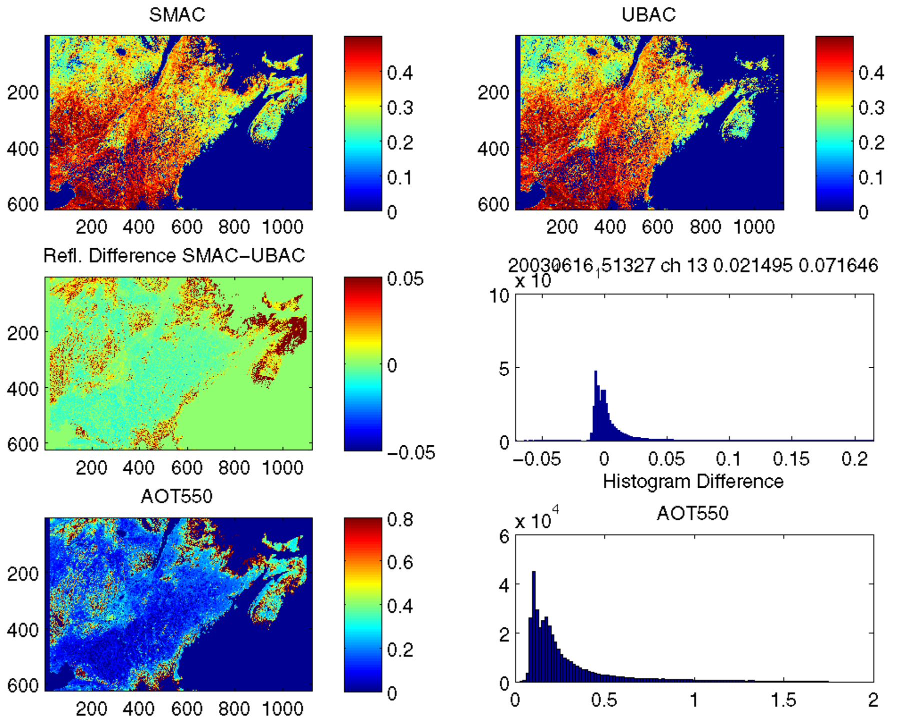

SMAC
UBAC
Refl. Difference SMAC−UBAC
20030616_51327 ch 13 0.021495 0.071646
Histogram Difference
AOT550
AOT550

MER_RR__2PP01R20030621_155918_000001102017_00269_06836_0001.N1.data

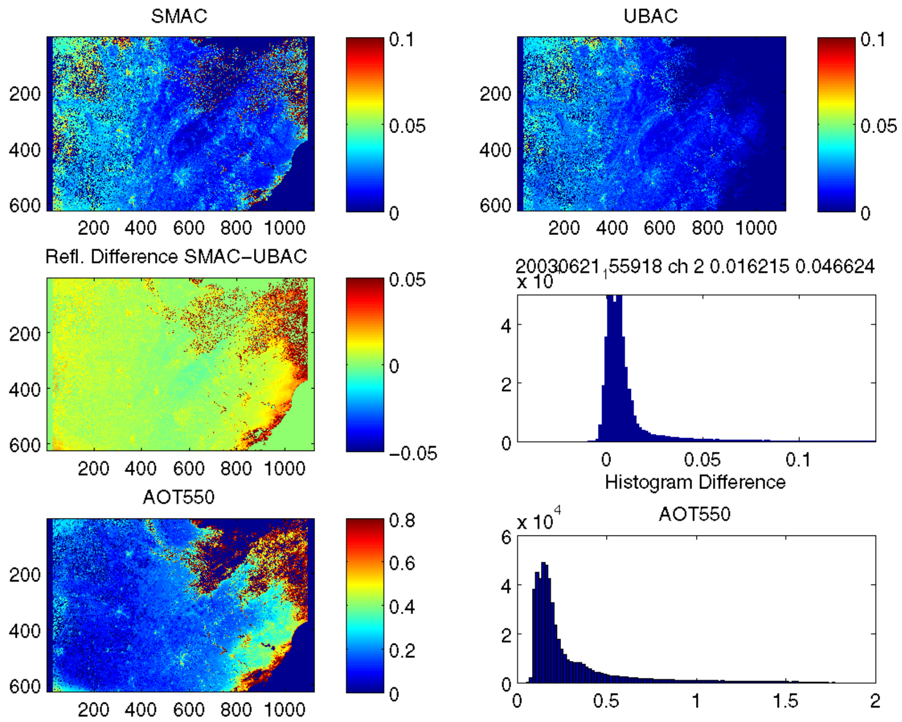

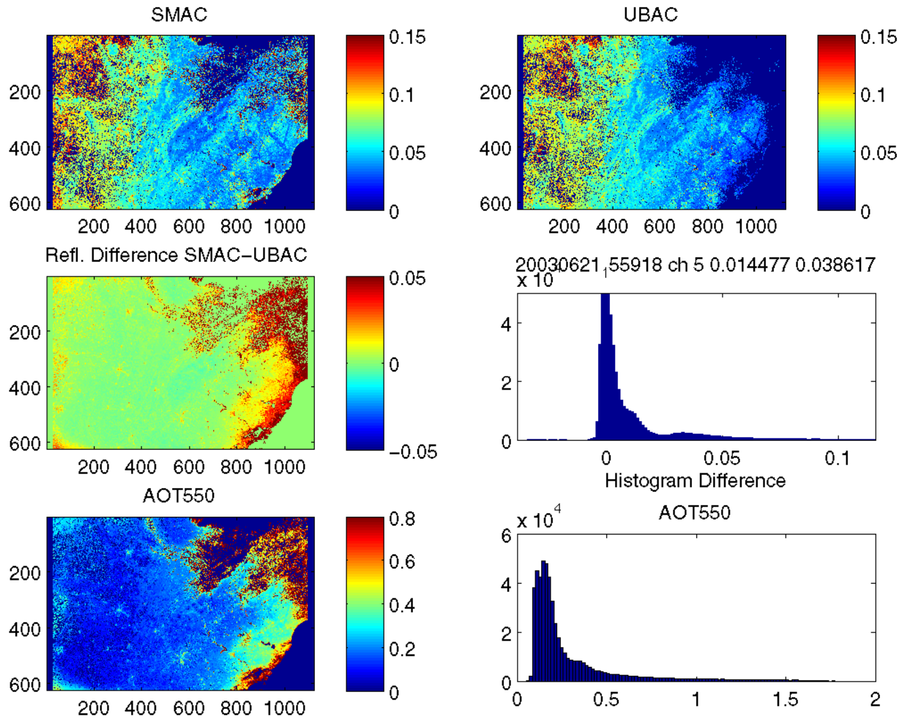

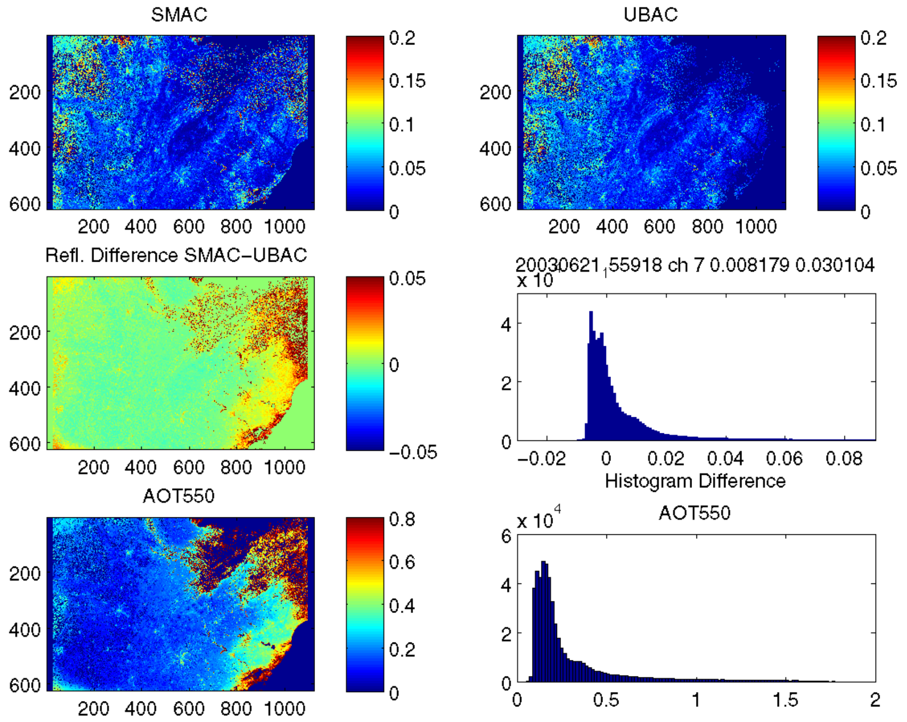

SMAC
UBAC
Refl. Difference SMAC−UBAC
20030621 55918 ch 7 0.008179 0.030104
Histogram Difference
AOT550
AOT550

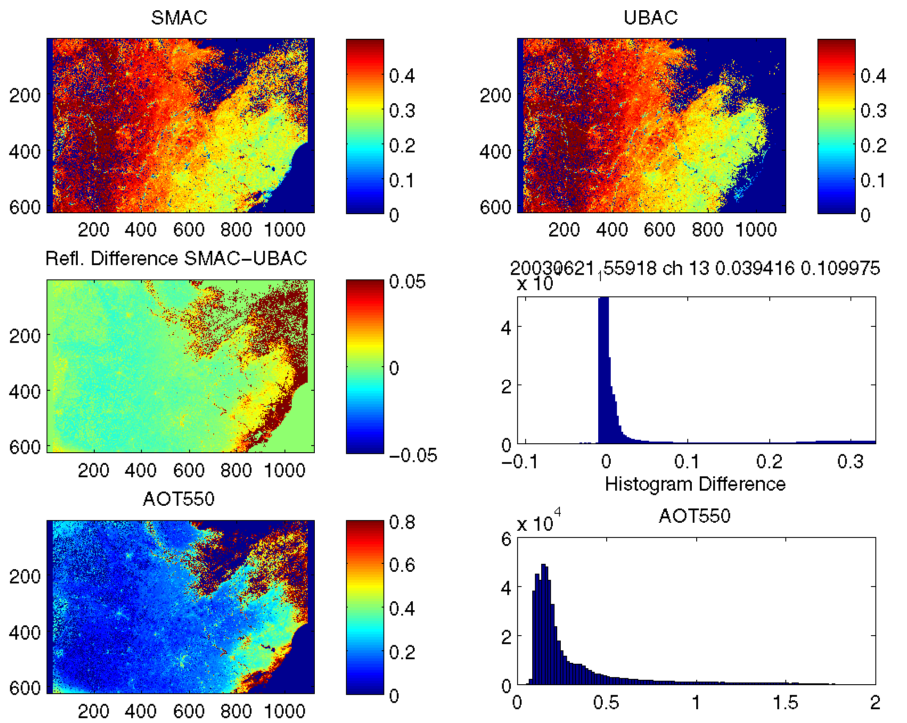

SMAC
UBAC
Refl. Difference SMAC−UBAC
20030621 55918 ch 13 0.039416 0.109975
Histogram Difference
AOT550
AOT550

MER_RR__2PP01R20030711_102624_000001072018_00051_07119_0001.N1.data

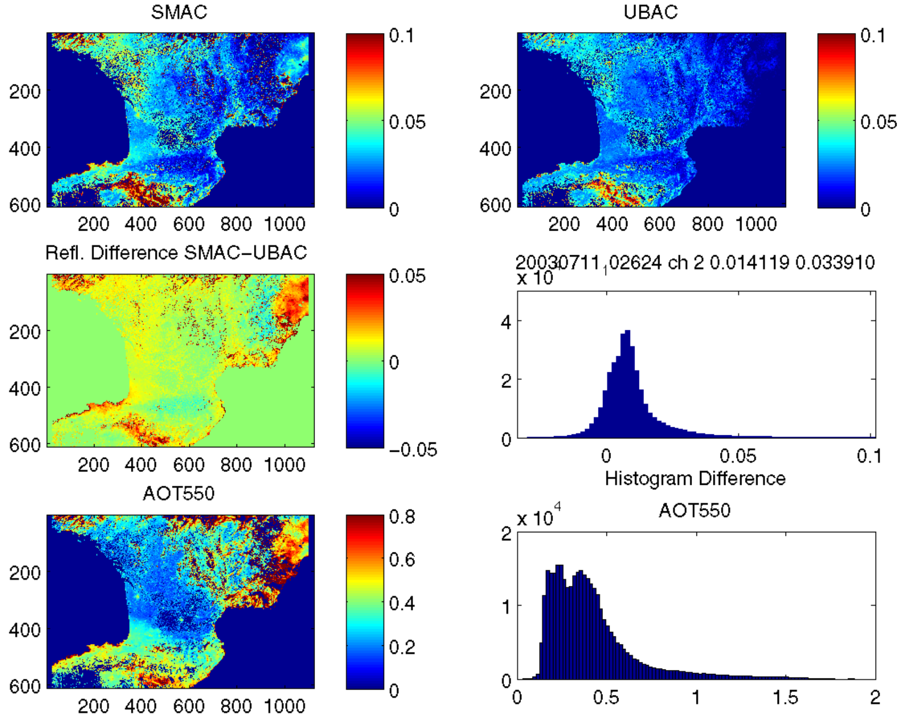

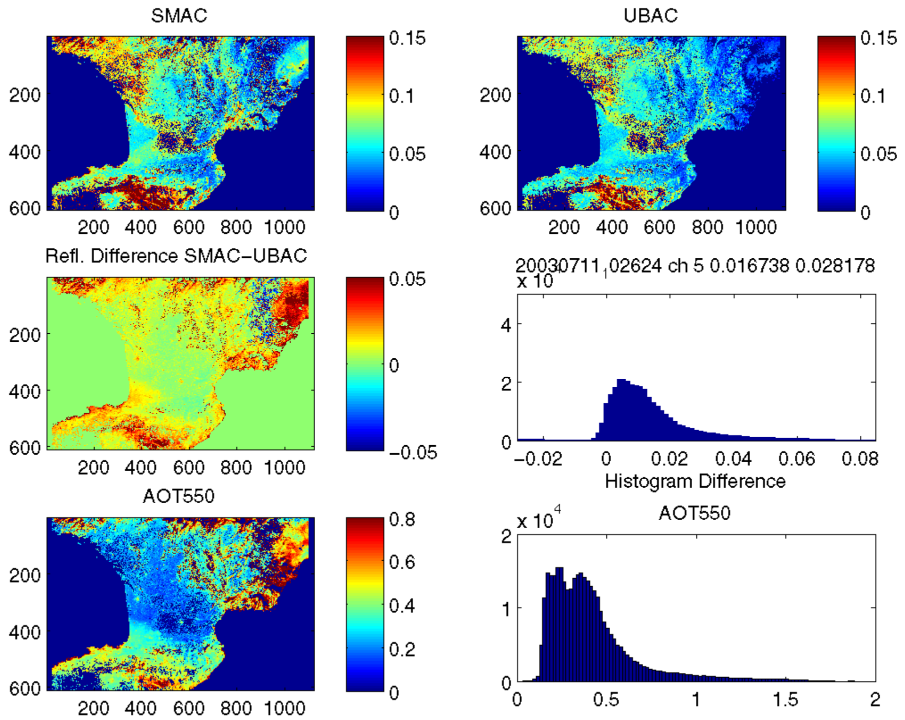

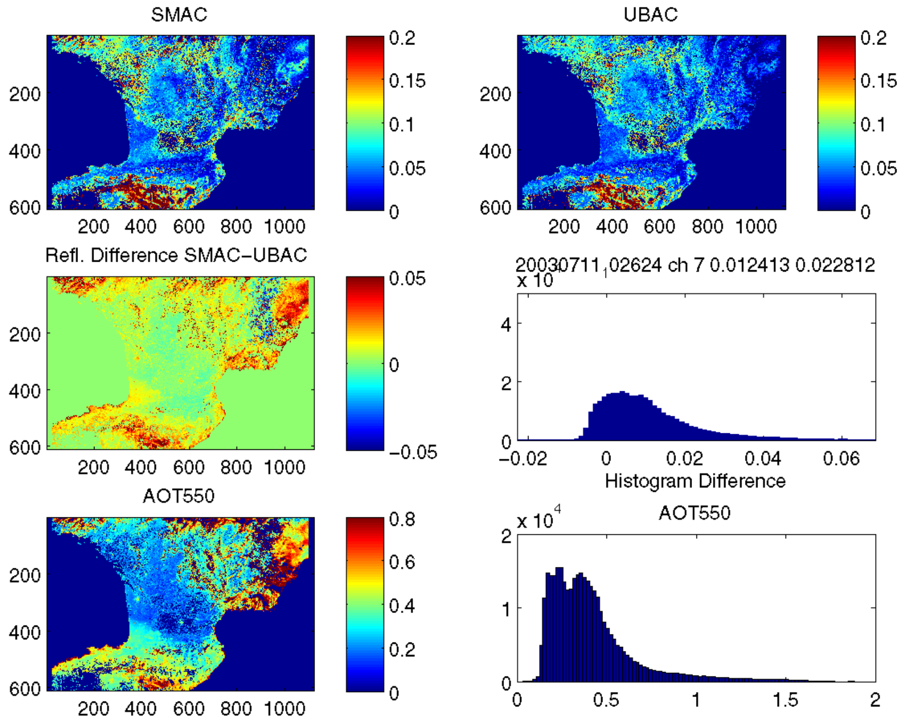
SMAC
UBAC
Refl. Difference SMAC−UBAC
20030711 02624 ch 7 0.012413 0.022812
Histogram Difference
AOT550
AOT550

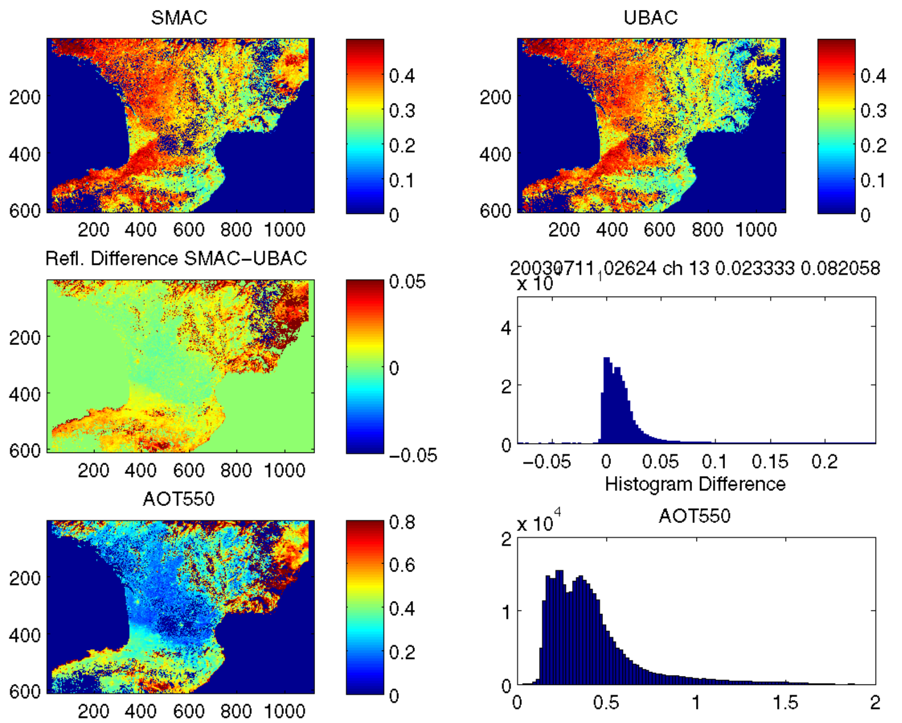
SMAC
UBAC
Refl. Difference SMAC−UBAC
20030711 02624 ch 13 0.023333 0.082058
Histogram Difference
AOT550
AOT550

MER_RR__2PP01R20030728_095206_000001102018_00294_07362_0001.N1.data

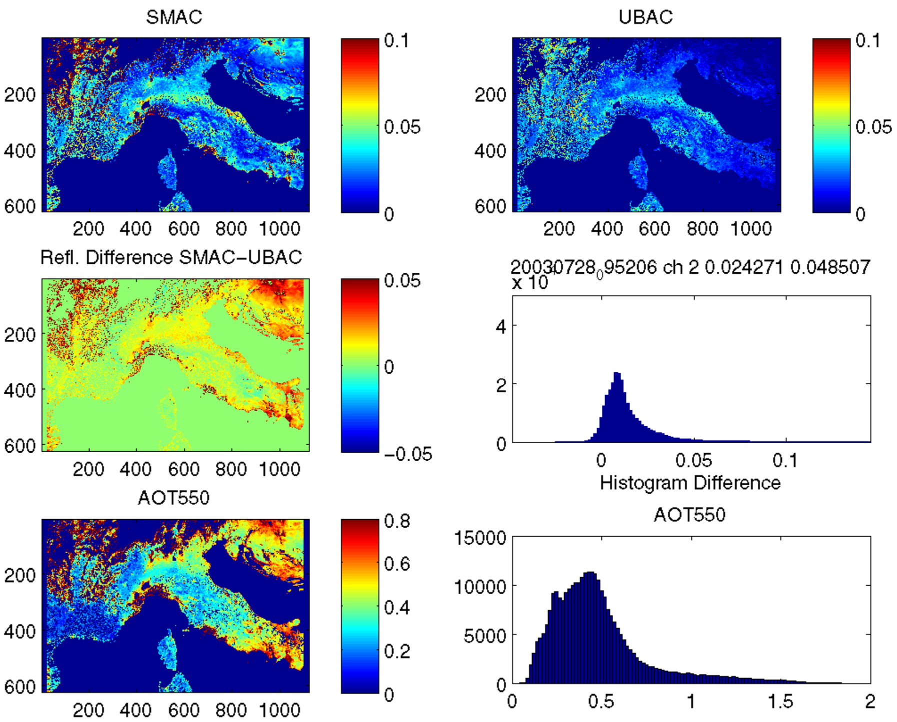

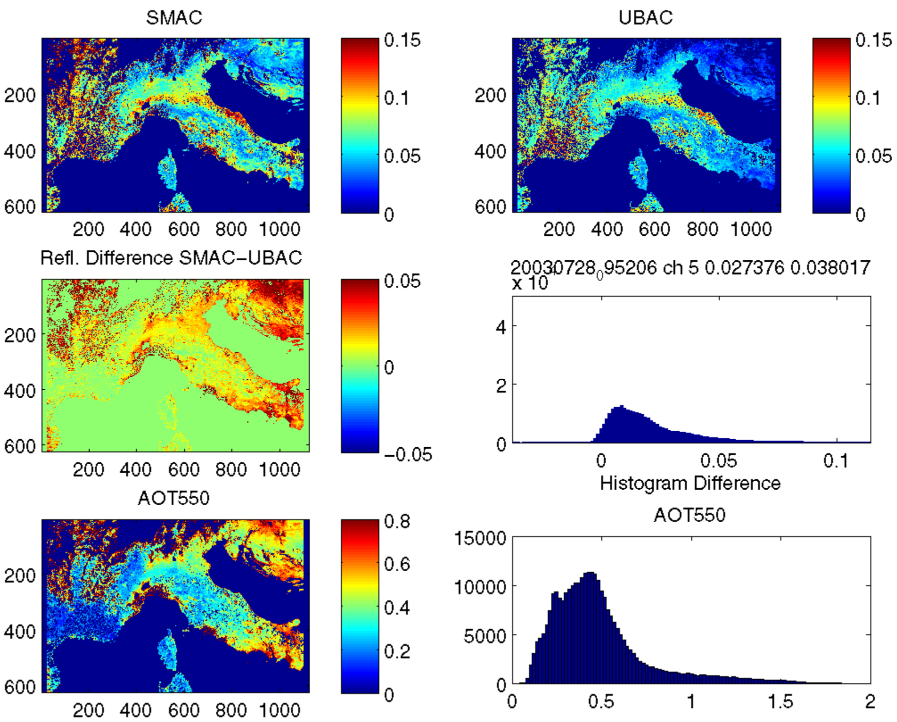

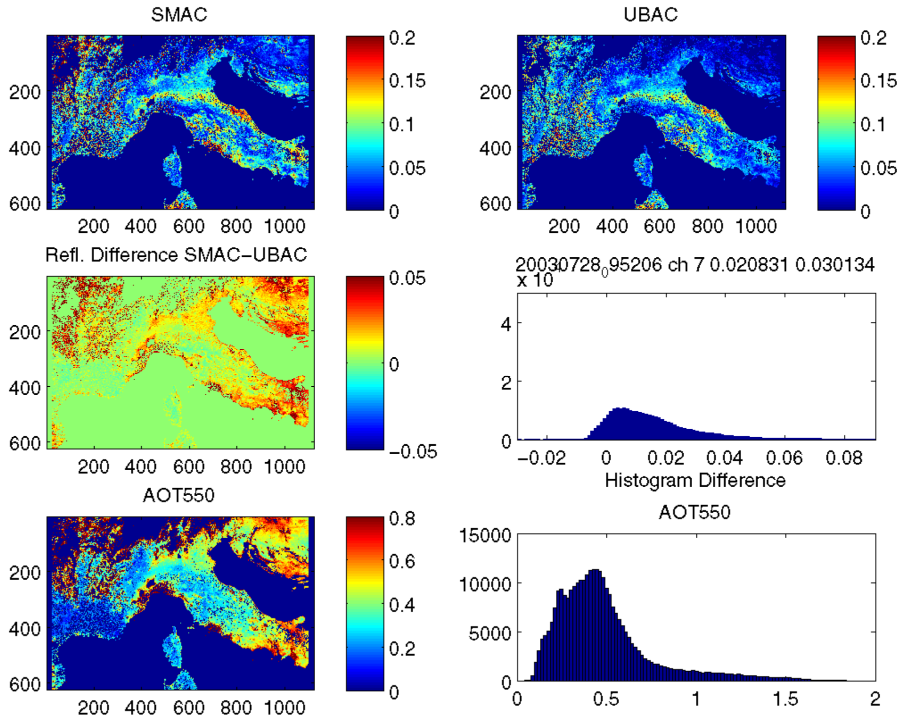

SMAC
UBAC
Refl. Difference SMAC−UBAC
20030728_95206 ch 7 0.020831 0.030134
Histogram Difference
AOT550
AOT550

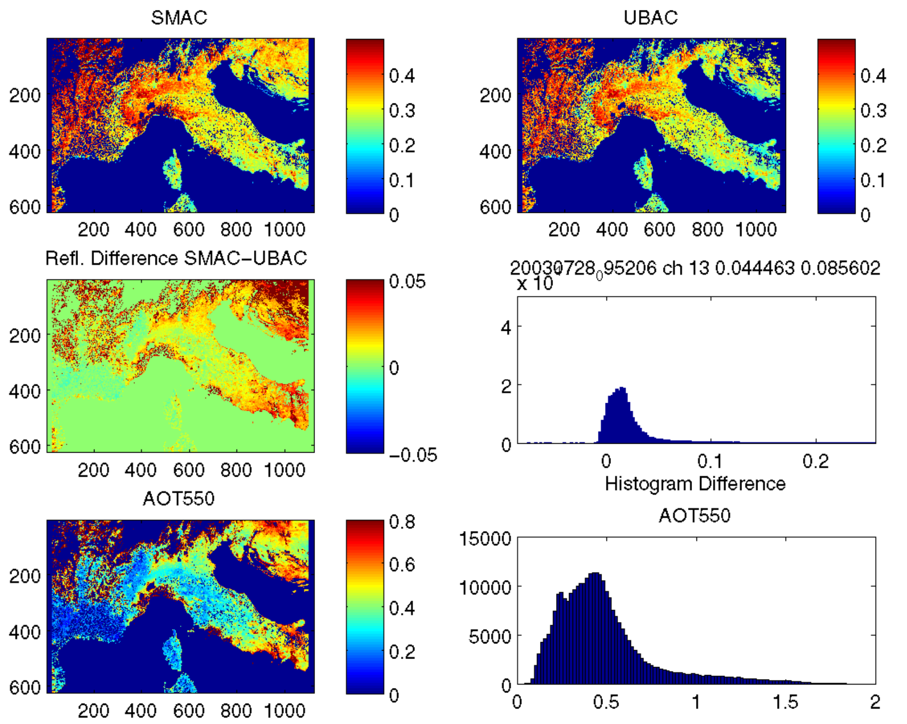

SMAC
UBAC
Refl. Difference SMAC−UBAC
20030728_95206 ch 13 0.044463 0.085602
Histogram Difference
AOT550
AOT550

MER_RR__2PP01R20030802_103459_000001102018_00366_07434_0001.N1.data

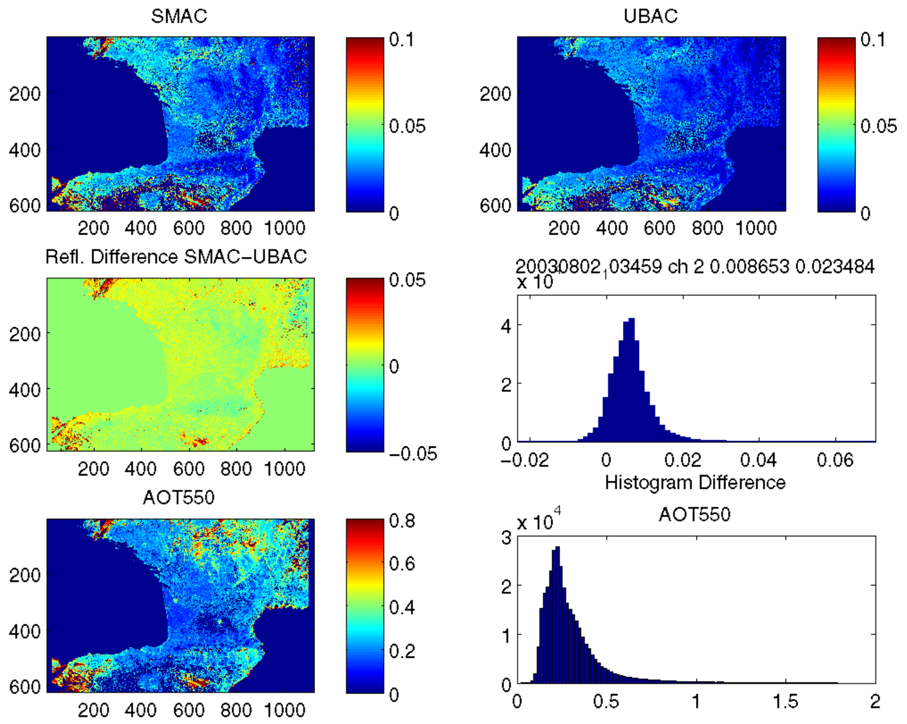

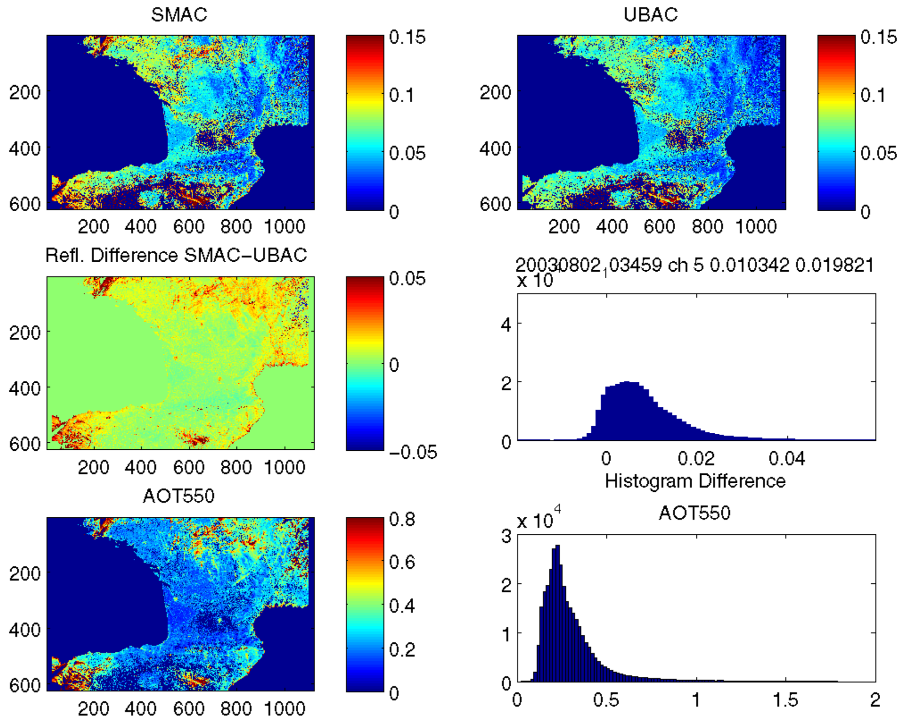

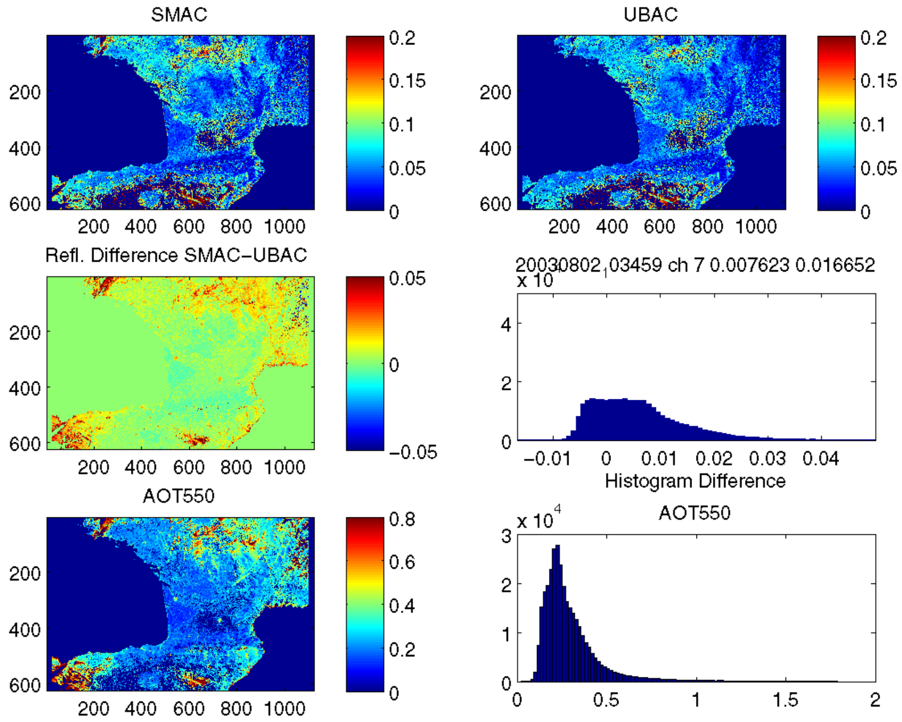
SMAC
UBAC
Refl. Difference SMAC−UBAC
20030802_03459 ch 7 0.007623 0.016652
Histogram Difference
AOT550

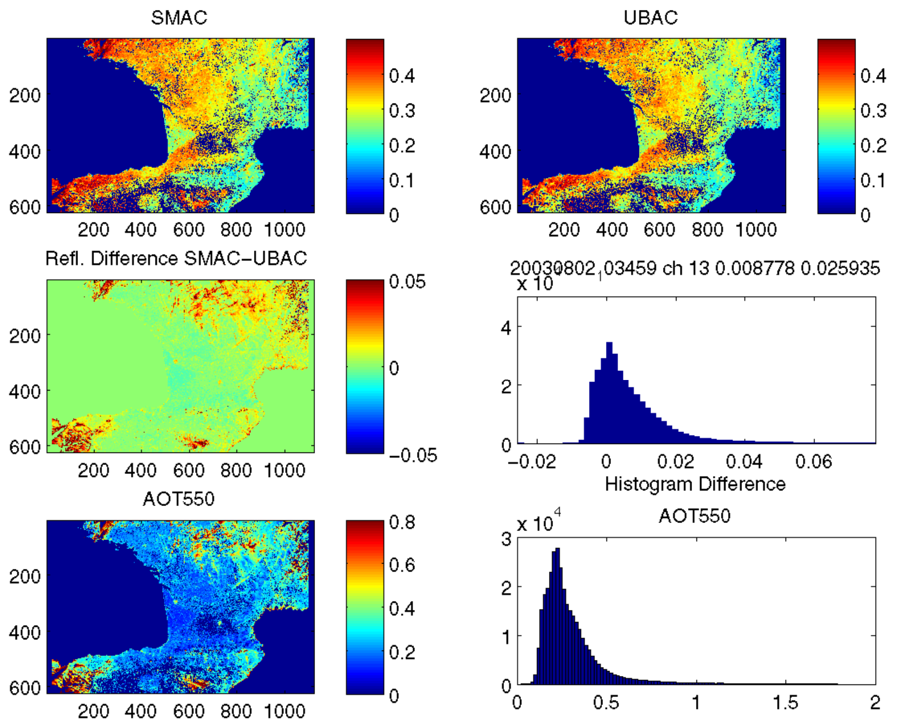
SMAC
UBAC
Refl. Difference SMAC−UBAC
20030802_03459 ch 13 0.008778 0.025935
Histogram Difference
AOT550

MER_RR__2PP01R20030825_101253_000001072019_00194_07763_0001.N1.data

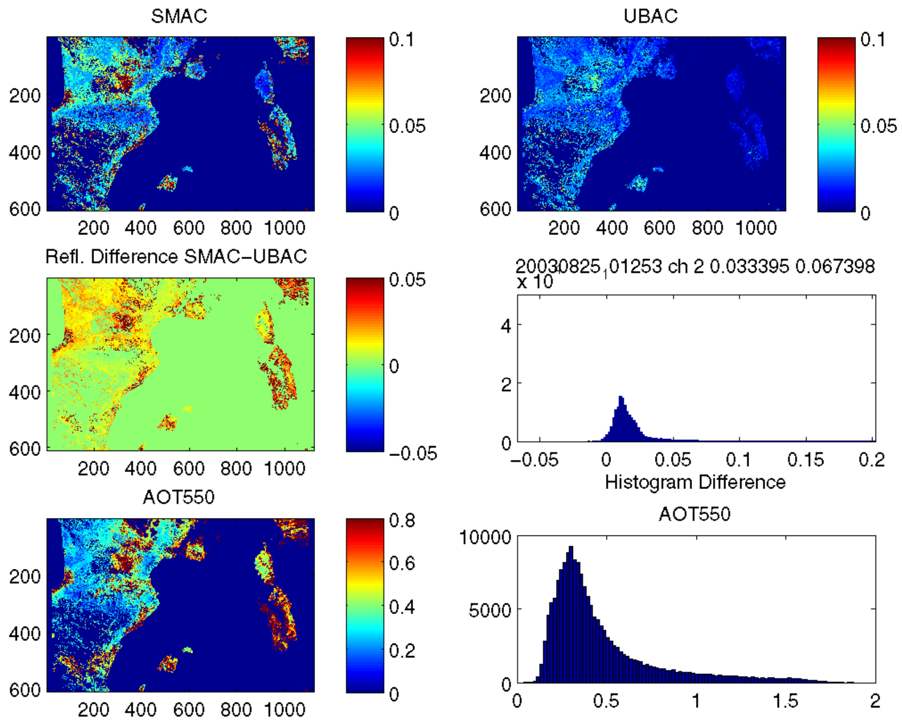

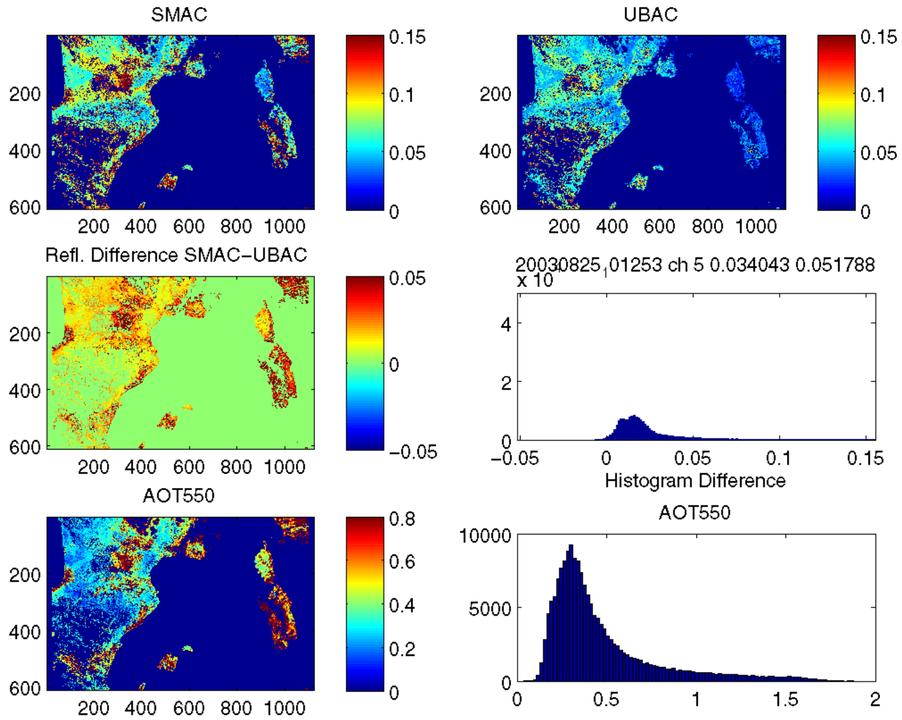

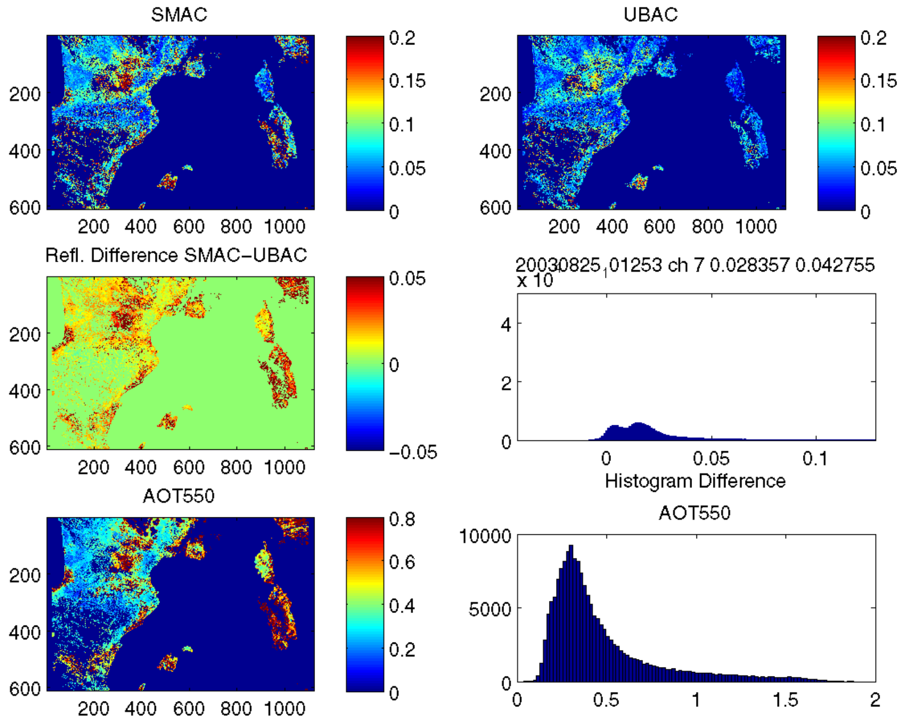

SMAC
UBAC
Refl. Difference SMAC−UBAC
20030825_01253 ch 7 0.028357 0.042755
Histogram Difference
AOT550
AOT550

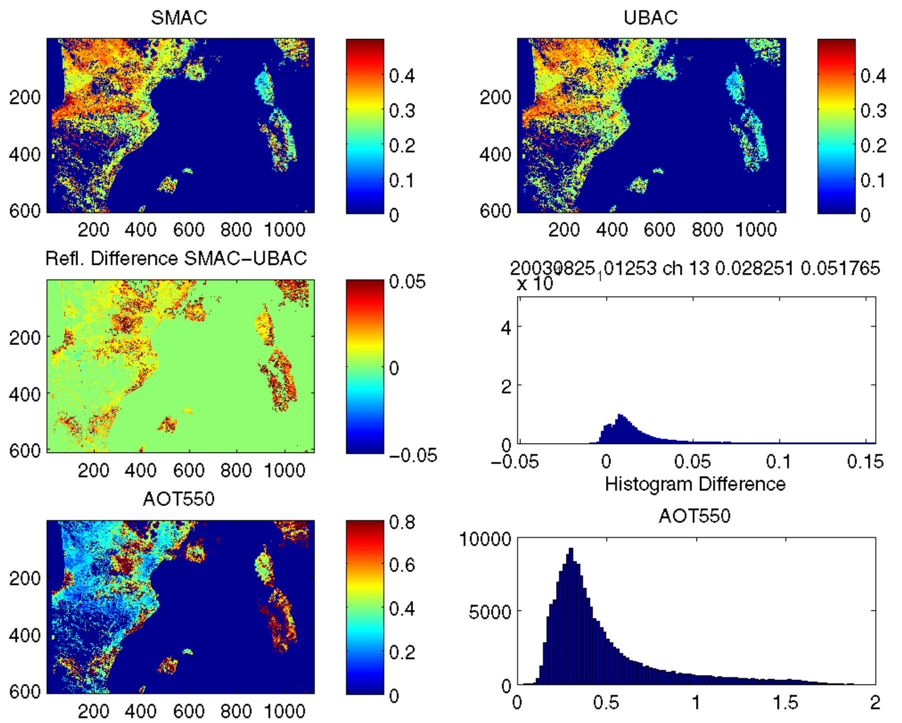

SMAC
UBAC
Refl. Difference SMAC−UBAC
20030825_01253 ch 13 0.028251 0.051765
Histogram Difference
AOT550
AOT550

MER_RR__2PP01R20030915_105232_000001102019_00495_08064_0001.N1.data

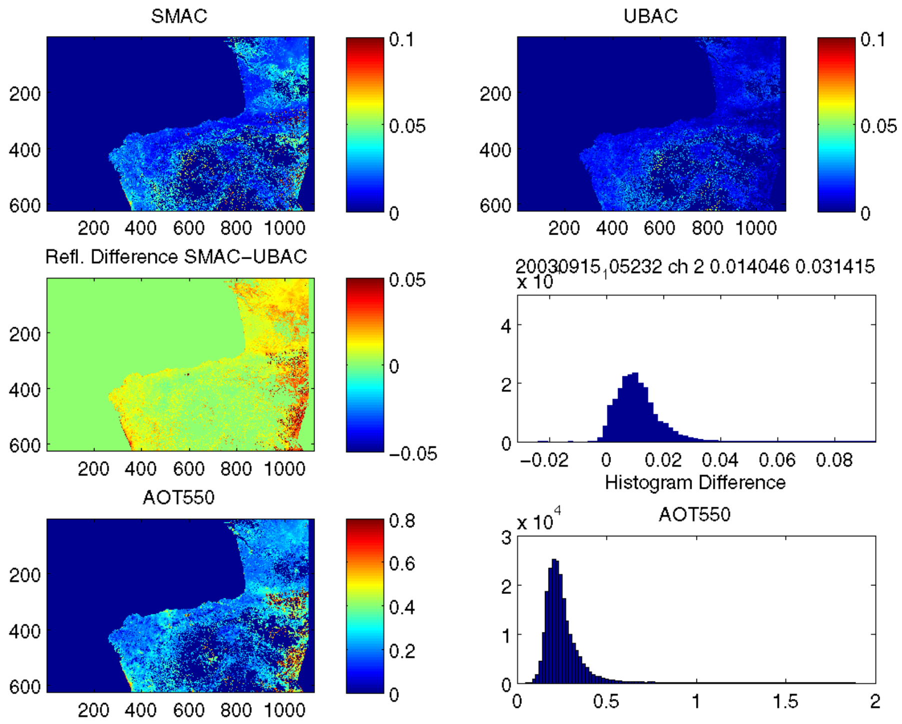

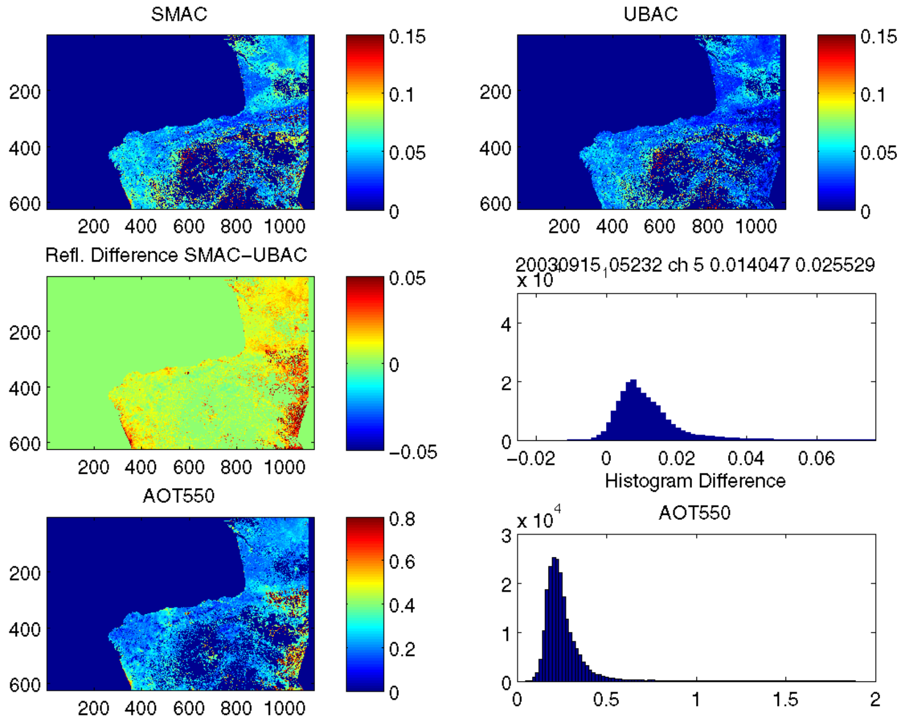

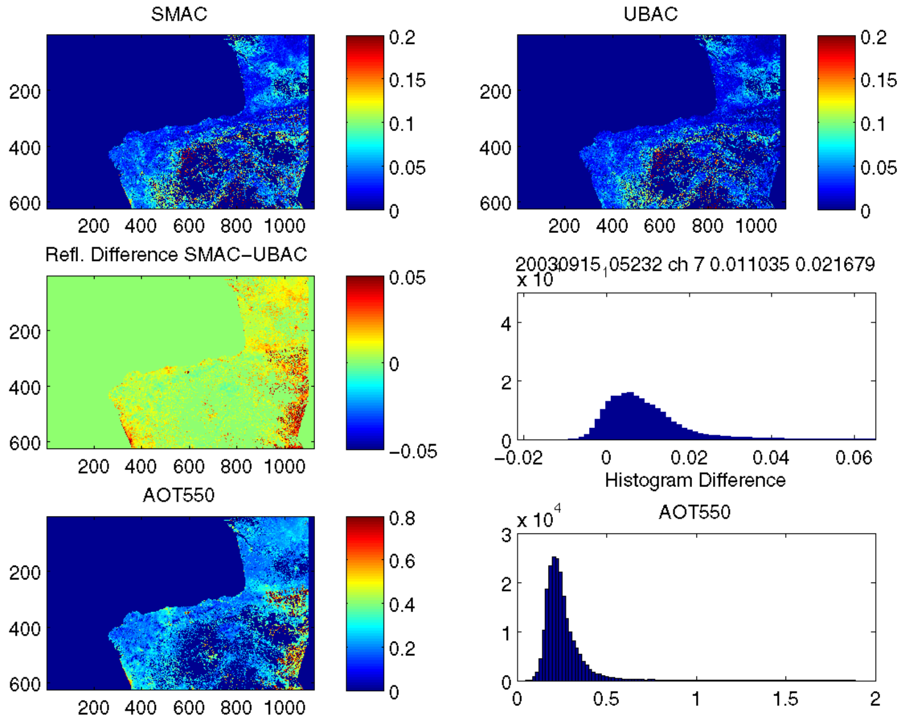
SMAC
UBAC
Refl. Difference SMAC−UBAC
20030915_05232 ch 7 0.011035 0.021679
Histogram Difference
AOT550
AOT550

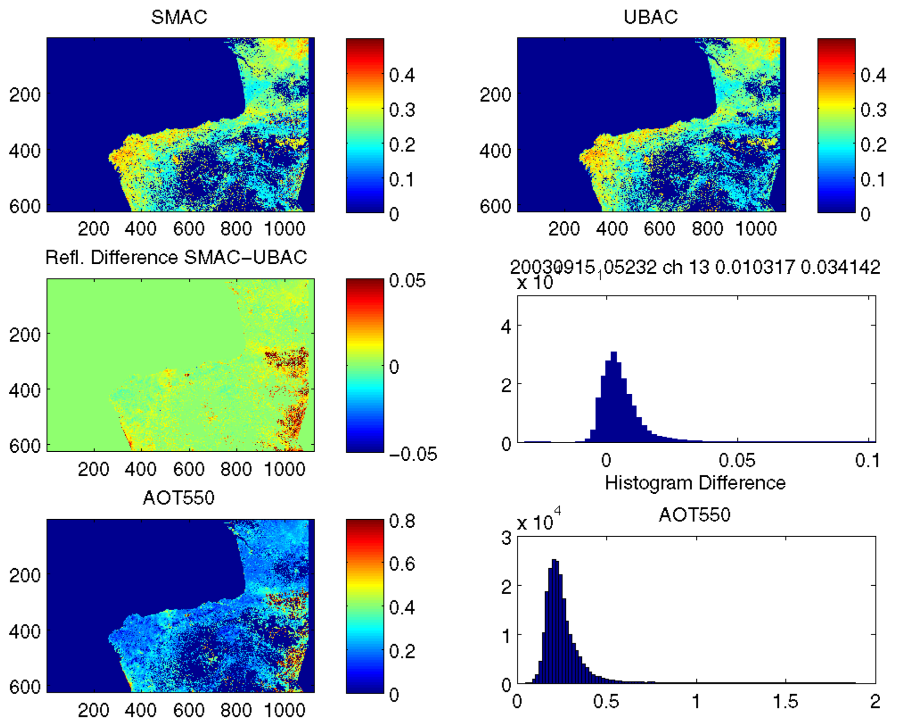
SMAC
UBAC
Refl. Difference SMAC−UBAC
20030915_05232 ch 13 0.010317 0.034142
Histogram Difference
AOT550
AOT550

MER_RR__2PP01R20030915_173807_000001072019_00499_08068_0001.N1.data

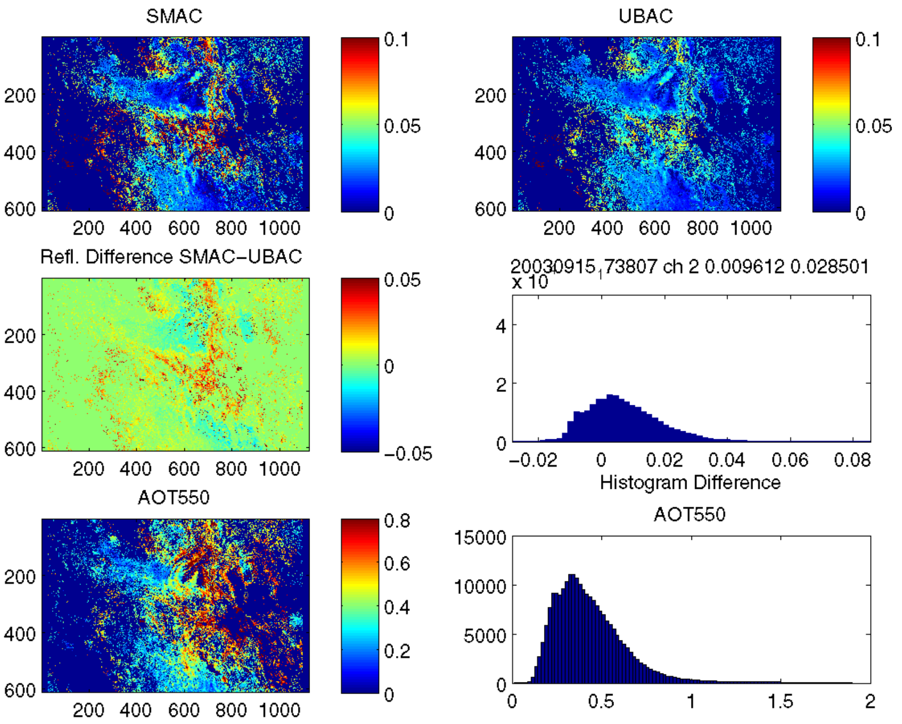

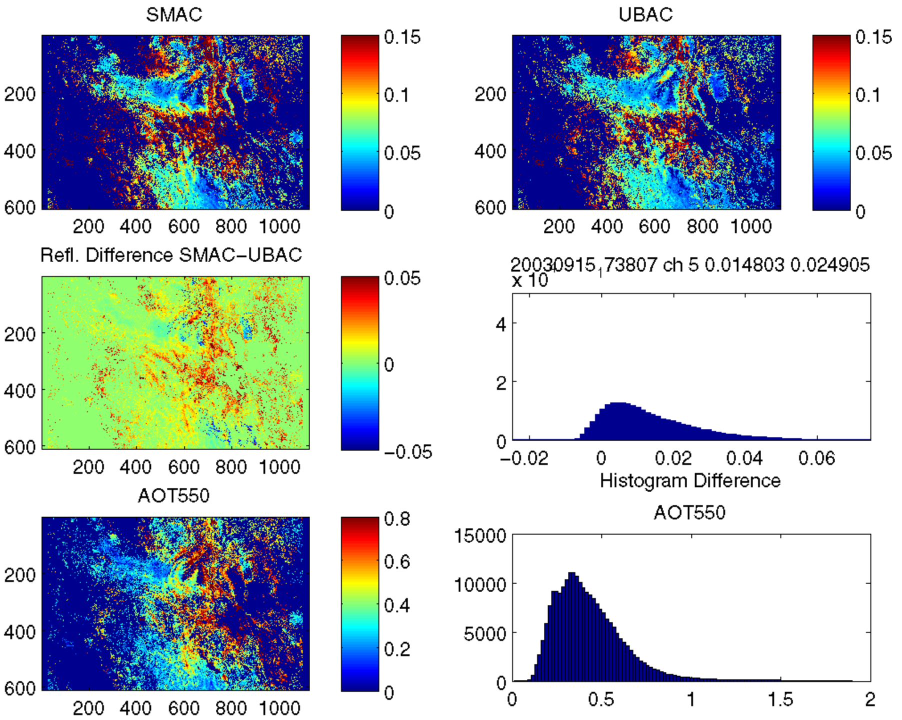

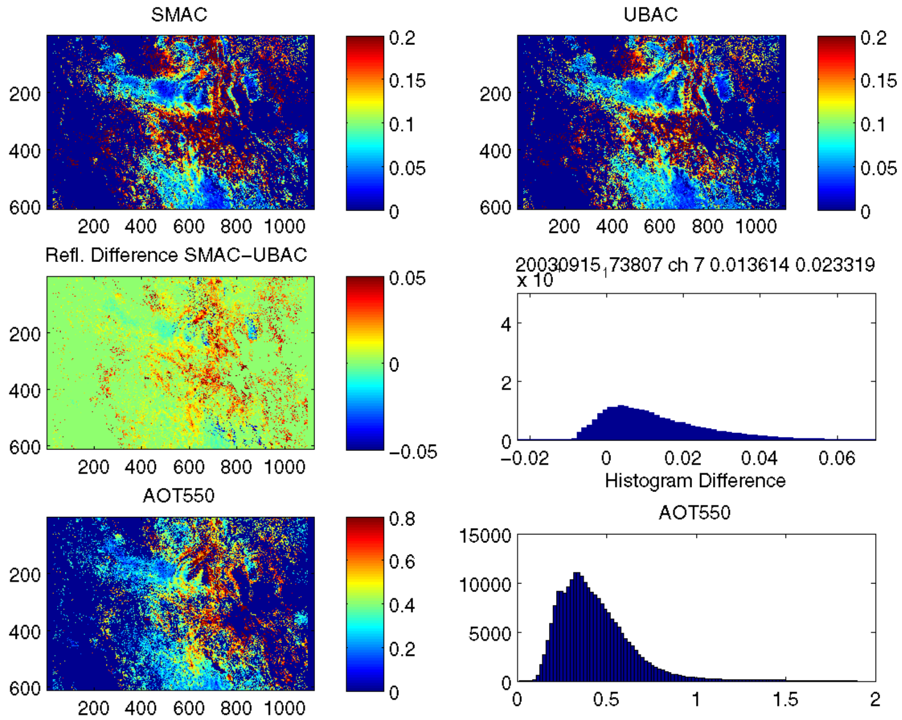

SMAC
UBAC
Refl. Difference SMAC−UBAC
20030915_73807 ch 7 0.013614 0.023319
Histogram Difference
AOT550
AOT550

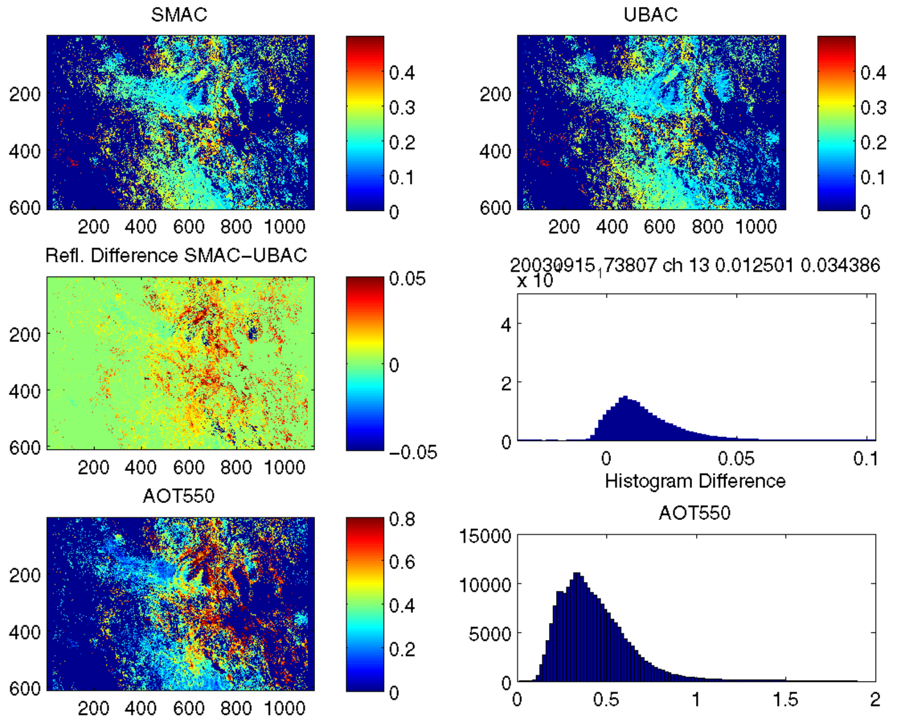

SMAC
UBAC
Refl. Difference SMAC−UBAC
20030915_73807 ch 13 0.012501 0.034386
Histogram Difference
AOT550
AOT550

MER_RR__2PP01R20031118_073905_000001072021_00407_08978_0001.N1.data

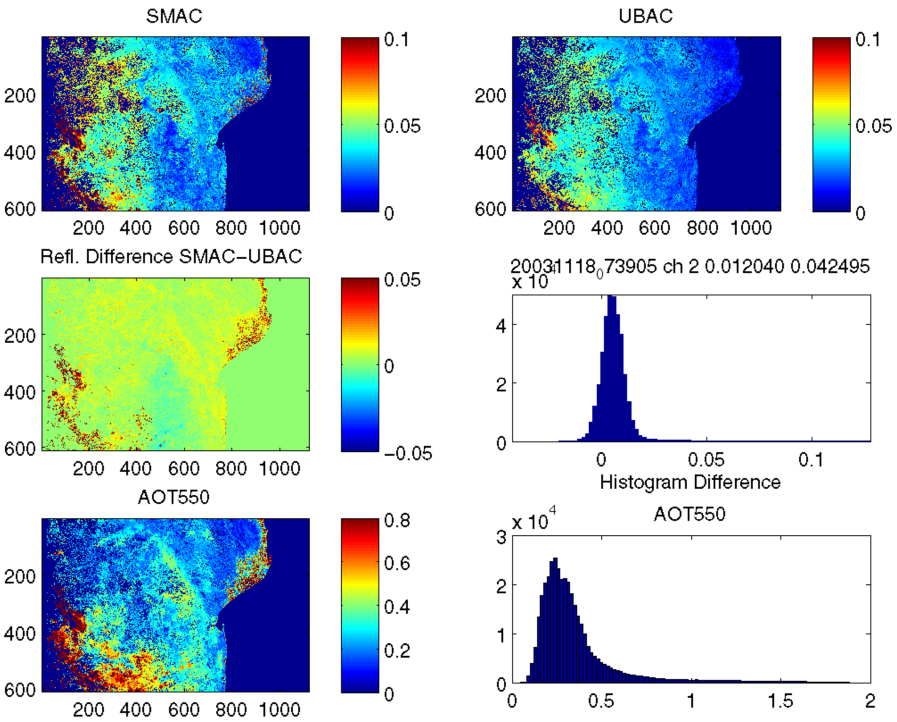

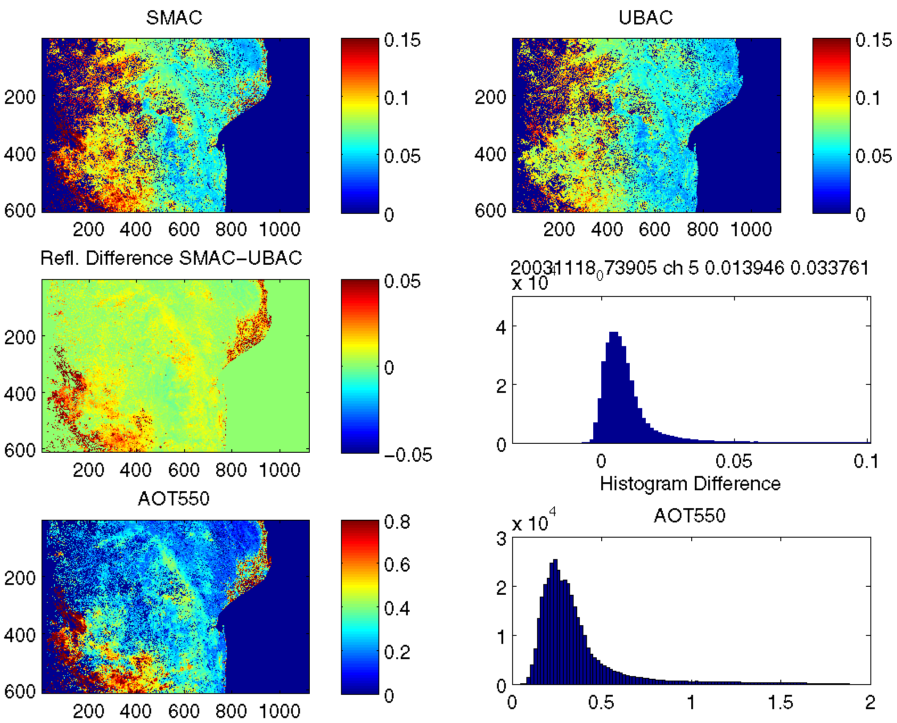

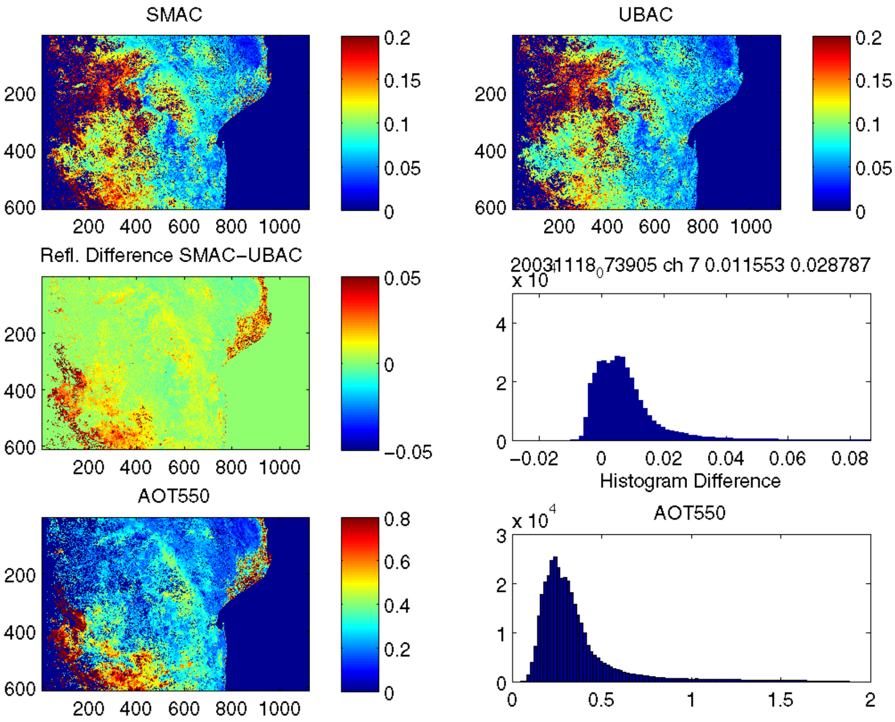
SMAC
UBAC
Refl. Difference SMAC−UBAC
20031118_0 73905 ch 7 0.011553 0.028787
Histogram Difference
AOT550
AOT550

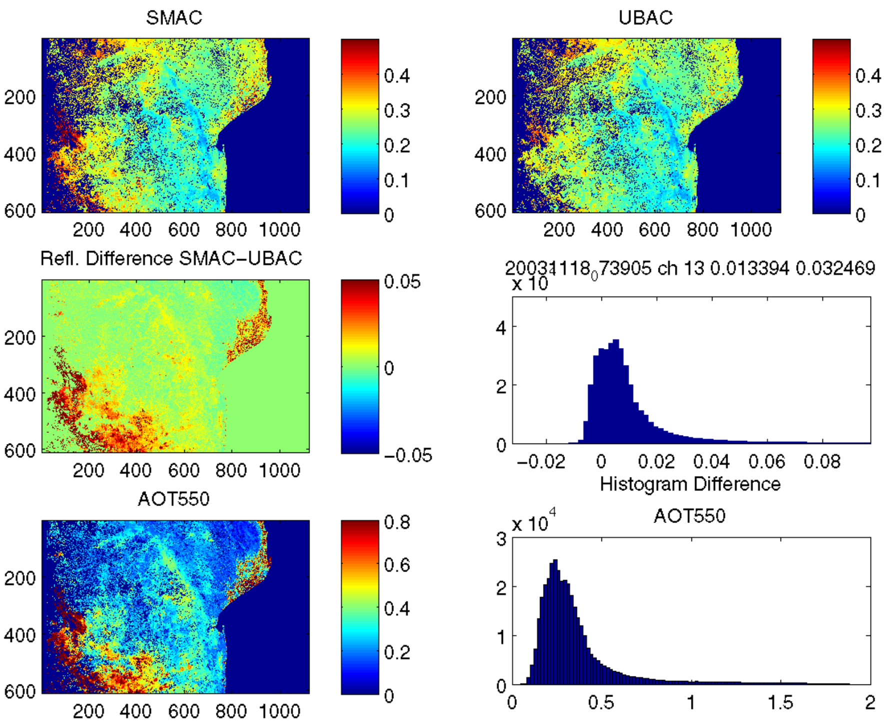
SMAC
UBAC
Refl. Difference SMAC−UBAC
20031118_0 73905 ch 13 0.013394 0.032469
Histogram Difference
AOT550
AOT550

MER_RR__2PP01R20031121_154959_000001072021_00455_09026_0001.N1.data

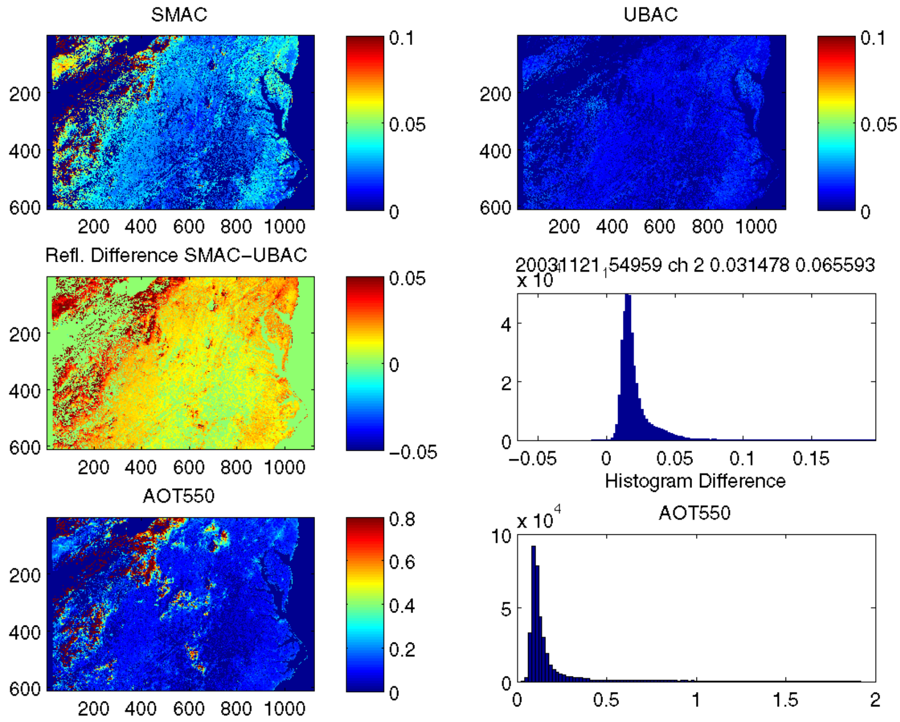

SMAC
UBAC
Refl. Difference SMAC−UBAC
20031121 54959 ch 2 0.031478 0.065593
Histogram Difference
AOT550
AOT550

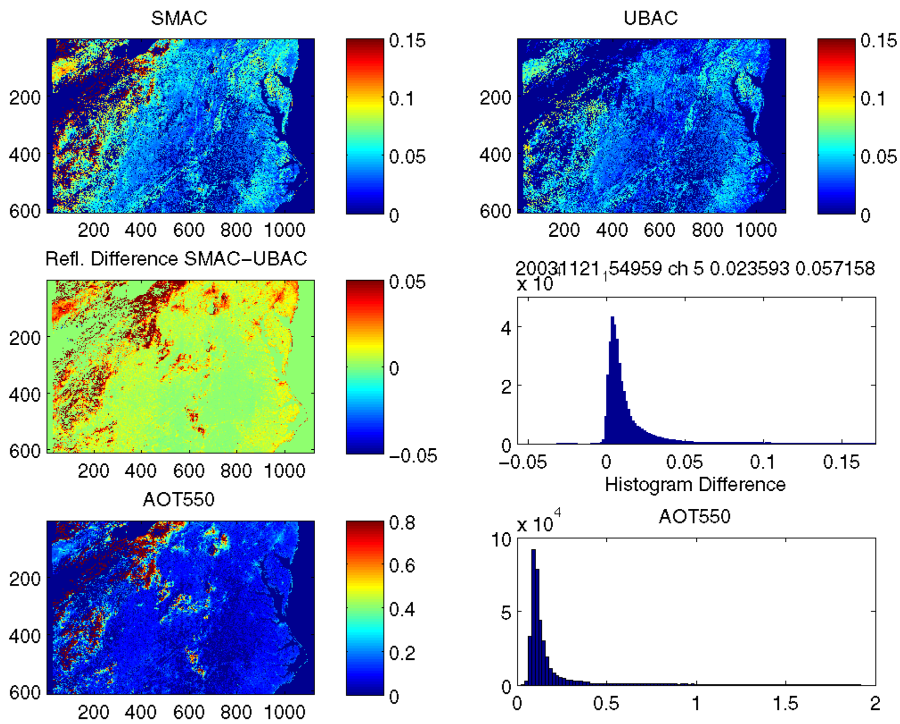

SMAC
UBAC
Refl. Difference SMAC−UBAC
20031121 54959 ch 5 0.023593 0.057158
Histogram Difference
AOT550
AOT550

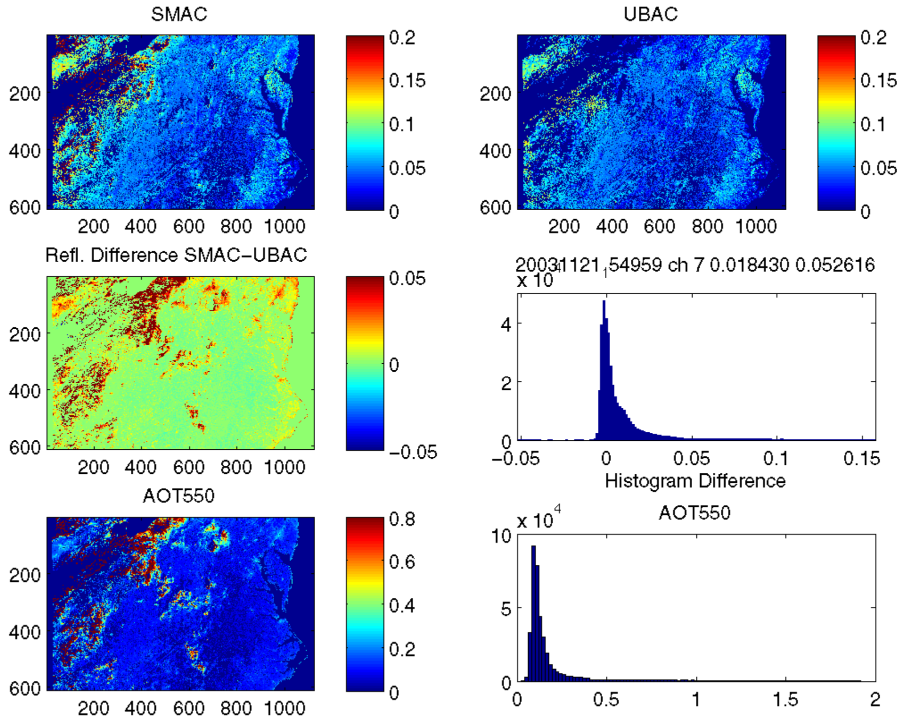
SMAC
UBAC
Refl. Difference SMAC−UBAC
20031121_54959 ch 7 0.018430 0.052616
Histogram Difference
AOT550
AOT550

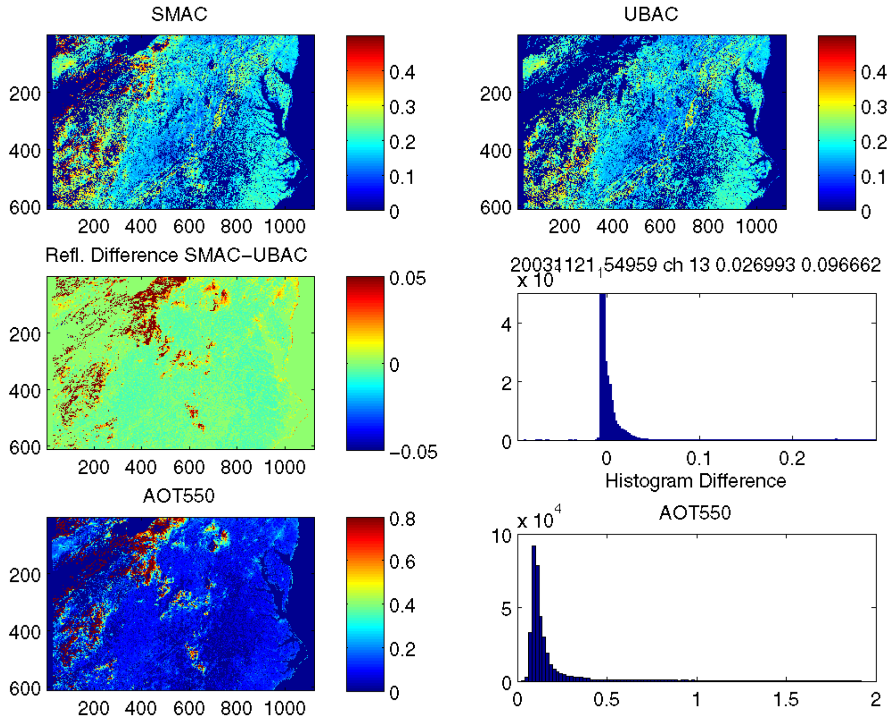
SMAC
UBAC
Refl. Difference SMAC−UBAC
20031121_54959 ch 13 0.026993 0.096662
Histogram Difference
AOT550
AOT550